Continuous homogeneous hydroformylation with integrated membrane separation : kinetics, mechanics and jet loop reactor technology

Continuous Homogeneous Hydroformylation with Integrated Membrane Separation:

Kinetics, Mechanism and Jet Loop Reactor Technology

PROEFSCHRIFT

ter verkrijging van de graad van doctor aan de Technische Universiteit Eindhoven, op gezag van de rector magnificus prof.dr.ir. C.J. van Duijn, voor een commissie aangewezen door het College voor Promoties, in het openbaar te verdedigen op maandag 2 december 2013 om 16:00 uur

door

Snezhana Asenova Hristova

geboren te Kardzhali, Bulgarije

Dit proefschrift is goedgekeurd door de promotoren en de samenstelling van de promotiecommissie is als volgt:

voorzitter:	prof.dr.ir. J.C. Schouten
1e promotor:	prof.dr. D. Vogt
2e promotor:	prof.dr. C. Müller
leden:	prof.dr. P.W.N.M. van Leeuwen (ICIQ)
	prof.dr. D. Cole-Hamilton (University of St Andrews)
	prof.dr. P. Wasserscheid (Friedrich-Alexander-Universität)
adviseur(s):	prof.dr. R. Franke (Evonik Industries AG)

"Essentially, all models are wrong, but some are useful"

George E. P. Box

A catalogue record is available from the Eindhoven University of Technology Library

ISBN: 978-90-386-3490-6

The research described in this thesis was part of the European Community's Seventh Framework Programme (FP7/2007-2013), F3 Factory and received financial support under grant agreement n° 228867.

Cover design by Sabriye Güven

Druk: TU/e PrintService

Continuous Homogeneous Hydroformylation with Integrated Membrane Separation: Kinetics, Mechanism and Jet Loop Reactor Technology

Table of Contents

Chapter 1

Continuous Homogeneous Hydroformylation with Integrated Membrane Separation: Kinetics, Mechanism and Jet Loop Reactor Technology

---

Hydroformylation is one of the most important examples of homogenously catalyzed reactions in industry. However, apart from advantages such as higher activity and selectivity, there is also a major challenge in homogeneous catalysis: the separation and reuse of the catalyst. This is relevant not only for recycling of the expensive metal but also for the product purity. It is therefore of great interest to build an optimal reaction-separation system that enables reuse of the catalyst. Recycling of homogeneous catalysts is conventionally achieved by phase separation (extraction) or by distillation. These techniques however have their limitations. We investigate the principle of catalyst compartmentalization by nanofiltration, ultimately enabling continuous operation. This can either be achieved by the use of catalysts that are sufficiently large in size themselves, or by molecular weight enlargement, using suitable molecular units to attach to the catalysts.

1.1 Hydroformylation

Hydroformylation is the reaction that transforms alkenes into aldehydes in the presence of Rh or Co catalysts under syngas pressure (Scheme 1). Discovered by Otto Roelen in 1938,[1] hydroformylation is one of the most important homogeneously catalyzed industrial reactions, with an annual production of approximately 10 million tons.[2] Aldehydes are used in the production of a range of products such as alcohols, detergents and plasticizers. Double bond isomerization, hydrogenation and formation of heavies via aldol condensation are possible side reactions.

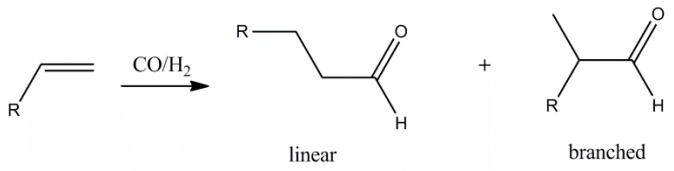

Scheme 1 Hydroformylation reaction

Currently, Rh is the most used metal for hydroformylation and the activity and selectivity of the catalyst can be tuned by phosphorus ligands. A large variety of phosphorus ligands are available, introducing different benefits in terms of activity and selectivity depending on their electronic and steric properties.[3] Although information on these properties allows a prediction of activity and selectivity to some extent, the kinetics for each alkene and catalyst combination are unique. This arises from a number of reasons; to start with, excess of ligand to metal ratio can change the number of ligands coordinated to the metal center and there can be a number of different metal-ligand complexes co-existing, acting slightly or dramatically different depending on the nature of the ligand. Another reason is the difference in accessibility of different positions in the molecule via double bond isomerization depending on the alkene molecule; steric hindrance and thermodynamically favored species being very molecule specific.[4]

The complexity of the reaction, especially in terms of existing number of catalyst species, leads to (semi)empirical modeling in many kinetic investigations.[5–7] However, a thorough investigation of the reaction mechanism is still crucial to rationalize any kinetic study and understand the reasons behind rate limiting steps and regioselectivity.

1.2 Hydroformylation Mechanism

The ligand-modified rhodium-catalyzed hydroformylation mechanism was postulated by Wilkinson as given in Scheme 2.[8] The reaction starts with dissociation of one ligand to form the active Rh hydride species (**I**) to which then the alkene can coordinate forming the π-complex (species **II**) followed by migratory insertion to form the alkyl species (**III**). This part of the mechanism is

important for the determination of the regioselectivity, since this insertion of the alkene determines whether a linear or a branched aldehyde will be formed. The cycle continues by addition of a carbonyl ligand to form species **IV**, and proceeds with the migratory insertion of CO into the Rh alkyl bond, forming species **V**. Addition of H_2 and reductive elimination of the aldehyde closes the cycle and reforms the active species **I**.

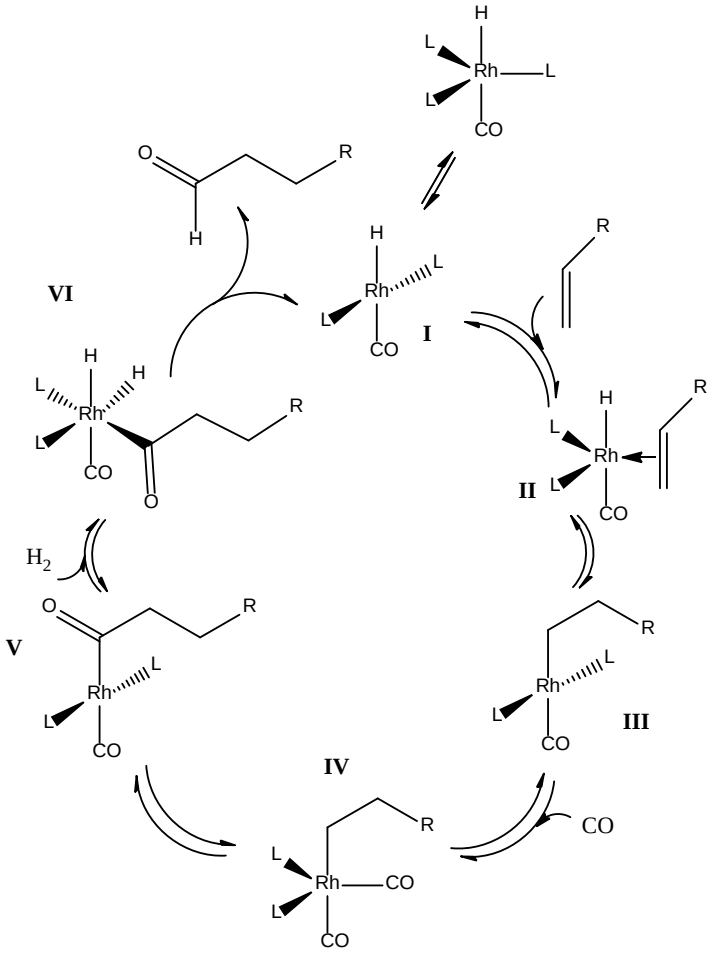

Scheme 2 Ligand modified hydroformylation mechanism[8]

Combining information about the coordination behavior, electronic and steric properties of the ligand, and the structure of the alkene to look at the mechanism will always prove useful for an initial guess of activity and parameters that should be taken into account for a kinetic study: Electronic properties of the ligand determine the ease of ligand dissociation and formation of the active species. For most substrate-catalyst pairs, the rate limiting step is either the coordination of the alkene to the metal center or hydrogenolysis of the acyl species (**V**). Steric nature of the ligand and number of ligands coordinated to Rh as well as the steric hindrance around the double bond of the alkene affect the ease of coordination to form the π-complex.

Naturally, in-situ investigation of the reaction intermediates using high pressure (HP) NMR, or HP IR is a very valuable tool in determining the rate limiting step and coordination behavior of the ligand.[9] Following reactions in time using these *in situ* tools also allows determination of kinetics of elementary steps.[10,11]

1.3 Kinetic Studies

Hydroformylation kinetics is a widely studied subject,[4–7,10,12–29] owing to the industrial relevance of the reaction and the huge number of catalyst-substrate-solvent combinations possible.

One pre-requisite to any kinetic study is to ensure that the kinetic experiments are performed under conditions free of mass-transfer limitation. For gas-liquid reactions, like most hydroformylation reactions catalyzed by homogeneous catalysts, the transfer of gaseous reactants to the liquid phase can become rate limiting when reaction rates are high. 'Kinetic' studies performed under mass transfer limitations will not only show false concentration dependencies but also will give lower than real activation energies.

As discussed before in Section 1.2; for one and the same catalyst, different steps in the reaction mechanism can be rate limiting for different alkene classes, i.e. linear, cyclic, vinylic, etc. Very bulky phosphite ligands typically lead to mono-ligated metal species, which are very active hydroformylation catalysts.[30] However, the coordination of sterically hindered alkenes might be rate limiting, resulting in a first order dependence on the alkene concentration (Type I Kinetics). Terminal linear alkenes on the other hand show very high activities with a first order dependence on H_2 concentration, with hydrogenolysis in this case being rate limiting (Type II Kinetics).[4] For ligands, which can coordinate in more than one possible fashion or when there are uncoordinated Rh centers, ligand concentration also shows up in the rate equations.[2]

$$(Type\ I) Rate = \frac{k[Alkene][Rh]}{K + [CO]}$$

$$(Type\ II) Rate = \frac{k[H_2][Rh]}{K + [CO]}$$

The regioselectivity of the reaction is also a function of various reaction parameters, such as temperature and/or reactant/ligand concentrations, depending on the catalyst and alkene used. For some alkenes, different steps of the mechanism can be rate limiting for the isomeric aldehydes.[31]

Finally, side reactions such as hydrogenation and especially double bond isomerization make the determination of kinetics for most substrates quite challenging.

1.4 Jet Loop Reactor

In loop reactors mixing is achieved by circulation of the reaction mixture via a pump through a tube connected to the reactor (Figure 1). They are especially important for multi-phase reactions where the gaseous reactants should dissolve in the liquid phase or a through mixing of two immiscible liquid phases is required. Feeding the reactant gas and the liquid reaction mixture through a restriction, like the nozzle of a jet, dissipates the gas phase into the liquid.[32]

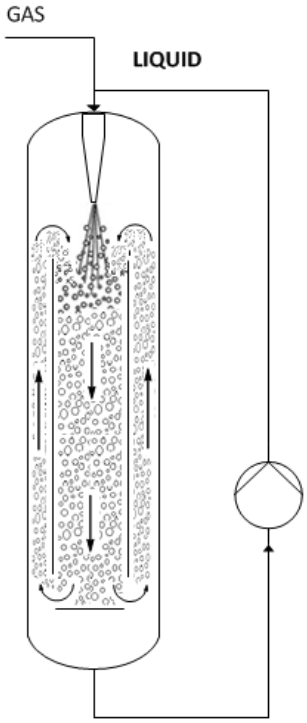

Figure 1 Jet loop reactor[32]

Jet loop reactors have superior dispersion characteristics[33,34] without the energy penalty, and are therefore very suitable for gas-liquid reactions like hydroformylation, where mass transfer limitations can be observed for very active catalysts. Figure 2 is taken from a publication by Behr. et al. and shows the specific interfacial area in different reactors for specific power input.[35] This intensive mixing capability enables a minimization of the reactor volume while maximizing the yield.

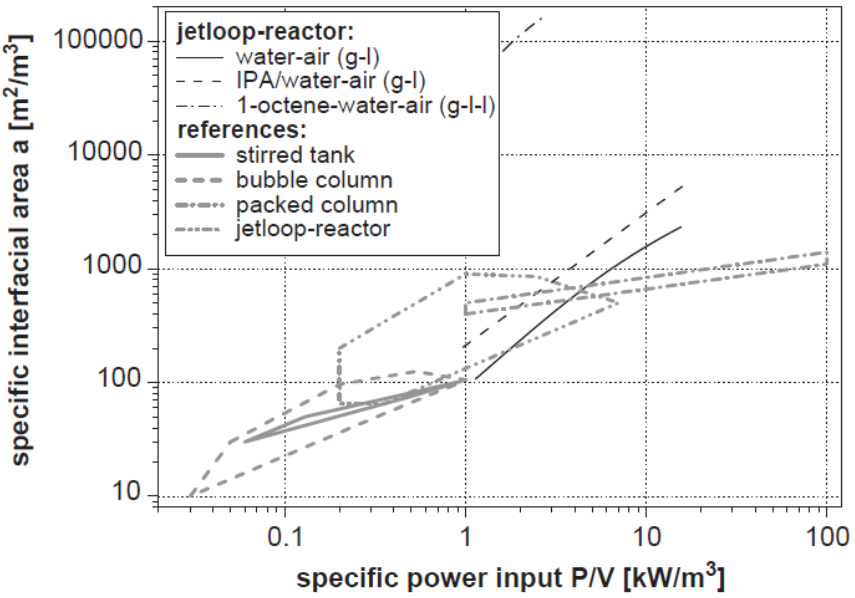

Figure 2 Specific interfacial areas for different reactor types[35]

For gas-liquid mixtures, having a downward flow is advantageous to increase the residence time of the gaseous phase.[34] Most commonly, a draft tube is added to the reactor to direct the flow through the nozzle along the body of the reactor, so entrained gas bubbles are pushed down against their buoyancy together with the liquid. An impact plate is placed in a way to allow an opening after the draft tube, and the flow is thus directed back up again, where it is drawn back into the jet enabling a very thorough mixing within the reactor (Figure 1).[35,36]

Important parameters for jet loop reactors are: i) gas hold-up (ε), which defines the ratio of volume of gas entrained in a liquid-gas mixture to the total volume, ii) bubble size measured as bubble diameter (d_B), and iii) residence time (τ) which is also defined as circulation time or in terms of circulation number. The effects of reactor geometry on gas holdup and residence time distribution are described in the literature.[34,37–39] There are also empirical models proposed for predicting the bubble size, gas hold-up, circulation time, and axial dispersion as a function of process variables.[34,38,40]

All these observations aim at one thing: to determine the mass transfer properties of the reactor as a function of design and process variables.

1.5 Catalyst Recycling in Continuous Hydroformylation

Figure 3 is adopted from the excellent review by Wiese and Obst[2] on hydroformylation and gives a very general representation of a hydroformylation process.

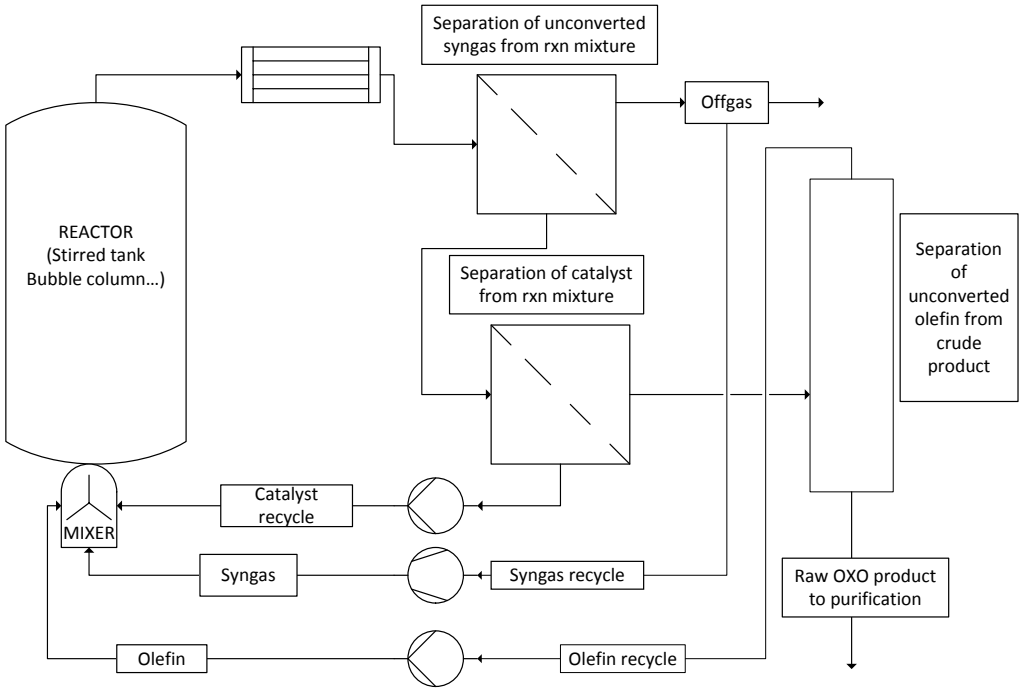

Figure 3 General scheme of an OXO process[2]

The reaction is carried out in a stirred tank or a bubble column reactor depending on the utilized reaction rates, under syngas pressure. Syngas is recycled back to the reactor after it is separated from the liquid reaction mixture as well as catalyst and unreacted olefin. The separation of catalyst from unreacted olefin and products is the trickiest part of any hydroformylation process. Different approaches for catalyst recycling is summarized in Chapter 8 of the book "*Rhodium Catalyzed Hydroformylation*" by P. van Leeuwen and C. Claver.[3]

The first application of rhodium-ligand catalyzed hydroformylation was the low pressure oxo (LPO) process, where catalyst remains in the reactor because the products and unconverted olefin are stripped using a big excess of syngas, which is recycled after the products and unreacted olefin are separated by condensation.[41] Apart from the huge amount of syngas recycle, this process is quite optimal in terms of catalyst and product separation and reuse of the homogeneous catalyst. The limitation however, is that this process is only feasible for low boiling aldehydes. The application is limited to propene hydroformylation since any longer alkene chain would require more syngas excess for stripping, which makes this process unfeasible for higher alkenes.

Another way to separate the catalyst from the products is distillation. Catalyst dissolved in high boiling side products, like aldol condensation products, is recycled back to the reactor after distillation. The process is again less attractive for higher alkenes because thermal strain introduced on the catalyst for distillation can lead to catalyst deactivation and to accumulation of heavies, in

which the catalyst is dissolved. This requires bleeding of the heavies, resulting in loss of catalyst. This process has been commercialized for butene hydroformylation by Mitsubishi Chemical and Union Carbide/Davy Process Technology.[3]

The Ruhrchemie-Rhône Poulenc process, which was introduced in the 1980s makes use of phase separation as a means of catalyst recycling.[42,43] The process employs two immiscible phases, usually an aqueous phase where the catalyst is dissolved and the product phase. The reaction rate is in this case limited by alkene solubility in the aqueous phase, so a very good mixing of the two phases (three including the reactant gases) is necessary. This approach has been extended to extraction after one phase reaction for systems where two phase reaction is extremely slow due to low solubility of reactants in the aqueous phase, i.e. the liquid-liquid mass transfer rate.[44,45] The basic principle in this case is to have polar catalyst-apolar product or vice versa. The phases separate after reaction by cooling or addition of a solvent and the reactants/products go to one phase whereas the catalyst goes to the other phase. Another method has been demonstrated by developing ligands changing solubility characteristics with temperature, enabling the catalyst to be in the organic phase at elevated reaction temperature and back in the aqueous phase when cooled.[46] Continuous homogeneous catalysis using supercritical (sc) CO_2[47] and ionic liquid/scCO_2 biphasic systems[48] has also been reported, which will not be discussed in detail here.

Recycling of the homogeneous catalyst can also be achieved by immobilization of the catalyst on a soluble or insoluble support, i.e heterogenization of the catalyst and recovering it by means of filtration.[49] For insoluble supports, the challenge might be that the heterogeneous catalyst is not as active as its homogeneous counterpart, or it leaches via formation of new bonds during catalysis leading to breaking of bonds between the support and the metal.[50] Using a film coating layer of ionic liquid on the supported catalyst was shown to improve activity and stability of the catalyst and there has been increasing research interest in this area in the past years.[51,52] Soluble supports are means of molecular weight enlargement to make the catalyst bulkier and thus easier to filter. Soluble polymers, dendrimers and polyhedral oligosilsesquioxane cages (POSS) are reported means of molecular weight enlargement.[53,54]

1.6 Ceramic Membrane Nanofiltration

Although the separation of organometallic complexes by membrane separation started to appear in the patent literature in the early 1970s,[55–57] the separation and recycling of homogeneous catalyst by means of nanofiltration was first reported around the early 2000s,[58–61] following the development of solvent resistant nanofiltration membranes.[62] According to the 1996 IUPAC-

nomenclature, nanofiltration is a "pressure-driven membrane-based separation process in which particles and dissolved molecules smaller than about 2 nm are rejected".[63] First organic solvent nanofiltration membranes developed were polymeric membranes.[62] Although ceramic membranes have been used in aqueous processes like waste water treatment for a long time, they have been applied only lately in organic solvent nanofiltration[64] due to challenges in obtaining smaller pore sizes.[62] By the end of the 20th century, ceramic zirconia and titania nanofiltration membranes, supported on silica or alumina were developed successfully and are commercially available under the name Inopor.[65] Ceramic membranes available by Inopor are given in Table 1.

Table 1 Ceramic ultra and nanofiltration membranes by Inopor[65]

Membrane	Material	Mean pore size	Cut-off	Open porosity
Ultrafiltration inopor® ultra	γ-Al_2O_3	10 nm		30 % - 55 %
		5 nm	7500 D	
	TiO_2	30 nm		
		5 nm	8500 D	
	ZrO_2	3 nm	2000 D	
Nanofiltration inopor® nano	SiO_2	1.0 nm	600 D	30 % - 40 %
	TiO_2	1.0 nm	750 D	
		0.9 nm	450 D	

Their superior chemical and mechanical stability in organic solvents and wider operating range in terms of temperature compared to polymeric membranes makes ceramic nanofiltration membranes a promising separation tool in chemical applications.[66,67]

An elegant example of continuous hydroformylation using ceramic membrane nanofiltration has been recently reported by Vogt and Müller et.al.[68] The researchers report an accumulated turn over number of 120 000 using a POSS-enlarged PPh_3 ligand in Rh-catalyzed hydroformylation of 1-octene. Figure 4 shows the nanofiltration coupled continuous reactor used for the study.

Recent research on ceramic membranes is focused on the prediction of solvent flux and rejection characteristics.[64,67,69]

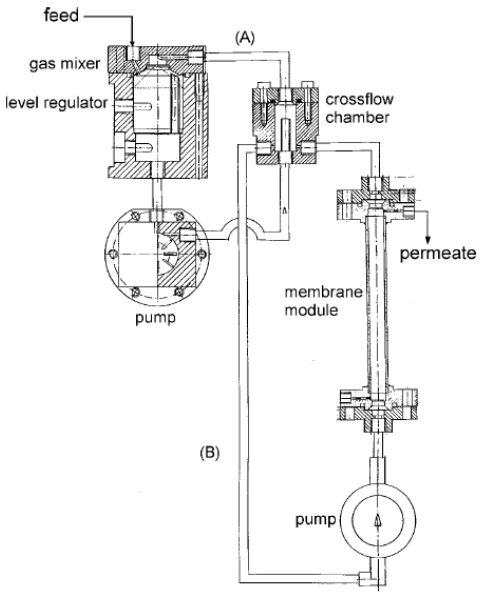

Figure 4 Continuous flow nano-filtration reactor by Vogt et. al.[68]

1.7 Aim and Scope of the Research

The separation and reuse of the homogeneous catalyst is a grand challenge in continuous hydroformylation. There are several approaches practiced in industry and others are under research; like phase separation, distillation, heterogenization of the catalyst on soluble/ insoluble supports. Recently, it was shown by our research group that molecular weight enlarged catalysts kept in the reactor by taking the products out as permeate from a nanofiltration membrane represents a viable solution to this challenge. [54,68]

Based on the expertise in the group and taking into account the other challenge of a fast two phase reaction, mass transfer limitation; we constructed a jet loop reactor with integrated membrane separation. Jet loop reactor technology enables a very good dispersion of gaseous reactants in the liquid without introducing extra energy demands. ***Chapter 2*** introduces the reactor setup and explains the design considerations taken into account.

The first step in planning a continuous reaction is to determine the reaction kinetics, which also makes it possible to understand the reaction mechanism. We investigated the hydroformylation kinetics of cyclooctene in order to plan a continuous hydroformylation reaction in the new setup. ***Chapter 3*** gives the kinetic results obtained from batch experiments and a continuous cyclooctene hydroformylation run in the setup is presented.

Hydroformylation kinetics of neohexene was also investigated, representing a different class of alkenes, i.e vinylic. The kinetic investigation led us to an interesting study on regioselectivity. We

investigated the reasons behind the temperature dependence of the l/b aldehyde selectivity using deuterium labeling and ^{2}H NMR as well as in-situ high pressure IR. Results of this study are presented in ***Chapter 4***.

Also a rather fast reaction, the hydroformylation of 1-pentene, was investigated. The results are presented in ***Chapter 5***. Mass transfer limitations are even more relevant for this very reactive terminal alkene. Kinetics of the reaction were used to plan a continuous reaction in the jet loop reactor. Effects of process conditions on isomerization and selectivity of the reaction are discussed.

Prediction of membrane permeability as a function of process variables and reaction mixture composition are obviously necessary to be able to operate a continuous reactor where the product flow is the permeate of a nanofiltration membrane. Also, characterizing the catalyst/ligand leaching behavior allows compensating for the lost ligand at an appropriate rate. Make-up of the lost ligand makes it possible to keep the ligand excess constant and prevent metal leaching since the metal centers will be more prone to leaching once they lose the ligand attached due to a shift in equilibrium. Membrane characterization is discussed in ***Chapter 6***.

1.8 References

[1] O. Roelen, *Verfahren Zur Herstellung von Sauerstoffhaltigen Verbindungen*, **1938**, DE 849548.
[2] K.-D. Wiese, D. Obst, in *Catal. Carbonylation React.* (Ed.: M. Beller), Springer Berlin Heidelberg, **2006**, pp. 1–33.
[3] P. W. N. M. van Leeuwen, C. Claver, *Rhodium Catalyzed Hydroformylation*, Springer, **2002**.
[4] A. van Rooy, E. N. Orij, P. C. J. Kamer, P. W. N. M. van Leeuwen, *Organometallics* **1995**, *14*, 34–43.
[5] A. Bernas, P. Mäki-Arvela, J. Lehtonen, T. Salmi, D. Y. Murzin, *Ind. Eng. Chem. Res.* **2008**, *47*, 4317–4324.
[6] R. Deshpande, *J. Catal.* **1989**, *115*, 326–336.
[7] R. M. Deshpande, R. V. Chaudhari, *Ind. Eng. Chem. Res.* **1988**, *27*, 1996–2002.
[8] D. Evans, J. A. Osborn, G. Wilkinson, *J. Chem. Soc. Inorg. Phys. Theor.* **1968**, 3133.
[9] P. C. J. Kamer, A. van Rooy, G. C. Schoemaker, P. W. N. M. van Leeuwen, *Coord. Chem. Rev.* **2004**, *248*, 2409–2424.
[10] J. Feng, M. Garland, *Organometallics* **1999**, *18*, 417–427.
[11] A. Torres, N. Molina Perez, G. Overend, N. Hodge, B. T. Heaton, J. A. Iggo, J. Satherley, R. Whyman, G. R. Eastham, D. Gobby, *Acs Catal.* **2012**, *2*, 2281–2289.
[12] C. Bergounhou, D. Neibecker, R. Mathieu, *J. Mol. Catal. Chem.* **2004**, *220*, 167–182.
[13] B. M. Bhanage, S. S. Divekar, R. M. Deshpande, R. V. Chaudhari, *J. Mol. Catal. Chem.* **1997**, *115*, 247–257.
[14] R. M. Deshpande, A. A. Kelkar, A. Sharma, C. Julcour-Lebigue, H. Delmas, *Chem. Eng. Sci.* **2011**, *66*, 1631–1639.
[15] C. Yang, Z.-S. Mao, Y. Wang, J. Chen, *Catal. Today* **2002**, *74*, 111–119.
[16] V. K. Srivastava, S. K. Sharma, R. S. Shukla, N. Subrahmanyam, R. V. Jasra, *Ind. Eng. Chem. Res.* **2005**, *44*, 1764–1771.
[17] S. N. Rush, Y. G. Noskov, T. E. Kron, G. A. Korneeva, *Kinet. Catal.* **2009**, *50*, 557–566.
[18] M. Rosales, A. González, Y. Guerrero, I. Pacheco, R. A. Sánchez-Delgado, *J. Mol. Catal. Chem.* **2007**, *270*, 241–249.
[19] M. Rosales, J. A. Durán, Á. González, I. Pacheco, R. A. Sánchez-Delgado, *J. Mol. Catal. Chem.* **2007**, *270*, 250–256.
[20] M. Rosales, G. Chacón, A. González, I. Pacheco, P. J. Baricelli, L. G. Melean, *J. Mol. Catal. Chem.* **2008**, *287*, 110–114.
[21] A. Riisager, R. Fehrmann, M. Haumann, B. S. K. Gorle, P. Wasserscheid, *Ind. Eng. Chem. Res.* **2005**, *44*, 9853–9859.
[22] S. I. Reut, G. L. Kamalov, P. S. Kildeev, G. I. Golodets, *React. Kinet. Catal. Lett.* **1991**, *44*, 197–199.

[23] C. P. Casey, L. M. Petrovich, *J. Am. Chem. Soc.* **1995**, *117*, 6007–6014.
[24] R. M. Deshpande, B. M. Bhanage, S. S. Divekar, S. Kanagasabapathy, R. V. Chaudhari, *Ind. Eng. Chem. Res.* **1998**, *37*, 2391–2396.
[25] V. S. Nair, S. P. Mathew, R. V. Chaudhari, *J. Mol. Catal. Chem.* **1999**, *143*, 99–110.
[26] R. M. Deshpande, Purwanto, H. Delmas, R. V. Chaudhari, *Ind. Eng. Chem. Res.* **1996**, *35*, 3927–3933.
[27] R. M. Deshpande, S. S. Divekar, B. M. Bhanage, R. V. Chaudhari, *J. Mol. Catal.* **1992**, *77*, L13–L17.
[28] D. Y. Murzin, A. Bernas, T. Salmi, *Aiche J.* **2012**, *58*, 2192–2201.
[29] D. Y. Murzin, A. Bernas, T. Salmi, *J. Mol. Catal. Chem.* **2010**, *315*, 148–154.
[30] T. Jongsma, G. Challa, P. W. N. . van Leeuwen, *J. Organomet. Chem.* **1991**, *421*, 121–128.
[31] A. L. Watkins, C. R. Landis, *J. Am. Chem. Soc.* **2010**, *132*, 10306–10317.
[32] J. C. Middleton, K. J. Carpenter, in *Ullmanns Encycl. Ind. Chem.*, Wiley-VCH Verlag GmbH & Co. KGaA, **2000**.
[33] A. P. Boyes, A. Chughtai, X. X. Lu, S. Raymahasay, S. Sarmento, M. W. Tilston, J. M. Winterbottom, *Chem. Eng. Sci.* **1992**, *47*, 3729–3736.
[34] M. Velan, T. K. Ramanujam, *Can. J. Chem. Eng.* **1991**, *69*, 1257–1261.
[35] A. Behr, M. Becker, J. Dostal, *Chem. Eng. Sci.* **2009**, *64*, 2934–2940.
[36] P. Zehner, A. Ulonska, R. Paciello, *Hydroformylation Process for the Production of Aldehydes And/or Alcohols or Amines*, **2003**, US 6642420.
[37] G. Padmavathi, K. Remananda Rao, *Can. J. Chem. Eng.* **1993**, *71*, 94–100.
[38] M. Velan, T. K. Ramanujam, *Bioprocess Eng.* **1994**, *11*, 101–106.
[39] A. Behr, M. Becker, J. Dostal, D. Kohlmann, *Chem. Ing. Tech.* **2008**, *80*, 1501–1508.
[40] N. N. Dutta, K. V. Raghavan, *Chem. Eng. J.* **1987**, *36*, 111–121.
[41] E. A. V. Brewester, R. L. Pruett, *Cyclic Hydroformylation*, **1981**, US 4247486.
[42] E. G. Kuntz, *Aldehydes by Hydroformylation of Olefins*, **1977**, FR 2314910.
[43] B. Cornils, J. Hibbel, W. Konkol, B. Lieder, J. Much, V. Schmidt, E. Wiebus, *Aldehydes*, **1984**, DE 3234701.
[44] Y. Harano, *Process for Obtaining Butanediols*, **1984**, US 4465873.
[45] M. Matsumoto, S. Miura, *Process for Continuous Hydroformylation of Allyl Alcohol*, **1986**, US 4567305.
[46] X. Zheng, J. Jiang, X. Liu, Z. Jin, *Catal. Today* **1998**, *44*, 175–182.
[47] P. B. Webb, D. J. Cole-Hamilton, *Chem. Commun.* **2004**, 612.
[48] P. B. Webb, M. F. Sellin, T. E. Kunene, S. Williamson, A. M. Z. Slawin, D. J. Cole-Hamilton, *J. Am. Chem. Soc.* **2003**, *125*, 15577–15588.
[49] M. Janssen, C. Müller, D. Vogt, *Green Chem.* **2011**, *13*, 2247.
[50] D. J. Cole-Hamilton, *Science* **2003**, *299*, 1702–1706.
[51] A. Riisager, R. Fehrmann, M. Haumann, P. Wasserscheid, *Eur. J. Inorg. Chem.* **2006**, *2006*, 695–706.
[52] C. Van Doorslaer, J. Wahlen, P. Mertens, K. Binnemans, D. De Vos, *Dalton Trans.* **2010**, *39*, 8377.
[53] C. Müller, M. G. Nijkamp, D. Vogt, *Eur. J. Inorg. Chem.* **2005**, *2005*, 4011–4021.
[54] M. Janssen, C. Müller, D. Vogt, *Dalton Trans.* **2010**, *39*, 8403.
[55] A. Goldup, M. T. Westaway, G. Walker, *Separation of Organometallic Catalysts by Silicon Latex Membranes Under Pressure*, **1971**, DE 1953641.
[56] A. Goldup, M. T. Westaway, G. Walker, *Separation of Organometallic Compounds from Organic Liquids*, **1972**, US 3645891.
[57] E. Bayer, V. Schurig, *Catalysis Using Soluble Metal Compounds of Synthetic Polymers*, **1974**, DE 2326489.
[58] S. S. Luthra, X. Yang, A. G. Livingston, L. M. Freitas dos Santos, L. S. White, *Chem. Commun.* **2001**, 1468–1469.
[59] D. Nair, S. S. Luthra, J. T. Scarpello, L. S. White, L. M. Freitas dos Santos, A. G. Livingston, *Desalination* **2002**, *147*, 301–306.
[60] K. De Smet, S. Aerts, E. Ceulemans, I. F. J. Vankelecom, P. A. Jacobs, *Chem. Commun.* **2001**, 597–598.
[61] D. Nair, J. T. Scarpello, L. S. White, L. M. Freitas dos Santos, I. F. . Vankelecom, A. G. Livingston, *Tetrahedron Lett.* **2001**, *42*, 8219–8222.
[62] "Koch Membrane Systems," can be found under http://www.kochmembrane.com/Membrane-Products.aspx**.**
[63] W. J. Koros, Y. H. Ma, T. Shimidzu, *J. Membr. Sci.* **1996**, *120*, 149–159.
[64] P. Marchetti, A. Butté, A. G. Livingston, *J. Membr. Sci.* **2012**, *415-416*, 444–458.
[65] "inopor," can be found under http://www.inopor.com/**.**
[66] C. Guizard, A. Ayral, A. Julbe, *Desalination* **2002**, *147*, 275–280.
[67] S. Darvishmanesh, A. Buekenhoudt, J. Degrève, B. Van der Bruggen, *Sep. Purif. Technol.* **2009**, *70*, 46–52.
[68] M. Janssen, J. Wilting, C. Müller, D. Vogt, *Angew. Chem. Int. Ed.* **2010**, *49*, 7738–7741.
[69] A. Dobrak, B. Verrecht, H. Van den Dungen, A. Buekenhoudt, I. F. J. Vankelecom, B. Van der Bruggen, *J. Membr. Sci.* **2010**, *346*, 344–352.

Chapter 2

Jet Loop Reactor with Integrated Membrane Separation:

Design Considerations

The separation of molecular catalysts by membrane nanofiltration is a promising technique for catalyst recycling in homogeneously catalyzed reactions. Taking another challenge of a fast two phase reaction, mass transfer limitations, into account; we constructed a jet loop reactor with integrated membrane separation for continuous hydroformylation. Jet loop reactor technology enables a very good dispersion of gaseous reactants in the liquid without introducing extra energy demands. A good selection of equipment gave us a flexible reaction system in terms of operating conditions like residence time, and the power input per unit volume on the fluid flow through the jet (P/V). (P/V) is an important parameter for achieved gas to liquid mass transfer rates.

2.1 Jet Loop Reactor with Integrated Membrane Separation for Continuous Hydroformylation

The separation of the catalyst from unreacted olefin and products is a very essential part of any hydroformylation process. Different approaches for catalyst recycling are summarized in Chapter 8 of the book "*Rhodium Catalyzed Hydroformylation*" by P. W. N. M. van Leeuwen and C. Claver. [1] The separation and recycling of homogeneous catalysts by means of nanofiltration has been reported first around the early 2000s,[2–5] following the development of solvent resistant nanofiltration membranes.[6] An elegant example of continuous hydroformylation using ceramic membrane nanofiltration has been recently reported by Vogt and Müller et al.[7] The researchers reported an accumulated turn over number of 120 000 using a POSS-enlarged PPh_3 ligand Rh catalyst for 1-octene hydroformylation. Figure 1 below shows the nano-filtration coupled continuous reactor used for the study.

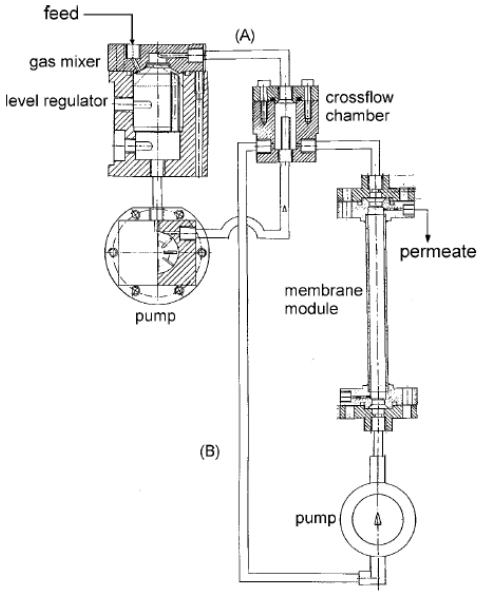

Figure 1 Continuous flow nano-filtration reactor by Vogt et al.[7]

Another challenge for hydroformylation, being a multiphase and exothermic reaction, is dispersion of the reactant gases into the liquid mixture and convenient removal of the heat generated. In loop reactors mixing is achieved by circulation of the reaction mixture via a pump through a tube connected to the reactor (Figure 2), where a heat exchanger can also be conveniently employed. Feeding gas and circulated liquid stream through a restriction, like the nozzle of a jet, dissipates the gas phase into the liquid.[8] Jet loop reactors have superior dispersion characteristic[9,10] without the energy penalty. Therefore they are very suitable for gas-liquid reactions like hydroformylation, where mass transfer limitations are observed for very active catalysts.

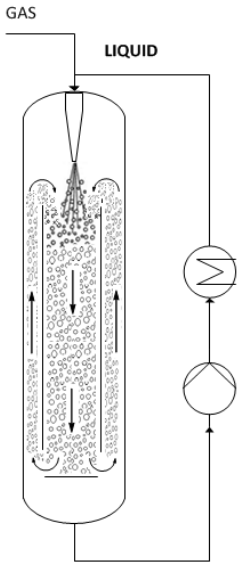

Figure 2 Jet loop reactor[8]

2.2 Reactor Setup

The basic jet loop reactor design used in this project has been adopted from earlier work reported in the literature.[11] A drawing of the reactor is given in Figure 3 together with a detailed drawing of the jet nozzle.

For gas-liquid mixtures, it is advantageous to apply a downward flow in order to increase the residence time of the gaseous phase.[10] A draft tube is added to the reactor to direct the flow through the nozzle along the body of the reactor, so entrained gas bubbles are pushed down against their buoyancy together with the liquid. An impact plate is placed in a way to allow an opening after the draft tube, and the flow is thus directed back up again, where it is drawn back into the jet enabling a very thorough mixing within the reactor[12,13] (Figure 2). The gas is fed into the nozzle through an inner tube and the liquid flow goes through the opening between this inner tube and an exchangeable nozzle head, via which the restriction applied to the liquid flow can be adjusted.

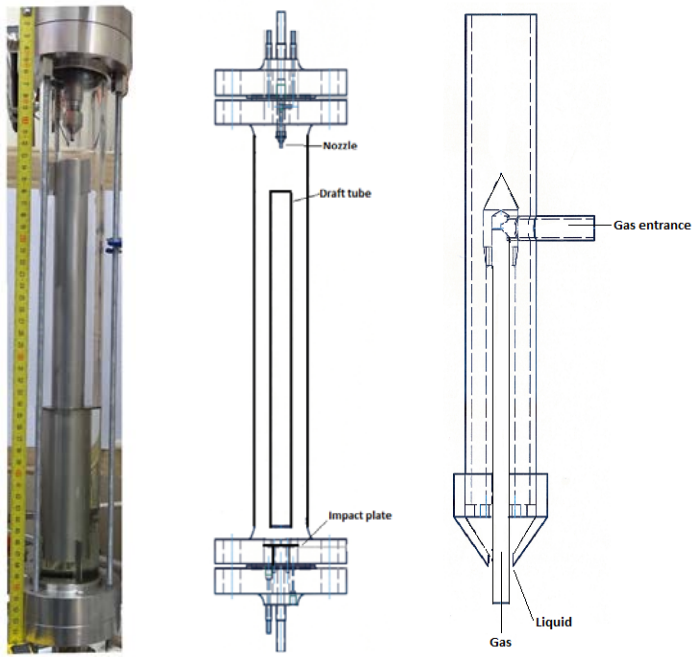

Figure 3 Jet-loop reactor (photo (left) and drawing (middle)) and the nozzle (right) used in this study

Dimensions belonging to the reactor and the nozzle are given in Table 1, along with the symbols which will be used to refer to them from now on.

Table 1 Dimensions of the jet-loop reactor and the nozzle

D_R: Reactor diameter (cm)	5
L_R: Reactor length (cm)	52
D_D: Draft tube diameters (cm)	1; 2.8
L_D: Draft tube length (cm)	35.5
D_I: Impact plate diameter (cm)	4
L_{DI}: Distance from the lower end of draft tube to impact plate (cm)	2.3
DI_N: Nozzle inner tube inner diameter (mm)	3
DO_N: Nozzle inner tube outer diameter (mm)	4
DI_{NH}: Nozzle restriction head inner diameters (mm)	4.3;4.4;4.6
L_{ND}: Distance from the tip of the nozzle to draft tube (cm)	4.7

There are two different draft tube sizes and the distance between the nozzle head and the upper end of the draft tube, L_{ND}, can be adjusted by lifting the draft tube up on a slide way to the point that the nozzle tip is immersed. There are also 3 different nozzle head diameters to increase/decrease the restriction of the liquid flow at the nozzle.

Figure 4 shows the flow sheet of the in-house built jet-loop reactor coupled with a nanofiltration membrane unit. The system consists of two loops: i) Reaction/gas saturation and ii) membrane

loop, which intersect at a cross-flow chamber. This chamber mixes the flows from the two loops and supplies volume for the gas bubbles entrained in the reactor outlet to buoy before the flow is fed to the membrane loop to minimize the syngas bleed through the membrane. In the membrane unit a ceramic membrane (TiO_2, pore size 0.9nm, MW cut-off 450D, length 0.5m, Inopor) is used to keep the catalyst within the system. The driving force for filtration is reaction pressure and the flux is regulated by an automated sampling unit that draws the permeate stream. The substrate solution is fed to the reactor by an HPLC pump which operates on feedback from a level sensor, so the liquid level in the reactor is kept constant. Total volume of the setup is 1000 mL, which can be considered as the reaction volume as all this volume is kept under reaction conditions. A mass flow controller keeps the reaction pressure constant and the gas uptake can be monitored to confirm conversion values obtained by GC sampling. The catalyst solution can be preformed in a heated compartment under pressure, the dropping funnel, connected to the reactor by a valve. This allows starting the reaction in a controlled manner, when a steady state of process variables is reached.

A list of equipment used in the setup is given in Table 2, showing the suppliers and operating window of the equipment and maximum temperature and pressure values where valid.

Table 2 List of Equipment used in the reaction setup, their providers and operating range

Equipment	**Provider and operation range**	**P_{max} ,T_{max}**
HPLC Pump	Knauer Smarline Pump 100 (0-50 ml/min)	400 bar
Membrane Loop Pump	K-Engineering HMH 060 (20-600 L water/h, gas content max 30%)	100 bar, 200°C
Reaction Loop Pump	K-Engineering HMH 070 (20-900 L water/h, gas content max 30%)	100 bar, 200°C
Level Sensor	Honsberg Nivolock NL-015HS/HK	160 bar, 100°C
Sampling valve	Rhodeyne MX Series II MXP7900-000	414 bar, 50°C
Flow meters	KEM-Küppers Electromechanik HM 005 R05.G.TC.15 (0.8 to 6 L/min)	630bar, 150C
Mass Flow Controller	Bronkhorst HI-TECH Model F-231M-TAD-33-V Multi-Bus DMFC (0-500 ml/min)	
Membrane	Inopor TiO_2, 450 D, 0.9nm pore size, 0.011 m^2 filtration area, channel diameter 7 mm, external 10 mm, length 0.5 m	

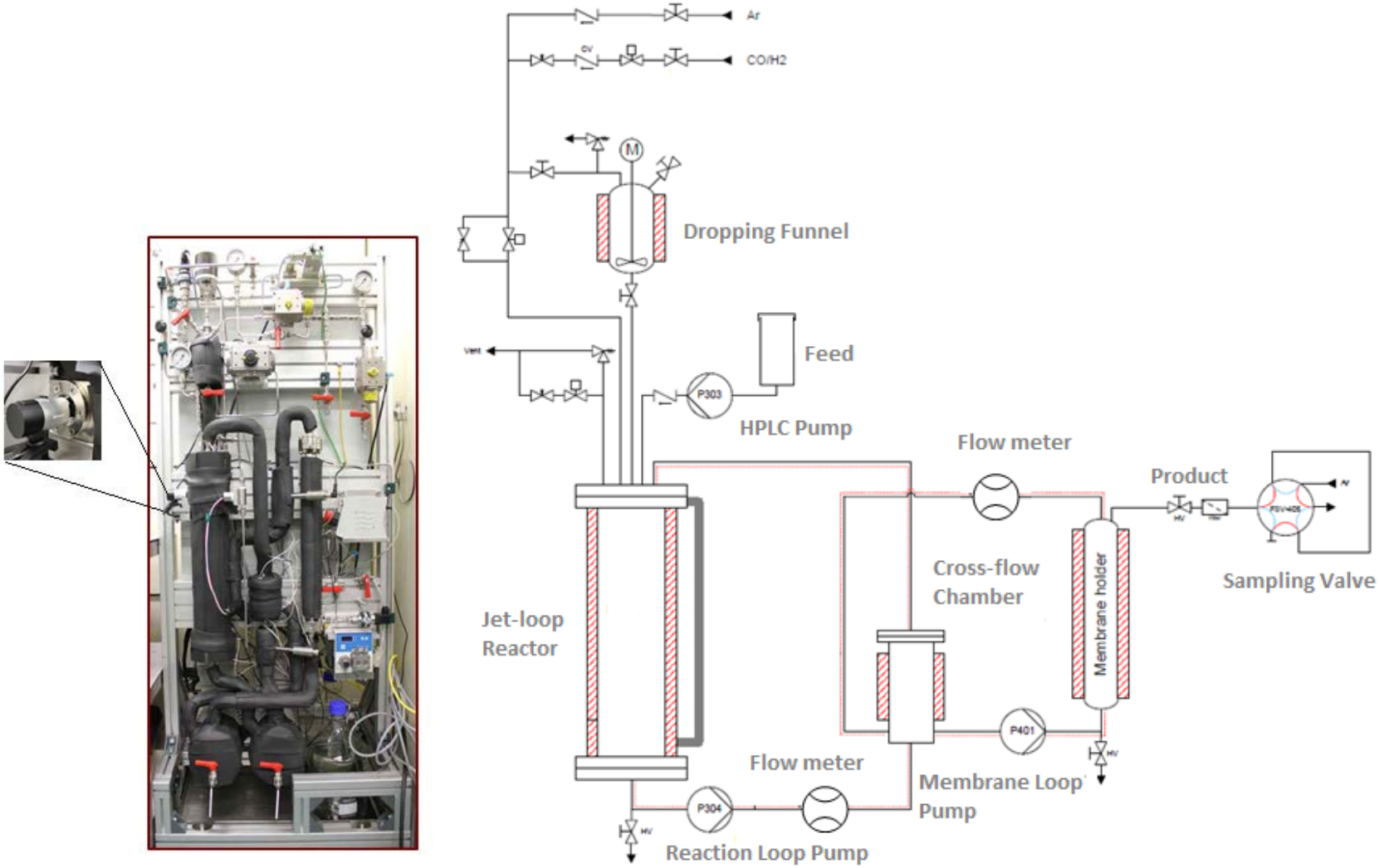

Figure 4 Picture (left) and flow sheet(right) of jet-loop reactor with integrated nanofiltration unit

The reactor also has a high pressure window, equipped with a live web-cam, which allows to observe the reactor behavior under reaction conditions at all times. Figure 5 shows pictures taken with this camera.

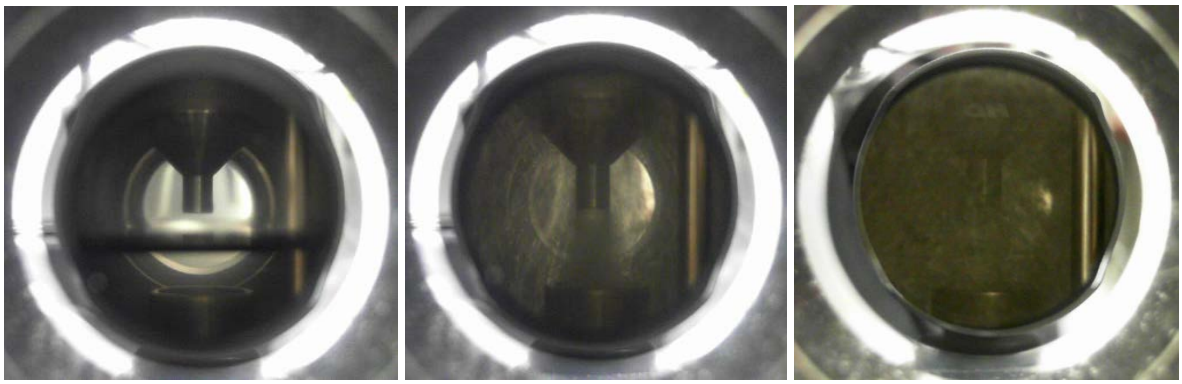

Figure 5 Pictures taken through the high pressure window: Liquid at the designated level (left), reaction loop pump running at 1.2 L/min (middle) and pump running at 2.1 L/min (right)

2.3 Design Considerations

2.3.1 Reactor

Important parameters for jet-loop reactors are: i) gas hold-up (ε) which defines the ratio of the volume of gas entrained in a liquid-gas mixture to the total volume, ii) bubble size measured as bubble diameter (d_B), and iii) residence time (τ), which is also defined as circulation time or in terms of circulation number. Studies on the effects of reactor geometry on gas holdup and residence time distribution have been reported in the literature. [10,14–16] There are also empirical models proposed for predicting the bubble size, gas hold-up, circulation time and axial dispersion as a function of process variables.[10,15,17]

All these observations aim at one thing, to determine the mass transfer properties of the reactor as a function of design and process variables: the so called $k_l a$ value, which is the volumetric mass transfer coefficient describing the mass transfer rate from gas bubbles to the liquid. The flux from gas to liquid phase is described by the equation given below:

$$\frac{dn_l}{dt} = V_l k_l a (C_l^* - C_l) \quad (1)$$

For a mass transfer limited reaction, the transfer of gas to the liquid phase is at its maximum since then the liquid phase concentration of the solute gas, C_l would be extremely small. Knowing the $k_l a$

value and the equilibrium concentration of the gas solute in the liquid, C_l^* allows to calculate the maximum rate of gas transfer possible at given reaction conditions.

A gas-liquid reaction is performed in the kinetic regime, only if the consumption rate of the gaseous reactants by reaction is well below this maximum gas to liquid transfer rate. The mass transfer coefficient $k_l a$ is a function of power input per unit volume as suggested by the empirical equation given in Equation 2.[17] And it is also a function of temperature although not included in Equation 2.

$$k_l a = m\left(\frac{P}{V_R}\right)^n \tag{2}$$

The power input *P* (W) can be calculated using Equation 3[17]

$$P = \frac{\pi \rho d^2 u_L^3}{8} \tag{3}$$

In the equations above V_R (m^3) is the reactor volume, ρ (kg/m^3) is the liquid density, u_L (m/s) is the velocity of liquid through the opening between the nozzle head and the inner tube and d (m) is given in Equation 4.

$$d = \sqrt{\frac{4A_{nozzle-opening}}{\pi}} \tag{4}$$

$A_{nozzle\text{-}opening}$ (m^2) defines the area of the opening between the nozzle head and the inner tube.

It is important to choose the pump on the reaction loop to enable the desired *P*/V values, also taking into account that the pressure drop over the nozzle will increase with increasing flow rates and the pump should be able to handle that differential pressure. The flow rates that can be achieved against certain pressures are listed in Table 3, specified by the supplier, for water.

Table 3 Flow rates that can be achieved against certain differential pressure values by the reaction loop pump

Flow (L water/min)	**ΔP (bar)**
13.33	0.40
10.00	4.90
6.67	6.00
5.00	6.50
3.33	6.90
2.50	7.00
0.00	7.40

The pressure drop ΔP over the nozzle is

$$\Delta P = \frac{K u^2 \rho}{2} \quad (5)$$

where K is the number of velocity heads, u is fluid velocity (m/s), ρ is fluid density (kg/m^3) and ΔP is in N/m^2. K was determined as 2.4 for the nozzle head with 4.4 mm diameter. The maximum rate of toluene flow through the nozzle is 4 L/min at a pressure drop of 6.6 bar. The *P*/V value achieved calculated using Equation 3 at this point is 21.2 kW/m^3. Maximum toluene flow rate and *P*/V value that can be achieved while using the 4.3 mm nozzle is 3 L/min and 16.5 kW/m^3 assuming that K is 2.4, which is probably higher; and for the nozzle head with a diameter of 4.6 mm can reach a maximum flow rate of 6 L/min and a *P*/V value of 29.6 kW/m^3, with the same assumption about the value of the velocity head, which should be now lower.

Obviously, the flow rate through smaller nozzle heads will be lower at the same *P*/V values, when compared to larger nozzle diameters. This also results in longer circulation times for smaller nozzle head diameters at given *P*/V values, as observed by Becker.[11]

The gas bubble diameter achieved in the reactor is important since the gas-liquid interface available for mass transfer increases when smaller bubbles are obtained. The bubble diameter decreases with increased power input. However, the effect is not at all as pronounced as the effect of liquid composition. Becker[11] found an increase by around 1000 times in the interfacial area per volume (*a* (m^2/m^3)), when 1-octene was added to the water-air system. We observed a similar behavior for air bubbles in the 1:1 sized, glass walled model when we added a small amount of aldehyde to toluene. Figure 6 below shows the lower part of the model reactor, and the air bubbles formed in different liquid compositions: water, toluene, 98% toluene+ 2% cyclooctanecarbaldehyde.

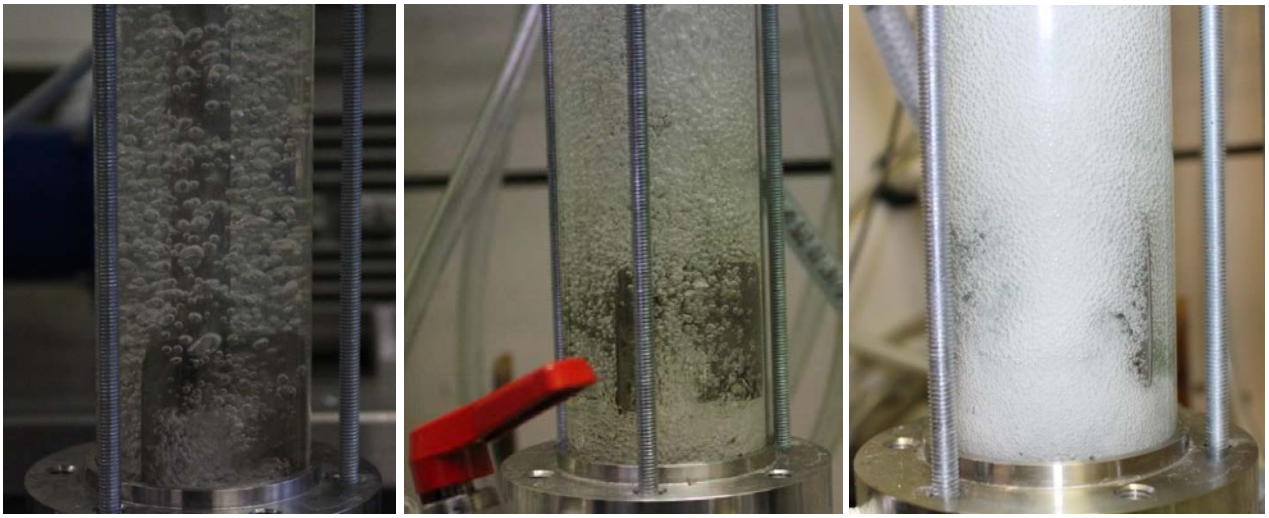

Figure 6 Lower part of the model reactor and the air bubbles formed in different liquid compositions: water (left), toluene (middle), 98% toluene+ 2% cyclooctanecarbaldehyde (right).

This improvement of bubble sizes has also been described in literature upon adding isopropanol into water.[18] The authors explained the reason behind this as formation of a polar isopropanol layer around the bubbles, which repels other bubbles and prevents coalescence.

Another important consideration is the gas holdup, the volume of gas in the gas-liquid mixture. By fixing the liquid level in the reactor and making sure to operate the reactor at full-height (the gas-liquid reaction mixture takes the whole reactor volume), we fixed the gas holdup as 18%.

Becker determined $k_l a$ values between 0.02 to 0.9 s^{-1} for water–CO and water-CO-octene systems,[11] the system temperature varying from 25 to 130°C and the power input from 1 to 10 kW/m^3. Considering the typical hydroformylation temperatures and the improvement on the bubble size in the presence of a polar component like the product aldehydes, one expects not to observe $k_l a$ values smaller than 0.1 s^{-1} in the jet loop reactor during hydroformylation.

2.3.1.1 Determination of volumetric mass transfer coefficient $k_l a$

We performed $k_l a$ measurements with toluene and a real reaction mixture of 1-pentene hydroformylation ([1-pentene]= 0.493 M, [2-pentene]= 0.073 M, [branched aldehydes]= 0.012 M, [hexanal]= 0.031 M, [toluene]= 2.575 M, [decane]= 0.003 M) in the jet loop reactor, using the batch absorption method. The experimental procedure was adopted from literature for these measurements with slight alterations.[19] Using the mole balance for gas dissolved in the liquid, given in Equation 1, it is possible to obtain Equation 6 below using ideal gas law and Henry's law, detailed derivation of which is reported.[19]

$$\frac{P_2 - P_0}{P_1 - P_0} ln\left(\frac{P_1 - P_2}{P - P_2}\right) = k_l a.t \quad (6)$$

Using this equation, it is possible to deduce $k_l a$ as slope of the line plotted for the left part of Equation 6 vs time. P_0 in the equation is the equilibrium pressure in the reactor before pressure is increased very quickly to P_1 and the mixing is started immediately; in our case by starting the reaction and membrane loop pumps. P_2 is the equilibrium pressure reached as the liquid is saturated with gas again. Pressure values over time are recorded from the start of mixing to the point at which a new equilibrium is reached to plot the mentioned graph. Figure 7 below shows the graphs plotted to determine the volumetric syngas transfer rate to toluene at 40°C at different specific power input values.

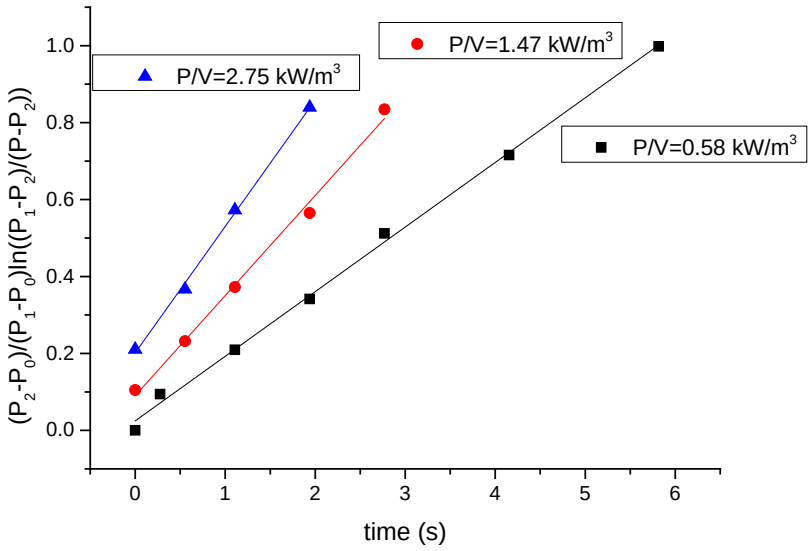

Figure 7 Determination of syngas-toluene gas-liquid mass transfer coefficient $\boldsymbol{k_l a}$ for the jet-loop reactor, performed at different specific power input values

We performed batch absorption experiments at 3 different temperatures for toluene, and also at different P/V values. Furthermore, we determined the $k_l a$ values for the 1-pentene hydroformylation reaction mixture also for a range of specific power input values. Figure 8 below shows the $k_l a$ values obtained as a function of P/V.

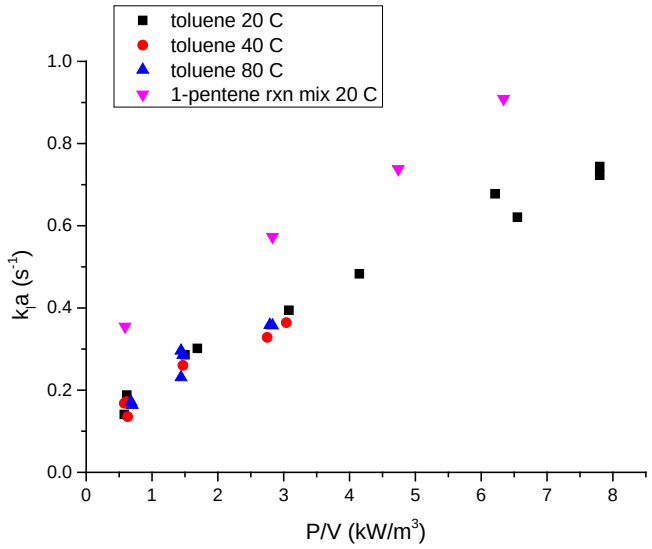

Figure 8 Syngas-toluene/1-pentene rxn mixture ([1-pentene]= 0.493 M, [2-pentene]= 0.073 M, [branched aldehydes]= 0.012 M, [hexanal]= 0.031 M, [toluene]= 2.575 M, [decane]= 0.003 M) gas-liquid volumetric mass transfer coefficient $\boldsymbol{k_l a}$ for the jet-loop reactor, performed at different specific power input values and temperatures

As seen in Figure 8, $k_l a$ for toluene is not temperature dependent in the temperature range we investigated and increases with increasing specific power input. It is possible to fit a curve to describe the P/V dependence of $k_l a$ as given in Equation 2 for the toluene data at 20°C, with R^2 = 0.985. Equation 7 shows the relation, which can be used to predict the $k_l a$ value for syngas-toluene at least till up to 80°C as well.

$$k_l a\ (toluene\ 20\ ℃) = 0.2188 \left(\frac{P}{V_R}\right)^{0.5813} \tag{7}$$

The $k_l a$ values found for the reaction mixture of 1-pentene are higher than those found for toluene, as expected, according to the previous discussion on the improvement of bubble sizes in the presence of polar aldehydes. Equation 8 describes $k_l a$ as a function of P/V for the reaction mixture, with R^2 = 0.972.

$$k_l a\ (1-pentene\ rxn\ mix\ 20\ ℃) = 0.4199 \left(\frac{P}{V_R}\right)^{0.3776} \tag{8}$$

These results confirm our previous assumption that we do not expect $k_l a$ values smaller than 0.1 s^{-1} in the jet-loop reactor during hydroformylation.

2.3.2 Membrane

There are two important considerations when it comes to designing the membrane module. First of all, the flow through the membrane channel must be turbulent to prevent concentration polarization on the membrane surface, which would lead to higher losses of the catalyst. And secondly, the membrane area should be large enough to ensure a good range of product flow rates through the membrane; since this also fixes what residence times can be achieved in the reactor together with the capabilities of the feed pump.

Darvishmanesh et al.[20] reported a permeability (L) of 2.3 L toluene/(h.m^2.bar) for HITK 275 (TiO_2, MWCO=275, 0.9 nm) ceramic membrane. The membrane we use will be Inopor TiO_2 membrane with a molecular weight cut-off of 450 D and 0.9 nm pore size.[21] It can be expected that the permeability will be similar to HITK 275. Considering the difficulty of storing a big amount of reactants and products from a long continuous reaction, we set the upper limit of product rate to 200 ml/h (4.8 L/day). Setting a minimum reaction pressure of 10 bar, the minimum pressure drop across the membrane (ΔP) was set to 8 bar. Equation 9 can now be used to calculate the membrane area (A), which is needed to obtain the desired flow at minimum available trans membrane pressure.

$$Desired\ permeate\ rate = Lx\Delta PxA \tag{9}$$

The membrane area found is 0.011 m^2 , which corresponds to 0.5 m of membrane with a filtration area of 0.026 m^2/1.2 m specified by the supplier.[21]

Fluid flow with a Reynolds number higher than 3000 should be achieved in the membrane channel for turbulent flow. The Re number is the product of density ρ (kg/m^3), fluid velocity u (m/s) and channel inner diameter d_i (m) which is given as 7 mm by the supplier; divided by viscosity μ(N.s/m^2) as given in Equation 10.

$$Re = \frac{\rho . u . d_i}{\mu} \tag{10}$$

Equation 10 allows us to estimate a minimum of 0.29 m/s toluene flow, which corresponds to around 40 L/h flow rate in the membrane tube. The operating point of the pump on the membrane loop is 100-180 L/h which corresponds to Re numbers of 8000-15000.

2.4 Conclusions

A new continuous hydroformylation setup was built; a jet-loop reactor was used since fast two phase reactions can be mass transfer limited and jet-loop reactors are known for their efficiency in dissipation of gas into liquid. Selection of equipment was done carefully to ensure a wide range of operating conditions. The pump used to circulate the reaction mixture was chosen carefully to supply a wide interval of power per unit volume, which affects the rate of mass transfer from gas to liquid. The gas-liquid volumetric mass transfer coefficient $k_l a$ was determined for toluene and a simulated reaction mixture as a function of specific power input. This will enable us to ensure operation in the kinetically controlled regime. The ceramic membrane, which enables withdrawing of the product stream while keeping the catalyst in the system, was chosen at a size to supply the filtration area needed to supply 200 ml/h of product with a differential pressure of 8 bar across the membrane. The maximum temperature and pressure that can be applied in the reactor are 100°C and 100 bar, according to the lowest T_{max}, P_{max} values of all the equipment used in the setup.

2.5 Experimental

2.5.1 Materials

Chemicals were purchased from Aldrich, Merck, Acros or Biosolve and 1-pentene was kindly supplied by Evonik Industries. The substrate solution containing 1-pentene and decane as internal standard was filtered over neutral alumina and degassed. A stock solution of catalyst (Rh precursor: $Rh(acac)(CO)_2$ and Ligand) was prepared in dry and degassed solvent. Solvents were dried and degassed using a custom-made alumina filled Ar flushed column. All air/water sensitive solutions were prepared under argon using Schlenk techniques. The reaction mixture for 1-pentene hydroformylation was prepared by performing a batch reaction in the jet-loop reactor.

2.5.2 Batch gas absorption experiments

The jet loop reactor was filled to the designated level with the solvent/mixture and the liquid was degassed by pressurizing the reactor with syngas to 4.5 bar and running the pumps to saturate the liquid with syngas. After the mixing was stopped, the pressure was released and this cycle was repeated 3 times. Starting from a low initial pressure at which the liquid was saturated by gas, the pressure was increased quite quickly and the pumps started immediately afterwards and a new equilibrium pressure was achieved within seconds. This new point was taken as the starting point of the next measurement and 4-5 measurements were performed between 1-20 bar. The temperature of the liquid was controlled during the measurements and was between ±2°C the set temperature during the experiments. Pressure in the reactor was registered digitally with a frequency of 3 data

points per second. The change in reactor pressure to reach the new equilibrium was fast enough to omit the liquid permeation through the membrane during the measurement and the pressure drop associated.

2.6 References

[1] P. W. N. M. van Leeuwen, C. Claver, *Rhodium Catalyzed Hydroformylation*, Springer, **2002**.
[2] S. S. Luthra, X. Yang, A. G. Livingston, L. M. Freitas dos Santos, L. S. White, *Chem. Commun.* **2001**, 1468–1469.
[3] D. Nair, S. S. Luthra, J. T. Scarpello, L. S. White, L. M. Freitas dos Santos, A. G. Livingston, *Desalination* **2002**, *147*, 301–306.
[4] K. De Smet, S. Aerts, E. Ceulemans, I. F. J. Vankelecom, P. A. Jacobs, *Chem. Commun.* **2001**, 597–598.
[5] D. Nair, J. T. Scarpello, L. S. White, L. M. Freitas dos Santos, I. F. . Vankelecom, A. G. Livingston, *Tetrahedron Lett.* **2001**, *42*, 8219–8222.
[6] "Koch Membrane Systems," can be found under http://www.kochmembrane.com/Membrane-Products.aspx**.**
[7] M. Janssen, J. Wilting, C. Müller, D. Vogt, *Angew. Chem. Int. Ed.* **2010**, *49*, 7738–7741.
[8] J. C. Middleton, K. J. Carpenter, in *Ullmanns Encycl. Ind. Chem.*, Wiley-VCH Verlag GmbH & Co. KGaA, **2000**.
[9] A. P. Boyes, A. Chughtai, X. X. Lu, S. Raymahasay, S. Sarmento, M. W. Tilston, J. M. Winterbottom, *Chem. Eng. Sci.* **1992**, *47*, 3729–3736.
[10] M. Velan, T. K. Ramanujam, *Can. J. Chem. Eng.* **1991**, *69*, 1257–1261.
[11] M. Becker, Der Strahlschlaufenreaktor Als Alternatives Reaktorkonzept Für Homogen Katalysierte Mehrphasenreaktionen Am Beispiel Der Hydroaminomethylierung, Technische Universität Dortmund, **2010**.
[12] A. Behr, M. Becker, J. Dostal, *Chem. Eng. Sci.* **2009**, *64*, 2934–2940.
[13] P. Zehner, A. Ulonska, R. Paciello, *Hydroformylation Process for the Production of Aldehydes And/or Alcohols or Amines*, **2003**, US 6642420.
[14] G. Padmavathi, K. Remananda Rao, *Can. J. Chem. Eng.* **1993**, *71*, 94–100.
[15] M. Velan, T. K. Ramanujam, *Bioprocess Eng.* **1994**, *11*, 101–106.
[16] A. Behr, M. Becker, J. Dostal, D. Kohlmann, *Chem. Ing. Tech.* **2008**, *80*, 1501–1508.
[17] N. N. Dutta, K. V. Raghavan, *Chem. Eng. J.* **1987**, *36*, 111–121.
[18] B. Hu, A. W. Nienow, E. Hugh Stitt, A. W. Pacek, *Chem. Eng. Sci.* **2006**, *61*, 6765–6774.
[19] A. Deimling, B. M. Karandikar, Y. T. Shah, N. L. Carr, *Chem. Eng. J.* **1984**, *29*, 127–140.
[20] S. Darvishmanesh, A. Buekenhoudt, J. Degrève, B. Van der Bruggen, *Sep. Purif. Technol.* **2009**, *70*, 46–52.
[21] "inopor," can be found under http://www.inopor.com/**.**

Chapter 3

Hydroformylation Kinetics of Cyclooctene:

Testing the Jet Loop Reactor with Integrated Nanofiltration

The kinetics of Rh-catalyzed cyclooctene hydroformylation were investigated for the tris(2,4-di-*tert*-butylphenyl) phosphite coordinated rhodium catalyst system. The rate limiting step was found to be the coordination of cyclooctene to the metal center as suggested in literature. The rate equation was derived according to the hydroformylation mechanism and parameters of the rate equation were estimated by nonlinear regression. Experimental data obtained from batch reactions were compared with model predictions and found to be in good agreement. The kinetics were used to plan a continuous hydroformylation run in the newly built reactor setup.

Part of this work is submitted for publication:
Sabriye Güven, Bart Hamers, Robert Franke, Markus Priske, Marc Becker and Dieter Vogt

3.1 Introduction

Hydroformylation is a widely applied reaction in industry, although the separation and reuse of the homogeneous catalyst is a major challenge. Aldehydes are key intermediates in the production of a number of important chemicals such as surfactants, softeners, and fragrances. Thus, despite many available industrial applications, it is still a hot research topic to develop an optimal reaction-separation system/technique that enables recycling of the homogeneous catalyst.

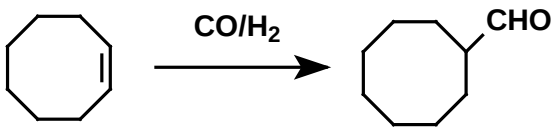

Scheme 1 Cyclooctene hydroformylation

To be able to plan a continuous reaction, the first step is to determine the reaction kinetics based on a plausible reaction mechanism. Rh-catalyzed hydroformylation kinetics have been widely studied since the rate equation and kinetic parameters of each catalyst-substrate system can be unique. The reason is that the rate equation depends on several factors such as properties of the coordinating ligand and the nature of the substrate. Bulky phosphite ligands for instance, are reported to result in very active catalysts. They give reasonable rates even for internal and hindered alkenes, which are not converted at all in the presence of some other catalysts.[1] The kinetics of hydroformylation catalyzed by bulky phosphite modified Rh were investigated for several substrates by van Leeuwen and co-workers. They proposed a reaction mechanism for this catalyst system and derived rate equations for cyclohexene, styrene, and 1-octene.[2]

The mechanism proposed has been widely accepted and used.[3] However, to our knowledge, estimates of kinetic parameters in a mechanistically derived rate equation have not been reported for any substrate for the catalyst in question.

The aim of this chapter is to demonstrate a continuous run in the jet-loop reactor with coupled nanofiltration, which is built combining the experience from recent research about continuous hydroformylation in our group[4,5] and jet-loop reactor technology developed by Behr et al.[6] For this reason we need to derive the rate equation for the hydroformylation of cyclooctene for the Rh-bulky phosphite-modified catalyst (Scheme 2) and estimate the kinetic parameters in the rate equation.

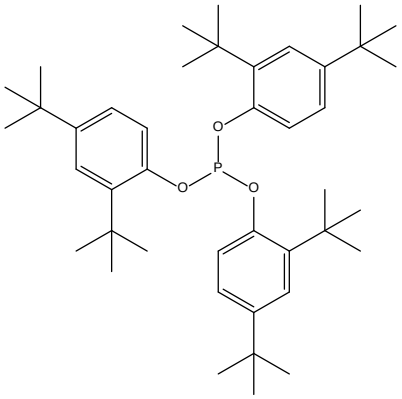

Scheme 2 Structure of the bulky phosphite ligand, tris(2,4-ditert-butylphenyl) phosphite

3.2 Batch Kinetic Experiments

3.2.1 Effect of stirring rate to eliminate mass transfer limitations

In order to ensure that the kinetic experiments are performed in the kinetically controlled regime, hydroformylation reactions at two different stirring rates were performed: 800 and 1200 rpm. The reactions were performed at the highest values of conditions like temperature and catalyst concentration planned in the experimental design. Reaction profiles obtained by plotting gas uptake values versus time were found to be almost identical, as shown in Figure 1, suggesting that already at 800 rpm, there is no gas to liquid mass transfer limitation for the reaction conditions applied. Based on this result, a stirring rate of 1200 rpm was used for all reactions performed.

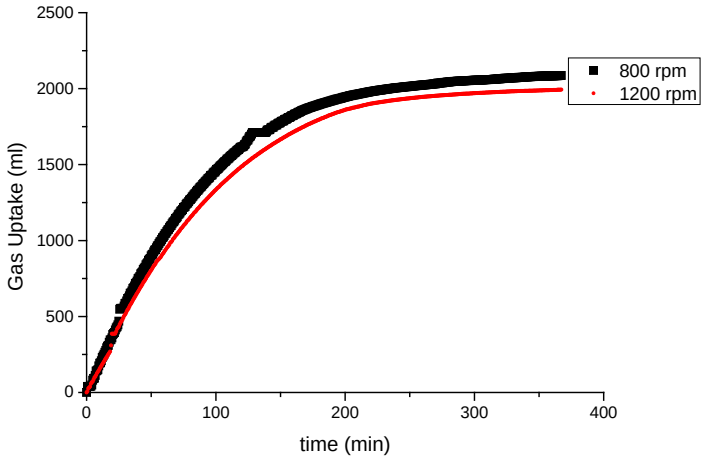

Figure 1 Gas uptake curves for stirring experiments: [cyclooctene] = 2.8 M, [Rh] = 2.9×10^{-4}M, [L] = 8.7×10^{-3} M and 50 vol. % toluene as solvent, under 45 bar syngas pressure (CO/H_2=1), T = 80°C

3.2.2 Mechanism

It is well reported[7,8] that the coordination of very bulky phosphite ligands results in mono-ligated Rh complexes. The mechanism of hydroformylation catalyzed by a mono-ligated Rh bulky phosphite catalyst is reported as given below in Scheme 3.

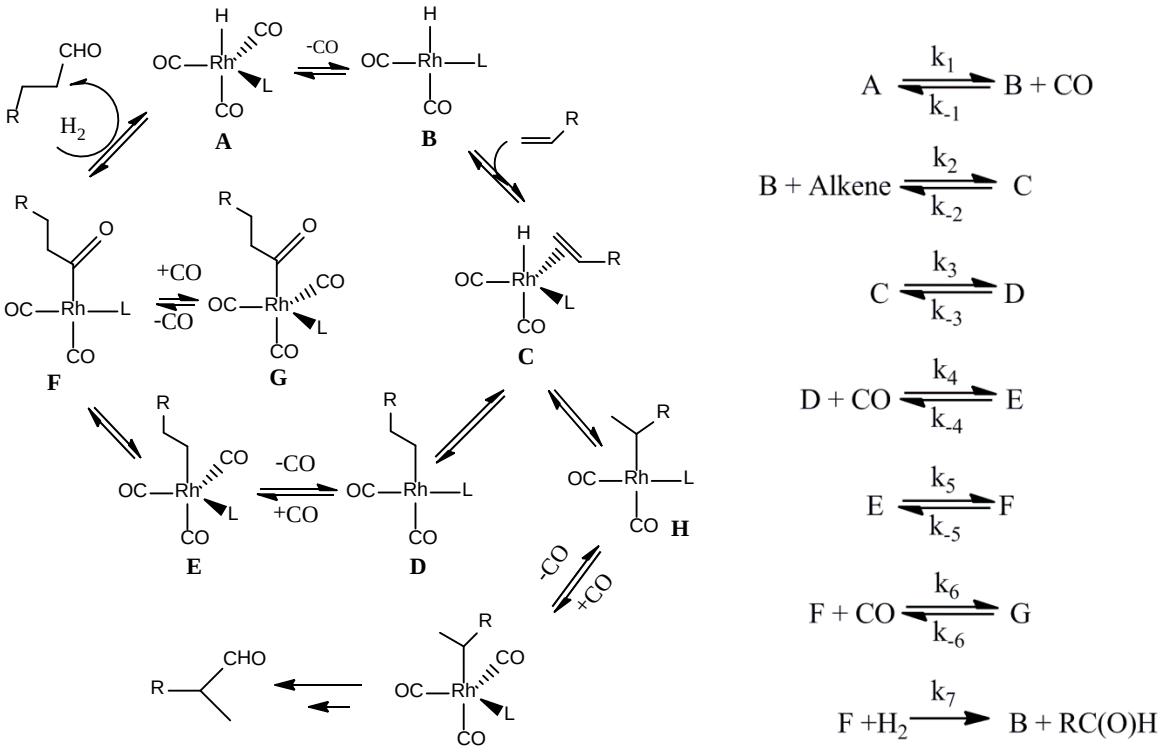

Scheme 3 Mechanism of Rh-catalyzed hydroformylation using bulky monophosphites[2]

A plot of the natural logarithm of cyclooctene concentration normalized to initial cyclooctene concentration; $\ln(C_{Alkene}/C_{Alkene\_0})$ vs time for these preliminary experiments, gives an obvious first order dependence in olefin concentration (Figure 2). This observation is in line with previous reports for the hydroformylation of cyclohexene with a slightly different bulky phosphite modified catalyst.[2]

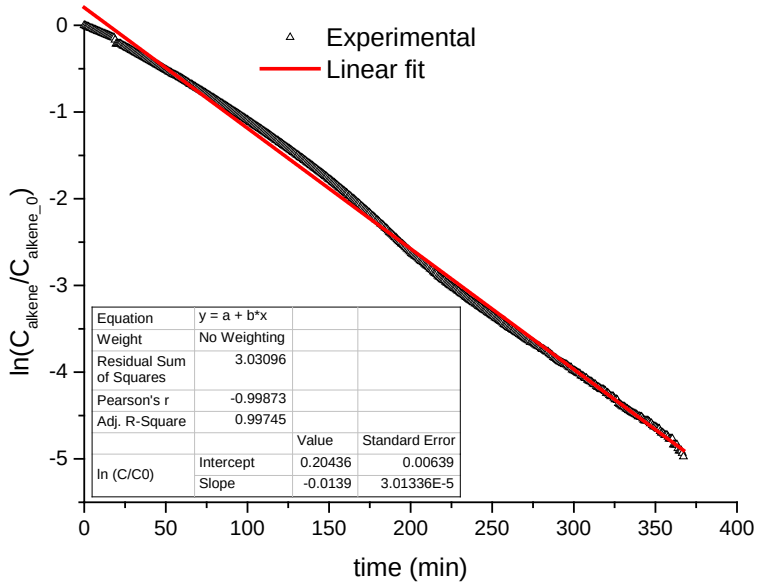

Figure 2 First order plot for the reaction at a stirring rate of 1200 rpm given in Figure 1

It was also shown that upon addition of cyclooctene to the catalyst system tri(o-*t*-butylphenyl) phosphite and Rh, the IR spectrum recorded *in situ* remained unchanged.[8] This suggests that the resting state during the reaction is species **A** and the rate limiting step is the coordination of cyclooctene to the hydrido complex **B**, preceded by a fast CO dissociation pre-equilibrium.[9]

To double-check that the hydrogenolysis step (**F** to **A**) is not rate limiting for this catalyst/substrate system, an experiment was performed where the hydrogen pressure was doubled compared to the stirring experiments presented in Figure 1. The conversion-time profiles of the experiments performed at 22.5 and 45 bar of H_2 (Figure 3) do not suggest any significant dependence of the reaction rate on the hydrogen concentration. The difference in the reaction profiles is probably due to an error in the total amount of cyclooctene added to the autoclaves, as suggested by the difference in the total gas uptake (GU) values. According to the GU values, the experiment performed at 45 bar H_2 has 1.1 times the amount of cyclooctene present for the 22.5 bar H_2 experiment. This difference makes the 45 bar H_2 experiment bit faster, but the reactions end around the same time; as expected for first order reactions. If there was any dependence on the hydrogen, the end time of the reaction would have shifted.

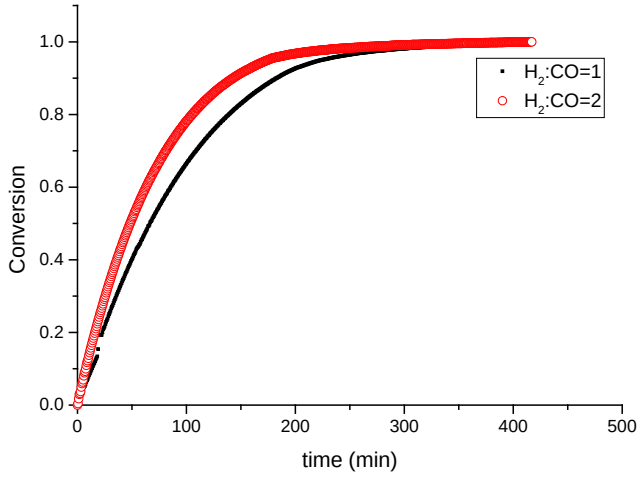

Figure 3 Conversion-time profiles for: [cyclooctene] = 2.8 M, [Rh] = 2.9x10^{-4} M, [L] = 8.7 x10^{-3} M and 50 vol. % toluene as solvent, 22.5 bar CO, 22.5 and 45 bar H_2, respectively, T = 80°C

3.2.3 Rate equation and experimental design

Based on the fact that the coordination of the alkene is the rate limiting step, preceded by a fast equilibrium; the following rate equation is derived, as already reported.[2]

$$r = \frac{k[Rh][alkene]}{1 + [CO]/\mathrm{K}} \quad (1)$$

$$where\ k = Aexp(\frac{-E_A}{RT}) \quad (2)$$

and K being the equilibrium constant for the pre-equilibrium step.

Batch experiments were planned according to a 2^4 central composite design[10] for the variables appearing in the rate equation; namely temperature, carbon monoxide partial pressure, catalyst and cyclooctene concentrations. Experimental conditions were varied according to the parameter levels given in Table 1 in order to estimate the parameters appearing in the rate equation. Hydrogen partial pressure was kept constant at 22.5 bar and a ligand/Rh ratio of 30 was used since a high molar excess is needed to ensure coordination of a ligand to each Rh center.[8]

Table 1 Variables and levels used for the 2^4 Central Composite Design

Variable	Level	Value	Variable	Level	Value
T (°C)	-2	60	P_{CO} (bar)	-2	15.00
	-1	65		-1	17.50
	0	70		0	20.00
	1	75		1	22.50
	2	80		2	25.00
$[cyclooctene]_0$ (M)	-2	2.24	[Rh] (M)	-2	$1.80x10^{-4}$
	-1	2.52		-1	$2.25x10^{-4}$
	0	2.80		0	$2.70x10^{-4}$
	1	3.08		1	$3.15x10^{-4}$
	2	3.35		2	$3.60x10^{-4}$

The experiments performed according to the experimental design and the rate of reaction observed at the first minute of reaction for each experiment are listed in Table 2 along with the turn over frequencies. Comparing the rates and Rh concentrations of entries 2 and 9; 3 and 6; 4 and 8; 5 and 7; 10, 11, 18, 19, 20, 21 and 17; 22 and 29; 23 and 28; 24 and 27; and 25 and 26 confirms that the reaction is first order in Rh concentration. The dependence in CO is not so strong and is harder to determine since it appears as (1+CO/K). Comparing entries 2 and 3, 4 and 5, 6 and 9, 7 and 8, 22 and 28, 23 and 29, 24 and 25, 26 and 27; it is not possible to deduce a clear influence of the CO concentration on the reaction rate.

Table 2 Kinetic experiments performed for parameter estimation

Entry	T (°C)	$[C.octene]_0$ (M)	P_{CO} (bar)	P_{H2} (bar)	[Rh] $x10^4$ (M)	Alkene / Rh	TOF @ 1st min (h^{-1})	Rate*100 @ 1st min (M/min)	[CO] (M)
1	60	2.76	20.0	22.5	2.70	10 236	1133	1.41	0.15
2	65	2.55	22.5	22.5	2.25	11 333	1413	1.35	0.18
3	65	2.52	17.5	22.5	2.25	11 200	1227	1.16	0.14
4	65	3.08	17.5	22.5	3.15	9 778	1219	1.96	0.14
5	65	3.04	22.5	22.5	3.15	9 651	1314	2.09	0.18
6	65	2.52	17.5	22.5	3.15	8 000	1257	1.66	0.14
7	65	3.11	22.5	22.5	2.25	13 822	1413	1.64	0.18
8	65	3.08	17.5	22.5	2.25	13 689	1280	1.47	0.14
9	65	2.49	22.5	22.5	3.15	7 905	1333	1.74	0.18
10	70	2.83	20.0	22.5	2.70	10 481	1600	2.03	0.16
11	70	2.80	20.0	22.5	2.70	10 370	1600	2.01	0.16
12	70	2.21	20.0	22.5	2.70	8 185	1422	1.41	0.16
13	70	3.32	20.0	22.5	2.70	12 296	1622	2.41	0.16
14	70	2.52	15.0	22.5	2.70	9 333	1733	1.96	0.12
15	70	2.80	23.8	23.8	2.70	10 370	1578	1.98	0.19
16	70	2.83	21.3	21.3	1.80	15 722	1800	1.52	0.17
17	70	2.80	20.0	22.5	3.60	7 778	1550	2.59	0.16
18	70	2.80	20.0	22.5	2.70	10 370	1533	1.93	0.16
19	70	2.80	20.0	22.5	2.70	10 370	1178	1.48	0.16
20	70	2.80	20.0	22.5	2.70	10 370	1578	1.98	0.16
21	70	2.76	20.0	22.5	2.70	10 222	1622	2.01	0.16
22	75	3.08	17.5	22.5	2.25	13 689	1947	2.24	0.14
23	75	3.08	22.5	22.5	3.15	9 778	1924	3.10	0.18
24	75	2.49	17.5	22.5	3.15	7 905	1981	2.58	0.14
25	75	2.55	22.5	22.5	3.15	8 095	1829	2.44	0.18
26	75	2.52	22.5	22.5	2.25	11 200	1973	1.86	0.18
27	75	2.49	17.5	22.5	2.25	11 067	1733	1.61	0.14
28	75	3.11	22.5	22.5	2.25	13 822	1973	2.29	0.18
29	75	3.11	17.5	22.5	3.15	9 873	2000	3.25	0.14
30	80	2.76	20.0	22.5	2.70	10 222	2422	2.99	0.17

3.2.4 Hydrogen and carbon monoxide concentrations in solution

The equilibrium concentration of carbon monoxide in toluene was calculated using a method presented in the literature, based on the theory of regular solution.[11] The mole fraction of dissolved CO in the reaction mixture (x_{co}) at 1 atm is estimated using Equation 3. The reaction mixture is assumed to be represented well by pure toluene for this calculation. Henry's law is used to calculate the CO concentration at reaction pressure.

$$\frac{1}{x_{CO}} = \frac{f_{CO}^{l}}{f_{CO}^{G}} \exp\left(\frac{\emptyset_{toluene}^{2}\vartheta_{CO}^{L}\left(\delta_{toluene}^{2} + \delta_{CO}^{2} - 2\delta_{CO}(\delta_{toluene}^{2} + \Delta_{toluene})^{1/2}\right)}{RT}\right) \quad (3)$$

Liquid and gas phase fugacities of CO; $f_{CO}^{l} and\ f_{CO}^{G}$ can be estimated using Equations 4 and 5, which are adopted from literature:[12]

$$f_{CO}^{l} = \exp(4.7475 + 588.52\mathrm{T}^{-1} - 1.3151\mathrm{x}10^{5}\mathrm{T}^{-2}) \quad (4)$$

$$f_{CO}^{G} = \exp\left[\frac{\mathrm{P_r}}{\mathrm{T_r}}\left(0.083 - \frac{0.422}{\mathrm{T_r}^{1.6}} + \omega(0.139 - \frac{0.172}{\mathrm{T_r}^{4.2}})\right)\right] 1.01325\ \mathrm{bar} \quad (5)$$

The solubility parameter for toluene, $\delta_{\mathrm{toluene}}$ can be estimated using Equation 6 given below[13] using vaporization enthalpy $\Delta\mathrm{H}_{\mathrm{toluene}}^{\mathrm{vap}}$ and molar volume $\vartheta_{\mathrm{toluene}}$ values reported in Table 3.

$$\delta_{\mathrm{toluene}} = \left(\Delta\mathrm{H}_{\mathrm{toluene}}^{\mathrm{vap}}/\vartheta_{\mathrm{toluene}}\right)^{1/2}\mathrm{J}^{0.5}\mathrm{m}^{-1.5} \quad (6)$$

The volume fraction of the solvent, Φ_{toluene} can be assumed as unity since the gases are sparingly soluble in the solvent. The values of the constants used in calculating these equations are listed in Table 3.

Table 3 Parameters for Regular Solution Theory

Parameter (Unit)	Value
$\vartheta_{\mathrm{toluene}}$ ($\mathrm{m^3mol^{-1}}$)	$1.06\mathrm{x}10^{-4}$
$\Delta_{\mathrm{toluene}}$ ($\mathrm{J.m^3}$) [13]	$7.49\mathrm{x}10^{6}$
$\Delta\mathrm{H}_{\mathrm{toluene}}^{\mathrm{vap}}$($\mathrm{J.mol^{-1}}$) [14]	38100
ϑ_{CO}($\mathrm{m^3mol^{-1}}$) [12]	$3.21\mathrm{x}10^{-5}$
δ_{CO}($\mathrm{J^{0.5}m^{-1.5}}$) [12]	$6.403\mathrm{x}10^{3}$
ω_{CO}	0.048
$\mathrm{T_{c\_CO}}$ (K)	132.9
$\mathrm{P_{c\_CO}}$ (bar)	34.99

The concentration of CO calculated according to the method explained here is given in Table 2 for all the kinetic experiments performed.

3.2.5 Estimation of rate equation parameters

Parameters in Equation 1 were estimated using a MATLAB script, developed according to the algorithm reported by A. Koeken et al.[15] The batch reactor design equation was numerically integrated to estimate the concentration as a function of time using the proposed rate equation

(Equation 7) and concentration data were used to calculate the rate. A built-in MATLAB function minimizes the difference between experimental and estimated rate values by finding the optimal values of the rate equation parameters A, E_A and K. These parameters and their 95% confidence intervals estimated are given in Table 4.

$$-\frac{dC_{cyclooctene}}{dt} = \frac{Aexp\left(\frac{-E_A}{RT}\right)[Rh][alkene]}{1+[CO]/\mathrm{K}} \quad (7)$$

Table 4 Parameter Estimates for Rate Equation (Equation 1) and 95% Confidence Intervals

Parameter	Estimated value	95% Lower	95% Upper
A ($L.min^{-1}.mol^{-1}$)	$2.09x10^8$	$1.27x10^8$	$2.91x10^8$
E_A (kJ/mol)	44.0	42.8	45.1
K (mol/L)	0.31	0.25	0.38

Figure 4 shows the parity plot comparing experimental rate data obtained from the kinetic batch experiments and rates estimated for these experiments according to the kinetic model; the values predicted by the model agree with the experimental data.

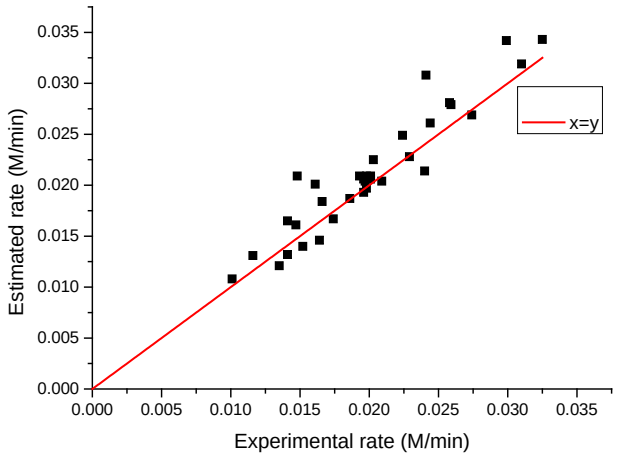

Figure 4 Parity plot for estimated vs. experimental reaction rates at the first minute of reaction

3.3 Continuous Reaction

A continuous hydroformylation experiment was planned using the kinetic data obtained from batch experiments. Full conversion at steady state was avoided since it might lead to idle catalyst molecules which are more prone to deactivation and it is also not possible to judge when deactivation/leaching starts in the case of full conversion. Figure 5 shows the conversion-time

profile of the continuous run together with the estimated reaction profile and 95% confidence intervals. Time dependent concentration data for the estimated reaction profile was obtained by integrating the CSTR design equation given below in Equation 8 with the initial condition that concentration in the reactor at time=0 is $C_{cyclooctene,0}$ and replacing $r_{cyclooctene}$ with Equation 1.

$$\frac{dC_{cyclooctene}}{dt} = \frac{1}{\tau}\left(C_{cyclooctene,f} - C_{cyclooctene}\right) - r_{cyclooctene} \tag{8}$$

Concentration as a function of time can then be expressed as given in Equation 9 below:

$$C_{cyclooctene}(t) = C_{cyclooctene,0}\exp\left(-\left(\frac{1}{\tau}+\epsilon\right)t\right) + \frac{C_{cyclooctene,f}}{1+k\tau}\left(1-\exp\left(-\left(\frac{1}{\tau}+\epsilon\right)t\right)\right) \tag{9}$$

where

$$\epsilon = \frac{Aexp(\frac{-E_A}{RT})[Rh]}{1+[CO]/\mathrm{K}} \tag{10}$$

calculated for given conditions using the parameter estimates reported in Table 4.

The reaction was stopped after 47 hours (~5 residence times) and a total turnover number (TTON) of 44 300 was achieved. The TTON can of course be improved by using a higher reaction temperature or by simply extending the reaction time. The kinetic model predicts the steady state behavior of the reactor well. Once the steady state conversion was reached, it stayed constant for about 4 residence times, at which the experiment was stopped. This suggests that the catalyst (MW = 835 g/mol) is retained reasonably well by the membrane (MW cut-off of 450 D) and that catalyst deactivation is not of major concern at this stage; ICP analysis of the product collected in the first 7.3 hours (0.9 residence times) confirmed that 98.75% of the initial rhodium content and 99.59% of the phosphorus content was retained.

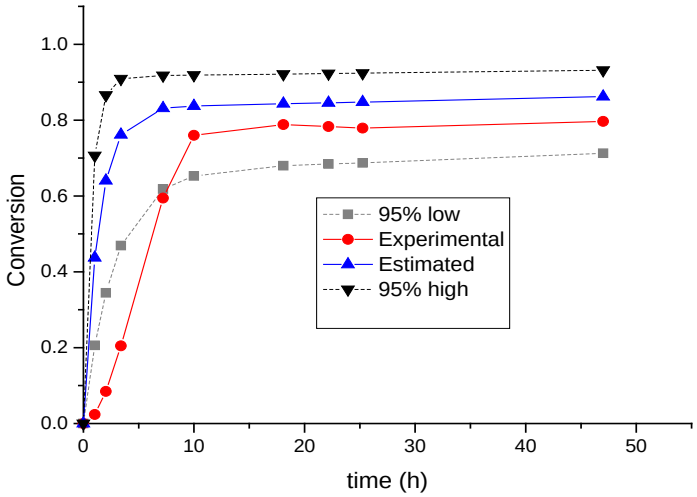

Figure 5 Continuous hydroformylation reaction performed with nanofiltration jet-loop reactor. [cyclooctene] = 1.34 M, [Rh] = 2.0×10^{-4} M, [L] = 5.9×10^{-3} M, p = 20 bar $CO:H_2$ (1:1), T = 80°C, $\tau \approx 9.3$ h

Although the steady state conversion is predicted quite well; the experimental conversion in the beginning is lower than the estimated. A partial explanation can be that gas bubbles formed in the beginning of the reaction are bigger than the ones that are formed later on when there is aldehyde in the reaction mixture, since the presence of aldehyde (acting as a surfactant-like agent) prevents coalescence, as explained in Chapter 2. Smaller bubbles supply a higher interfacial surface area for gas to liquid mass transfer which can be limiting in the beginning of the reaction. This explanation, however, would be valid for the lower conversion ranges since a small amount of aldehyde is enough to obtain small bubbles.

The residence time changed gradually over time from 8.2 h^{-1} in the beginning to 10.4 h^{-1} at the end of the reaction. This trend in residence time is taken into account for the estimated conversion profile.

3.4 Conclusions

Cyclooctene was used as the model substrate to test the constructed jet-loop reactor with integrated membrane nanofiltration. A rate equation was derived to express the kinetics of cyclooctene hydroformylation for the Rh/tris(2,4-di-tert-butylphenyl) phosphite system, according to the reaction mechanism. It was shown that the reaction is first order in cyclooctene with an activation energy of 44±1.2 kJ/mol. Although the bulky-phosphite catalyst system is known to be a very active catalyst, the highest turnover frequency obtained for the conditions in this work is around 2500 h^{-1}. The reason behind low reaction rates is the steric bulk of cyclooctene, which hampers

coordination of the molecule to the metal center. Parameter estimates for the rate model were determined within narrow confidence intervals and allows a good prediction and interpretation of continuous reaction data.

A continuous hydroformylation run was successfully performed in the developed reaction setup, giving a total turnover number of 44 300 in a total reaction time of 47 hours, which corresponds to 5 residence times. Steady state conversion was reached after about one residence time and remained constant till the experiment was stopped. This result is important since it is achieved with a commercially available ligand without any further MW enlargement or immobilization on a support and can be improved by applying higher reaction temperatures or simply by running the reaction longer.

3.5 Experimental

3.5.1 Materials

Chemicals were purchased from Aldrich, Merck, Acros or Biosolve. All air/water sensitive solutions were prepared under argon using Schlenk techniques. The substrate solution containing cyclooctene and decane as internal standard was filtered over neutral alumina and degassed. A stock solution of catalyst (Rh precursor: $Rh(acac)(CO)_2$ and Ligand) was prepared in dry and degassed solvent. Solvents were dried and degassed using a custom-made alumina-filled Ar-flushed column.

3.5.2 Batch reactions

Batch reactions were performed in custom built high pressure stainless steel autoclaves (100 ml) equipped with a mechanical gas-impeller stirrer and a mass flow controller (MFC) to monitor the gas uptake. Conversion was measured on a Shimadzu GC-2010 gas chromatograph (GC) using an Agilent DB1 column (30m x0.32mm i.d.) at the end of the reaction time to normalize the values obtained from gas uptake data.

The substrate solution was filled into a dropping funnel (30 ml) and the catalyst solution was charged in the autoclave where it was preformed under reaction conditions for an hour, after which the reaction was started by adding the substrate solution.

3.5.3 Continuous reaction in jet loop reactor and nanofiltration setup

For hydroformylation, the reaction start-up was performed as follows: The reactor was purged with syngas pressure before the reactor was filled with substrate solution under argon flow to the designated level by the HPLC pump. The catalyst solution was added into the dropping funnel,

which is connected to the reactor by a valve, under argon. It is possible to preform the catalyst in this heated compartment under pressure. The reactor was heated and pressurized to the reaction conditions and after the flux through the membrane reached steady state, preformed catalyst solution was added to start the reaction. A mass flow controller kept the reaction pressure constant and the gas uptake was monitored to confirm conversion values obtained by GC sampling.

3.6 References

[1] P. W. N. M. van Leeuwen, C. F. Roobeek, *J. Organomet. Chem.* **1983**, *258*, 343–350.
[2] A. van Rooy, E. N. Orij, P. C. J. Kamer, P. W. N. M. van Leeuwen, *Organometallics* **1995**, *14*, 34–43.
[3] K.-D. Wiese, D. Obst, in *Catal. Carbonylation React.* (Ed.: M. Beller), Springer Berlin Heidelberg, **2006**, pp. 1–33.
[4] M. Janssen, C. Müller, D. Vogt, *Dalton Trans.* **2010**, *39*, 8403.
[5] M. Janssen, J. Wilting, C. Müller, D. Vogt, *Angew. Chem. Int. Ed.* **2010**, *49*, 7738–7741.
[6] A. Behr, M. Becker, J. Dostal, D. Kohlmann, *Chem. Ing. Tech.* **2008**, *80*, 1501–1508.
[7] C. Kubis, R. Ludwig, M. Sawall, K. Neymeyr, A. Börner, K.-D. Wiese, D. Hess, R. Franke, D. Selent, *ChemCatChem* **2010**, *2*, 287–295.
[8] T. Jongsma, G. Challa, P. W. N. . van Leeuwen, *J. Organomet. Chem.* **1991**, *421*, 121–128.
[9] A. van Rooy, E. N. Orij, P. C. J. Kamer, F. van den Aardweg, P. W. N. M. van Leeuwen, *J. Chem. Soc. Chem. Commun.* **1991**, 1096–1097.
[10] G. E. P. Box, J. S. Hunter, W. G. Hunter, *Statistics for Experimenters: Design, Innovation, and Discovery*, Wiley-Interscience, **2005**.
[11] J. H. Hildebrand, *Solubility of Non-electrolytes*, Reinhold Pub. Corp., **1936**.
[12] U. J. Jáuregui-Haza, E. J. Pardillo-Fontdevila, A. M. Wilhelm, H. Delmas, *Lat. Am. Appl. Res.* **2004**, *34*, 71–74.
[13] L. C. Yen, J. J. McKetta, *Aiche J.* **1962**, *8*, 501–507.
[14] M. V. Roux, M. Temprado, J. S. Chickos, Y. Nagano, *J. Phys. Chem. Ref. Data* **2008**, *37*, 1855.
[15] A. C. J. Koeken, L. J. P. van den Broeke, B.-J. Deelman, J. T. F. Keurentjes, *J. Mol. Catal. Chem.* **2011**, *346*, 1–11.

Chapter 4

Kinetics as a Tool in Understanding the Regioselectivity of Neohexene Hydroformylation

The kinetics of neohexene hydroformylation were investigated for a Rh catalyst modified with bulky monodentate tris(2,4-di-*tert*-butylphenyl) phosphite, based on the mechanism reported for mono-ligated Rh-catalyzed hydroformylation. The rate limiting step was shown to be the hydrogenolysis of the Rh-acyl intermediate for both the linear and the branched aldehydes. Rate equations for both aldehydes were derived and the kinetic parameters were estimated. To elucidate the increased aldehyde linearity at higher temperature, deuterioformylation experiments were performed. At 100°C the linear Rh-alkyl formation was found to be more reversible than the branched one. The ratio of linear to branched Rh-acyl species was determined using *in situ* High Pressure (HP) IR experiments in order to quantify the difference in activation energies of the hydrogenolysis steps towards the isomeric aldehydes.

Part of this work is submitted for publication:
Sabriye Güven, Marko M. L. Nieuwenhuizen, Bart Hamers, Robert Franke, Markus Priske, Marc Becker, and Dieter Vogt

4.1 Introduction

The hydroformylation of alkenes, discovered in 1938 by Otto Roelen, is widely applied in industry and has been studied extensively.[1] Rhodium and cobalt are used as catalyst metal and a great variety of phosphorus ligands is available to tune the activity and selectivity of the homogeneous catalyst. The influence of ligands on the catalyst arising from their steric and electronic properties enables a good prediction of the activity and selectivity of a catalyst system. Bulky, monodentate π-acceptor ligands give rise to extremely active but less selective catalysts, while chelating ligands possessing a large bite angle result in very high selectivity towards the linear aldehyde.[2] However, knowledge about the catalyst itself alone is not enough; different elementary steps in the mechanism can become rate limiting for different substrates, even for isomers, depending on the position of the double bond in the molecule.[3]

Regioselectivity in the Rh-catalyzed hydroformylation is a widely studied subject[4–7] since normally only one of the product aldehydes (usually linear) is the desired product and optimization of selectivity has great industrial relevance. The Rh-alkyl formation step in the reaction mechanism is generally accepted to be the step that determines the regioselectivity, especially at low temperatures where Rh-alkyl formation is not reversible.[4] With increasing temperature, the linear aldehyde has been shown to be favored over the branched one, commonly attributed to increased reversibility of the branched Rh-alkyl.[2,8,9] However, for styrene hydroformylation, a detailed *in situ* kinetic study on the rate limiting Rh-acyl hydrogenolysis step showed a difference in energetics for the linear and branched isomers. The role of these different energetics in determining the regioselectivity should be considered.[5] The latest studies agree that hydroformylation regioselectivity is governed by a combination of different steps in the mechanism depending on reaction conditions, catalytic system, and substrate.[6,10]

The kinetics of neohexene hydroformylation (Scheme 1) has been investigated for the tris(2-*tert*-butyl-4-methylphenyl) phosphite modified rhodium catalyst by van Rooy et al.[11] The reaction rate was found to be first order in alkene concentration and hence alkene coordination was proposed as the rate limiting step. Under the conditions applied, these authors did not observe the branched product and drew the conclusion that the steric bulk of the substrate, which hampers the coordination of the alkene, also prevented its coordination in the branched fashion.

Under the same conditions used by van Rooy et al., using the bulky tris(2,4-di-*tert*-butylphenyl) phosphite rhodium catalyst, Selent et al.[12] observed 5% branched aldehyde in the product. Both aldehydes followed pseudo first order kinetics: a constant reaction rate in the beginning of the

reaction followed by a first order alkene dependence at higher conversions. The authors revealed the reformation of Rh-hydride species together with Rh-acyl species as observable intermediates during the reaction using *in situ* IR. According to these researchers, the rate limiting step is the hydrogenolysis of the Rh-acyl species over the whole course of the reaction. The authors also observed an increase in the amount of branched aldehyde produced with decreasing temperature and proposed that it might arise from the difference in activation energies of the hydrogenolysis steps of the isomeric aldehydes.

We investigated the kinetics of neohexene hydroformylation for the tris(2,4-di-*tert*-butylphenyl) phosphite rhodium catalyst and the reason behind the temperature dependence of the regioselectivity using the kinetic information.

4.2 Kinetics

Aldehydes produced by neohexene hydroformylation are 4,4-dimethylpentanal and 2,3,3-trimethylbutanal as shown in Scheme 1, which will be called linear and branched aldehyde respectively from here on.

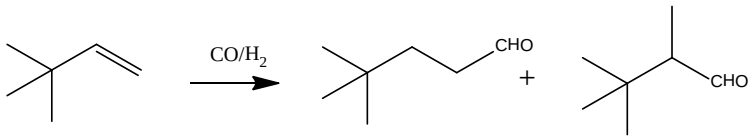

Scheme 1 Neohexene Hydroformylation

Bulky phosphites are reported to give mono-coordinated active Rh species.[12–14] The hydroformylation mechanism proposed for bulky phosphite ligated Rh catalysts is given in Scheme 2.[3]

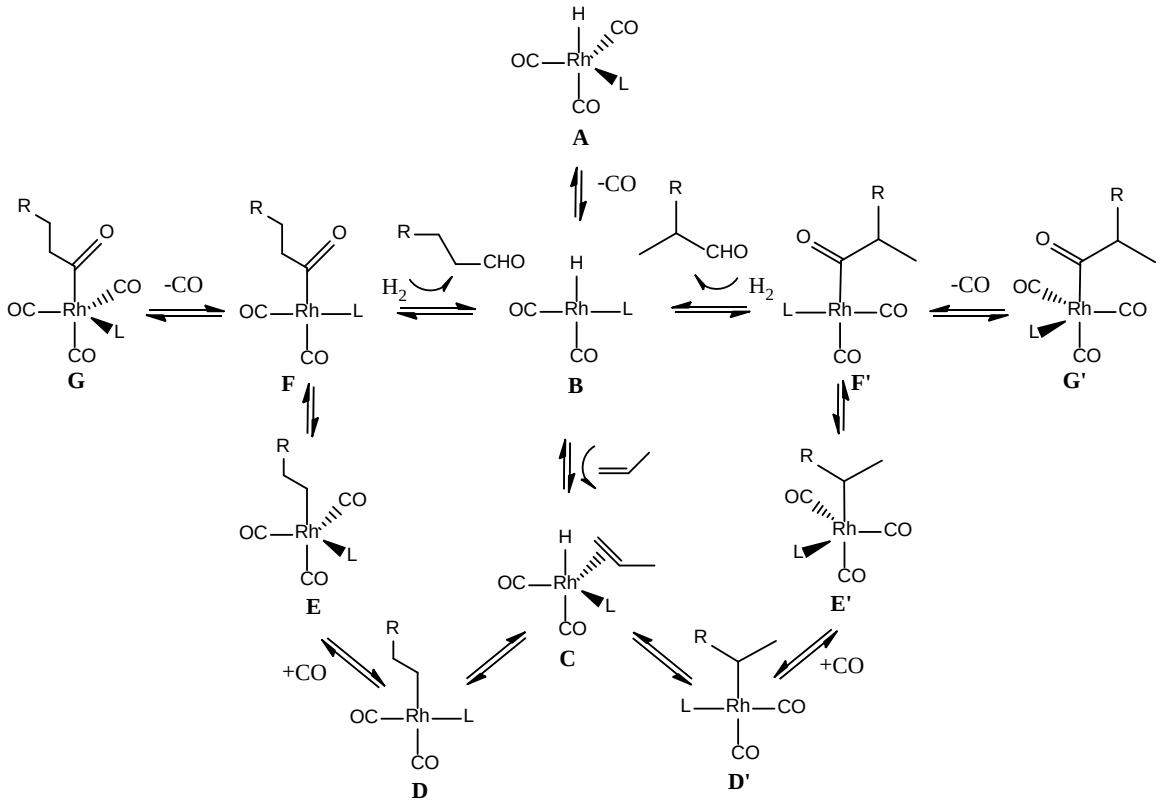

Scheme 2 Mechanism of Rh-catalyzed hydroformylation using bulky monophosphites[3]

To check the assumption that hydrogenolysis really is the rate limiting step for both aldehydes, two reactions were performed at 80˚C, 20 bar CO, 20 and 40 bar H_2, respectively. The linear to branched aldehyde ratio would change, since one product would be formed faster, if one of the aldehydes had a different rate limiting step. The reaction profiles obtained by logged gas uptake data confirmed that hydrogenolysis is the rate limiting step (Figure 1) and the experiments gave the same linear to branched aldehyde ratio of 18.5, confirming hydrogenolysis as the common rate limiting step.

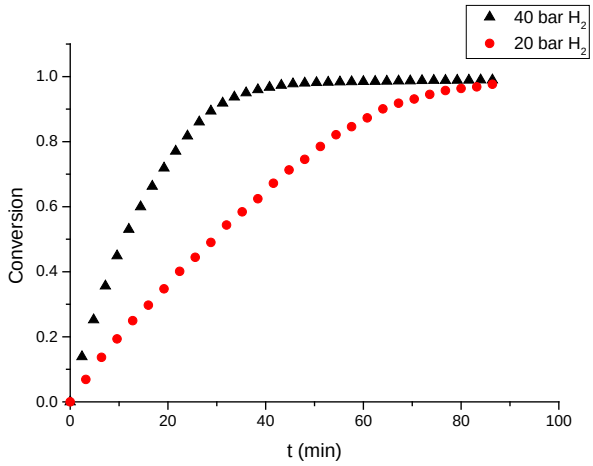

Figure 1 Reaction profiles for hydroformylation reactions performed under 40 bar and 20 bar H_2 , other conditions were kept same: [neohexene] = 2.2 M, [Rh] =1.12x10^{-4} M, L/Rh=30, CO =20 bar, 80˚C

Moreover, monitoring the reaction profile by sampling gave very similar profiles for both aldehydes as shown in Figure 2.

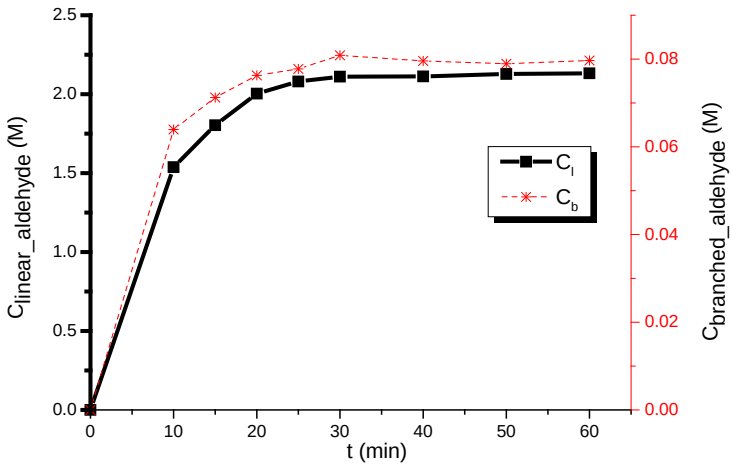

Figure 2 Hydroformylation reaction showing reaction profiles for both linear and branched aldehydes. Reaction conditions: [neohexene] = 2.2 M, [Rh] =1.2x10^{-4} M, L/Rh=30, 40 bar syngas CO/H_2=1, 80˚C

Both the experiment with doubled hydrogen pressure and the sampling experiment confirm that hydrogenolysis is the common rate limiting step for both aldehydes. According to these results and the findings in literature,[12] rate equations for linear and branched aldehydes were derived (Equations 1 and 2), assuming that the hydrogenolysis step is rate limiting in the mechanism given in Scheme 2 for both aldehydes. Detailed derivation of these equations are given in the Appendix.

$$r_l = \frac{k_{FA}K_{AB}K_{BC}K_{CF}[Rh][Alkene][H_2]}{1 + K_{AB}K_{BC}(K_{CF}K_{FG} + K'_{CF}K'_{FG})[Alkene][CO]} \quad (1)$$

$$r_b = \frac{k'_{FA}K_{AB}K_{BC}K'_{CF}[Rh][Alkene][H_2]}{1 + K_{AB}K_{BC}(K_{CF}K_{FG} + K'_{CF}K'_{FG})[Alkene][CO]} \quad (2)$$

where k stands for the rate constant and K for the equilibrium constant of the step specified by the subscript. These equations can be simplified as given in Equations 3 and 4 below by lumping equilibrium constants together;

$$r_l = \frac{k_l[Rh][Alkene][H_2]}{1 + K[Alkene][CO]} \quad (3)$$

$$r_b = \frac{k_b[Rh][Alkene][H_2]}{1 + K[Alkene][CO]} \quad (4)$$

$k_l = A_l \exp\left(-\Delta E_l^A / RT\right)$ and $k_b = A_b \exp\left(-\Delta E_b^A / RT\right)$ are Arrhenius type rate constants with frequency factors A_l and A_b for linear and branched aldehydes, respectively, where ΔE_l^A and ΔE_b^A stand for the activation energies, R for the universal gas constant and T for the temperature.

Batch hydroformylation experiments were performed to determine the parameters in the rate equations: frequency factors, activation energies and the equilibrium constant K. Reaction variables appearing in the rate equation; Rh and alkene concentrations, H_2 and CO pressures and reaction temperature were varied as given in Table 1. The l/b ratios as well as the times to reach 10, 30, 50 and 70% conversion are reported in Table 1.

Table 1 Reaction conditions, obtained l/b values and reaction times at 10, 30, 50 and 70% conversion for batch experiments performed in the kinetic study

Entry	T(K)	$[alkene]_0$ (M)	$[Rh]x10^4$ (M)	P_{H2} (bar)	P_{CO} (bar)	[L/Rh]	l/b	t (min) @ x=0.1	t (min) @ x=0.3	t (min) @ x=0.5	t (min) @ x=0.7
1	334	1.25	1.77	25.7	14.3	30.0	6.0	5.48	17.53	29.73	43.97
2	333	2.01	1.77	22.8	17.2	22.5	5.5	6.63	21.85	37.82	55.40
3	344	1.35	1.18	25.4	19.6	30.0	9.4	3.87	12.05	21.43	33.50
4	344	2.88	2.36	20.4	14.6	15.0	11.5	3.08	12.42	23.32	35.55
5	344	2.82	2.36	25.4	19.6	22.5	10.9	2.15	8.18	15.78	24.52
6	344	1.35	2.36	25.9	14.1	22.5	13.1	1.08	3.52	6.48	11.07
7	344	2.82	1.18	20.0	20.0	22.5	12.2	7.28	25.28	44.65	64.62
8	343	2.88	1.18	23.1	14.4	22.5	11.4	4.05	16.20	29.42	44.95
9	354	2.13	1.77	26.0	14.0	15.0	15.4	1.25	4.75	8.17	12.92
10	354	1.39	1.77	25.5	19.5	30.0	12.1	1.13	3.60	7.55	12.22
11	353	2.50	1.12	20.0	20.0	30.0	18.5	3.20	16.00	28.80	41.60
12	353	1.95	1.12	42.0	18.0	30.0	18.5	1.73	4.80	9.60	16.80
13	353	2.21	1.12	24.1	25.9	30.0	15.0	7.07	25.77	46.95	71.53
14	354	2.28	1.12	24.1	35.9	30.0	14.3	8.10	27.97	50.33	75.07
15	354	2.17	1.12	24.1	35.9	30.0	14.0	5.58	19.28	35.17	53.13
16	353	2.03	1.77	23.0	17.0	22.5	15.7	1.50	4.50	7.80	12.28
17	353	2.37	1.77	23.0	17.0	22.5	16.1	1.73	5.65	11.30	19.57
18	353	2.21	1.77	22.5	22.5	22.5	14.9	1.37	5.17	9.27	14.20
19	353	1.58	0.59	23.0	17.0	22.5	15.7	4.25	14.88	25.70	37.93
20	353	2.03	2.95	23.0	17.0	22.5	15.1	0.88	2.12	4.25	6.73
21	353	2.03	1.77	23.0	17.0	22.5	16.3	1.00	3.30	5.88	9.60
22	353	2.03	1.77	23.0	17.0	22.5	12.6	1.28	4.62	8.20	13.85
23	354	2.03	1.19	20.0	20.0	30.0	10.7	2.90	9.83	18.10	27.60
24	353	2.23	2.36	21.0	9.0	15.0	10.7	0.75	1.97	4.17	7.02
25	353	1.80	2.36	42.0	18.0	15.0	14.0	0.83	2.22	4.23	7.08
26	363	2.87	1.18	26.2	13.8	22.5	24.3	0.95	2.87	5.98	9.95
27	363	2.93	2.36	20.0	20.0	30.0	15.8	1.00	3.03	6.05	10.07
28	363	1.16	2.36	20.6	14.4	30.0	14.1	0.89	2.01	2.63	4.03
29	363	1.35	2.36	25.6	19.4	22.5	19.8	0.47	1.32	2.27	3.12
30	363	1.35	1.18	20.0	20.0	15.0	22.1	1.35	3.57	6.68	10.03
31	363	2.86	1.18	26.2	13.8	30.0	22.1	1.23	4.63	9.27	14.83
32	363	1.21	1.18	23.4	14.1	22.5	15.1	0.67	1.83	3.17	5.32
33	363	2.41	1.18	22.8	19.7	22.5	13.0	1.95	5.85	11.22	18.53

Nonlinear regression analysis was performed using a MATLAB routine which minimizes the difference between experimental and estimated concentrations and l/b values at times given in Table 1, by changing the values of the parameters in the rate equations, i.e. A_l, A_b , ΔE_l^A, ΔE_b^A and

K. The optimum values of the parameter estimates are presented below in Table 2 with their 95% confidence intervals:

Table 2 Parameter estimates for rate equations of linear and branched aldehydes (Equations 3 and 4)

Parameter	Estimated value
A_l ($M^{-2}min^{-1}$)	(1.45±0.66) x10^{17}
ΔE_l^A (kJ/mol)	85.54±1.86
A_b ($M^{-2}min^{-1}$)	(5.83±0.90) x10^{11}
ΔE_b^A (kJ/mol)	56.87±0.31
K (M^{-2})	40.00±1.05

4.2.1 Gas solubilities in the reaction mixture

The solubility of carbon monoxide and hydrogen in toluene required for the kinetic calculations was calculated as explained before in Chapter 3 for carbon monoxide, according to the method presented in the literature based on the theory of regular solution.[15] Equation 5 was used to estimate the mole fraction of dissolved gas in the reaction mixture (x_{co} and x_{H2}), which was assumed to be represented well by pure toluene for this calculation at 1 atm.

$$\frac{1}{x_g} = \frac{f_g^l}{f_g^G} \exp\left(\frac{\emptyset_{solvent}^2 \vartheta_g^L \left(\delta_{solvent}^2 + \delta_g^2 - 2\delta_g(\delta_{solvent}^2 + \Delta_{solvent})^{1/2}\right)}{RT}\right) \tag{5}$$

Liquid phase fugacities of carbon monoxide and hydrogen; $f_{CO}^l and\ f_{H2}^l$ can be estimated using Equations 6 and 7 respectively, and gas phase fugacities of both gases, $f_{CO}^G and\ f_{H2}^G$,can be estimated using Equation 8:[16]

$$f_{CO}^l = \exp(4.7475 + 588.52\mathrm{T}^{-1} - 1.315110^5\mathrm{T}^{-2}) \tag{6}$$

$$f_{H2}^l = exp(-7.4246\mathrm{x}10^{-2} + 4336T^{-1} - 9.3595\mathrm{x}10^5T^{-2} + 6.3853\mathrm{x}10^7T^{-3}) \tag{7}$$

$$f_g^G = \exp\left[\frac{\mathrm{P_r}}{\mathrm{T_r}}\left(0.083 - \frac{0.422}{\mathrm{T_r}^{1.6}} + \omega(0.139 - \frac{0.172}{\mathrm{T_r}^{4.2}})\right)\right] 1.01325\ \mathrm{bar} \tag{8}$$

The solubility parameter for the solvent, $\delta_{solvent}$ can be estimated using Equation 9 given below[17] using vaporization enthalpy $\Delta H_{solvent}^{vap}$ and molar volume $\vartheta_{solvent}$ values reported in Table 3.

$$\delta_{solvent} = \left(\Delta H_{solvent}^{vap}/\vartheta_{solvent}\right)^{1/2} \mathrm{J}^{0.5}\mathrm{m}^{-1.5} \tag{9}$$

The volume fraction of the solvent, $\Phi_{solvent}$ can be assumed as unity since the gases are sparingly soluble in the solvent. The values of the constants used in evaluating these equations are listed in Table 3.

Table 3 Parameters for Regular Solution Theory

Parameter (Unit)	**Value**	
$\vartheta_{toluene}$ (m^3mol^{-1})	$1.06x10^{-4}$	
$\Delta_{toluene}$ ($J.m^3$) [16]	$7.49x10^6$	
$\Delta H^{vap}_{toluene}$($J.mol^{-1}$) [18]	38100	
ϑ_{hexane} (m^3mol^{-1})	$3.68x10^{-4}$	
Δ_{hexane} ($J.m^3$) [non-ploar solvent=0]	0	
ΔH^{vap}_{hexane}($J.mol^{-1}$) [19]	28850	
	Carbon monoxide	**Hydrogen**
ϑ(m^3mol^{-1}) [16]	$3.21x10^{-5}$	$3.73x10^{-5}$
δ($J^{0.5}m^{-1.5}$) [16]	$6.403x10^3$	$7.835x10^3$
ω	0.048	-0.216
T_c (K)	132.9	33.19
P_c (bar)	34.99	13.13

After mole fractions are converted into concentrations, they are used to calculate the Henry's constants (K_H) which will be used to correct the liquid concentration of gas solutes (C_g^l) for pressure. Henry's law is given in Equation 10.

$$P_g = K_H C_g^l \tag{10}$$

4.3 Regioselectivity

Using the estimates given in Table 2, it is possible to model the regioselectivity as given in Equation 11:

$$\frac{l}{b} = \frac{r_l}{r_b} = \frac{A_l \exp\left(-\Delta E_l^A / RT\right)}{A_b \exp\left(-\Delta E_b^A / RT\right)} \tag{11}$$

Equation 11 suggests that the regioselectivity is a function of temperature only. Figure 3 shows the percentage of linear aldehyde in the product depending on the reaction temperature; obtained from the batch hydroformylation reactions performed for the kinetics (Table 1) and estimated using Equation 5, in good agreement. There is a clear increase in the percentage of linear aldehyde in the product with increasing temperature, especially evident in the lower temperature region.

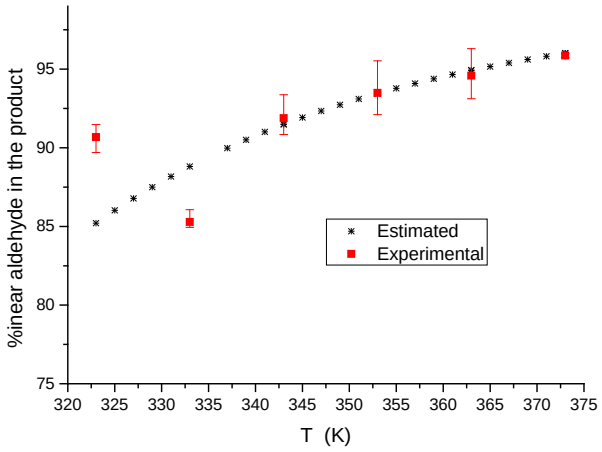

Figure 3 Percentage of linear aldehyde in the product as a function of temperature, values obtained from kinetic hydroformylation experiments and estimated by Equation 8. (Data at 323K and 373K belong to deuterioformylation experiments)

This behavior can be the result of a shift in the Rh-alkyl formation equilibrium with increasing temperature; i.e. the linear Rh-alkyl being favored.[20] Another reason could be a difference in activation energies of the hydrogenolysis steps; rate of linear aldehyde formation increasing faster with temperature compared to the branched aldehyde, i.e linear aldehyde having a higher activation energy.[12]

For the sake of simplicity, we have lumped together the equilibrium and rate constants in Equations 1 and 2 and expressed them in the form of Arrhenius dependency. Writing them in their original forms as in Equation 12 will help to show the roles of these two probable sources of temperature effects on the regioselectivity.

$$\frac{r_l}{r_b} = \frac{k_{FA}K_{CF}}{k'_{FA}K'_{CF}} = \frac{A_{FA}\exp\left(-\Delta E^{\#}_{FA}/RT\right)\exp\left(-\Delta G_{CF}/RT\right)}{A'_{FA}\exp\left(-\Delta E^{\#\prime}_{FA}/RT\right)\exp\left(-\Delta G'_{CF}/RT\right)} \qquad (12)$$

Lumped activation energies $\Delta E_l^A \; and \; \Delta E_b^A$ representing the whole cycle for linear and branched aldehydes have 28.7 kJ/mol difference as shown in Equation 11. This difference is a combination of differences in activation energies ($\Delta E_{FA}^{\#} \; and \; \Delta E_{FA}^{\#\prime}$) of the hydrogenolysis steps and the Gibbs free energies of the equilibrium steps ($\Delta G_{CF} \; and \; \Delta G'_{CF}$) between the π-complex (species **C**, **C'**) and the Rh-acyl (species **F**, **F'**).

In the following, deuterioformylation and *in situ* IR experiments were performed to quantify these effects.

4.3.1 Deuterioformylation experiments

Hydroformylation experiments performed under D_2 pressure instead of H_2 give direct information on the reversibility of the Rh-alkyl formation step (**C** to **D**).[8,21] The Rh catalyst preformed under D_2 labels the alkene reversed from a branched Rh-alkyl at its terminal carbon atom C1, whereas the alkene reversed from a linear Rh-alkyl gets labeled at C2 carbon, as shown in Scheme 3.

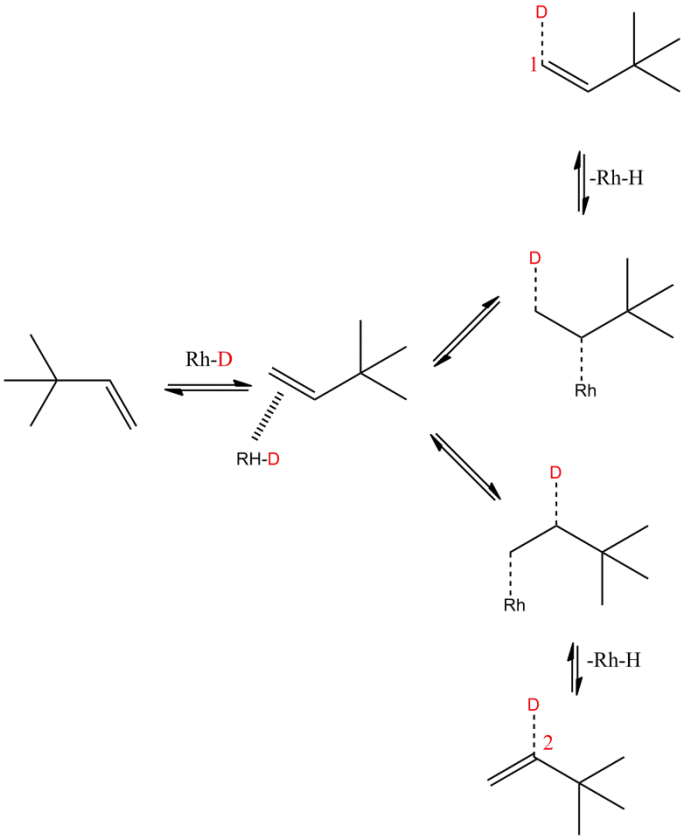

Scheme 3 Deuterium labeling of alkene molecules reversed from Rh-alkyl formation under deuterioformylation conditions

Three deuterioformylation reactions were performed with D_2:CO (20:20 bar), at 50, 80 and 100˚C, respectively, to investigate the effect of temperature on Rh-alkyl reversibility. A fourth experiment was also carried out at 50°C and 20:10 bar D_2:CO to check if the CO pressure has any effect on the reversibility of Rh-alkyl species, since it might have a different effect on the equilibrium following linear Rh-alkyl formation (**D** to **E**) compared to the branched one (**D'** to **E'**).[22] One of these equilibria could be more sensitive to CO concentration, shifting the rate limiting step to CO insertion into the Rh-alkyl species (**D** to **E**) at lower CO concentrations. However, care should be

taken to prevent CO depletion; since these results might be misleading. Deuterium incorporation into C1 (terminal) and C2 (internal) positions were determined by ^{2}H NMR of samples taken during the course of the reactions (Figure 4).

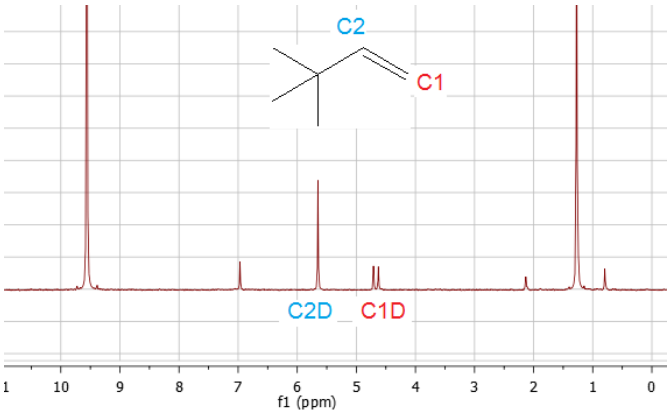

Figure 4 ^{2}H NMR spectra of a reaction sample at 65% conversion, 100°C deuterioformylation reaction, [neohexene] = 2.7 M, [Rh] =1.0x10^{-4} M, L/Rh=27, CO=20 bar, D_2=20 bar

As seen from Figure 5, the number of deuterium atoms incorporated normalized to the number of aldehyde molecules produced, increases with increasing temperature for both positions.

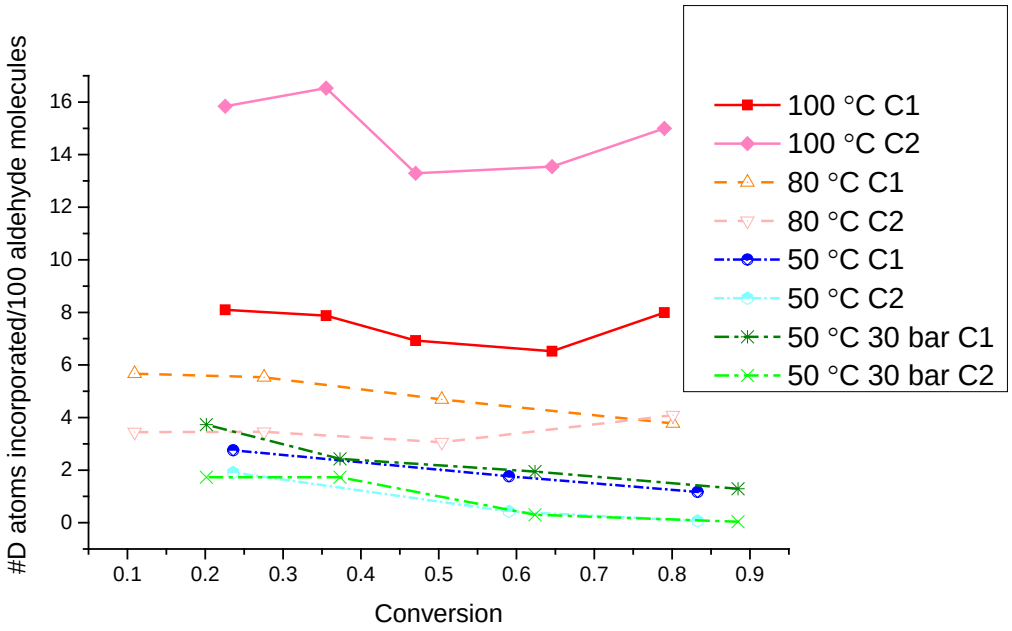

Figure 5 Deuterium incorporation into C1(terminal) and C2 (internal) positions of neohexene during deuterioformylation: [neohexene] = 2.7 M, [Rh] =1.0x10^{-4} M, L/Rh=27, CO =20 bar unless otherwise stated, D_2=20 bar

An important observation is that at 100˚C, the number of D atoms in C2 position is higher than in C1. Hence, the equilibrium for linear Rh-alkyl formation is more temperature sensitive than that for

the branched one. This behavior is easily observed in Figure 6, where the numbers of D atoms in C1 and C2 positions are averaged out for the whole conversion range.

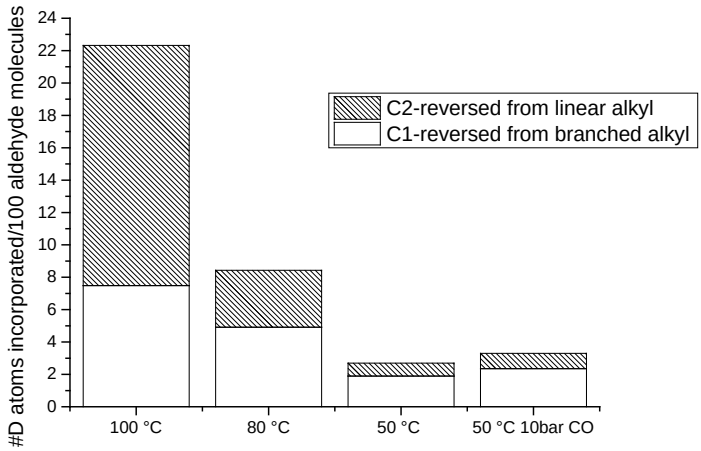

Figure 6 Average Deuterium incorporation into C1(terminal) and C2 (internal) positions of neohexene during deuterioformylation for conditions given in Figure 5

These trends are confirmed also by investigating the deuterium incorporation into the linear aldehyde. When deuterioformylation proceeds without any reversion, the linear aldehyde has two D, one on the aldehyde and another one on the β-position, as shown in Scheme 4.

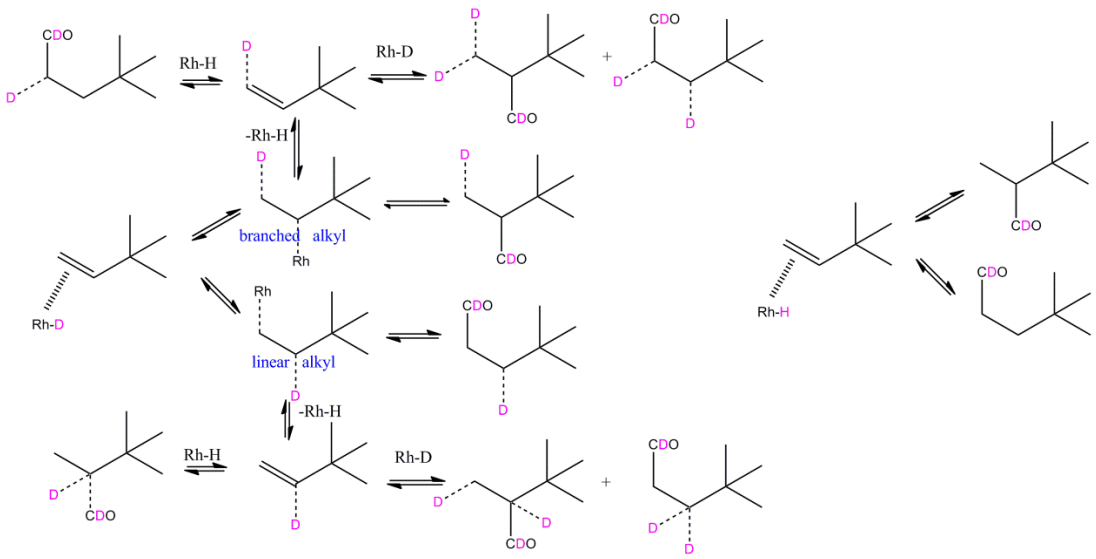

Scheme 4 Deuterium incorporation into alkene and aldehyde molecules during deuterioformylation

The carbon atom closest to the aldehyde function, α-carbon, contains a D atom when an alkene molecule reversed from branched-alkyl confirmation is deuterioformylated. The number of D

atoms in this position is a direct measure of branched alkyl reversibility. Table 4 below gives the number of D atoms in α and β positions of the linear aldehyde at different conversions for each deuterioformylation experiment, normalized to the amount of aldehyde.

Table 4 Number of D atoms in α and β positions of linear aldehyde per 100 aldehyde molecules at different conversions (x)

100°C			**80°C**			**50°C**			**50°C,30 bar**		
x	α	β	x	α	β	x	α	β	x	α	β
0.23	2.37	77.03	0.11	1.74	94.85	0.24	0.28	86.87	0.20	0.23	87.90
0.36	1.61	76.59	0.28	1.40	86.56	0.59	1.18	89.28	0.37	1.05	89.02
0.47	2.40	76.83	0.50	2.07	86.19	0.83	1.14	88.86	0.62	1.38	89.45
0.65	2.16	77.16	0.80	3.45	83.80				0.88	1.66	89.17
0.79	4.05	77.45									

As seen in Table 4, the number of D atoms in α position increases with increased temperature, and the number of D in β position decreases. The former confirms increased branched alkyl reversion at elevated temperatures whereas the latter is due to increased formation of Rh-H species from increased alkene reversion.

The number of D atoms incorporated in the linear aldehyde was also determined by GC-MS. Figure 7 shows the relative amount of aldehyde produced with 1, 2, 3 and 4 D atoms for each deuterioformylation experiment, at 80% or higher conversion. If there would be no reversed alkyl species, there should be only aldehydes with two D atoms. It is evident from Figure 7 that the number of aldehydes with one D only increases with increased temperature, as suggested by the ^{2}H NMR measurements, because of the Rh-H species generated when Rh-alkyl species goes back to alkene. The presence of 4 D atoms suggest that there are alkene molecules that were reversed from Rh-alkyl species more than once.

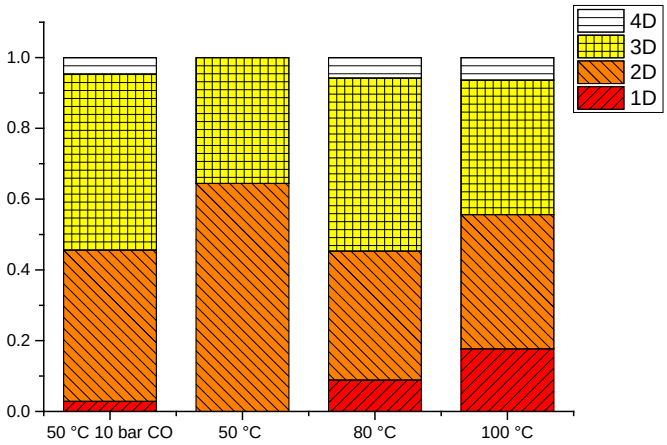

Figure 7 Relative amount of aldehyde with 1 to 4 D atoms incorporated at different temperatures

The temperature sensitivity of an equilibrium arises from the entropy change associated with this step, as should be clear from the following expression: $\Delta G = \Delta H - T\Delta S$; i.e the entropy term will affect the equilibrium more at higher temperatures. Rh-alkyl formation should have negative entropy since one molecule is formed from two molecules and a negative change in entropy will favor the reverse reaction, even more so at increased temperature. Thus, the increase in reversed linear Rh-alkyl with temperature suggests that the negative change in entropy for linear Rh-alkyl formation is higher than it is for the branched one, meaning that the linear Rh-alkyl has lower entropy. Reducing CO pressure does not seem to have an effect on the reversibility at 50°C. This is an expected result, confirming that hydrogenolysis is the common rate limiting step.

The kinetic isotope effect observed when comparing deuterioformylation experiments to hydroformylation at similar conditions also confirm that the rate limiting step is the hydrogenolysis step here. Figure 8 compares conversion time profiles of a hydroformylation and a deuterioformylation experiment.

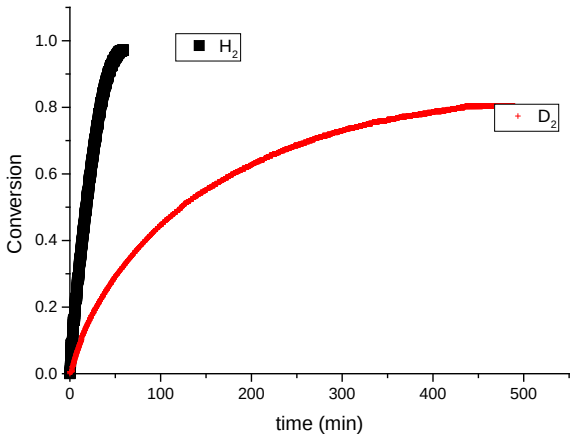

Figure 8 Deuterioformylation: [neohexene] = 2.7 M, [Rh] =1.0x10^{-4} M, L/Rh=27, CO =20, D_2=20 bar, 80°C
Hydroformylation: [neohexene] = 2.23 M, [Rh] =1.19x10^{-4} M, L/Rh=30, CO =20, D_2=20 bar, 80°C

4.3.2 HP-IR experiments

Although deuterioformylation experiments give a clear idea about the reversibility of linear and branched Rh-alkyl species, they do not help to quantify the activation energy difference in the hydrogenolysis step. Only an analysis of respective amounts of Rh-acyl species would give direct information on that,[5] as explained in the derivation below:

$$\frac{dC_{l-aldehyde}}{dt} = k_{FA}[F][H_2] \tag{13}$$

$$\frac{dC_{l-aldehyde}}{dt} = \frac{k_{FA}[G][H_2]}{K_{FG}[CO]} \tag{14}$$

According to the justified assumption that l/b is constant during the reaction, it is possible to write Equation 15 and comparing Equation 15 to Equation 12, Equation 16 can be written as given.

$$\frac{dC_{l-aldehyde}}{dC_{b-aldehyde}} = \frac{l}{b} = \frac{k_{FA}[G]K'_{FG}}{k'_{FA}[G']K_{FG}} = \frac{A_{FA}\exp\left(-\Delta E^{\#}_{FA}/RT\right)[G]\ exp\left(\frac{\Delta S'_{FG}}{R}\right)exp\left(\frac{-\Delta H'_{FG}}{RT}\right)}{A'_{FA}\exp\left(-\Delta E^{\#'}_{FA}/RT\right)[G']\ exp\left(\frac{\Delta S_{FG}}{R}\right)exp\left(\frac{-\Delta H_{FG}}{RT}\right)} \tag{15}$$

$$\frac{[G]}{[G']} = \frac{K_{FG}exp\left(-\Delta G_{CF}/RT\right)}{K'_{FG}exp\left(-\Delta G'_{CF}/RT\right)} = exp\left(\frac{\Delta S_{CG} - \Delta S'_{CG}}{R}\right)exp\left(\frac{-\Delta H_{CG} + \Delta H'_{CG}}{RT}\right) \tag{16}$$

The ratio of linear to branched Rh-acyl $[G]/[G']$ also gives direct information on the Gibbs free energy differences of steps between Species **C** and **G**, as given in Equation 16. *In situ* IR

experiments were performed to quantify the respective amounts of linear and branched Rh-acyl species. Figure 9 shows the spectra recorded in the first ten minutes of a reaction performed at room temperature.

Negative peaks appearing after the addition of neohexene ($\tilde{\nu}$=1824.4 cm^{-1}) belong to the hydride species (**A**) characterized by peaks at 2013, 2043 and 2092 cm^{-1}. These values are in close agreement with the ones reported by Selent et al.[12] ($\tilde{\nu}_{CO}$=2013, 2041 and 2091 cm^{-1}). They are negative since the background spectrum was measured after complete conversion of the catalyst into Rh-hydride and after substrate addition some of this species turns into Rh-acyl. Rh-acyl species (**G, G'**) is characterized by three peaks in the terminal CO region; 1994.6, 2019.8 and 2078 cm^{-1} appearing immediately after substrate addition, also in agreement with the values reported by Selent et al.[12] ($\tilde{\nu}_{CO}$ = 1995, 2017, 2079 cm^{-1}).

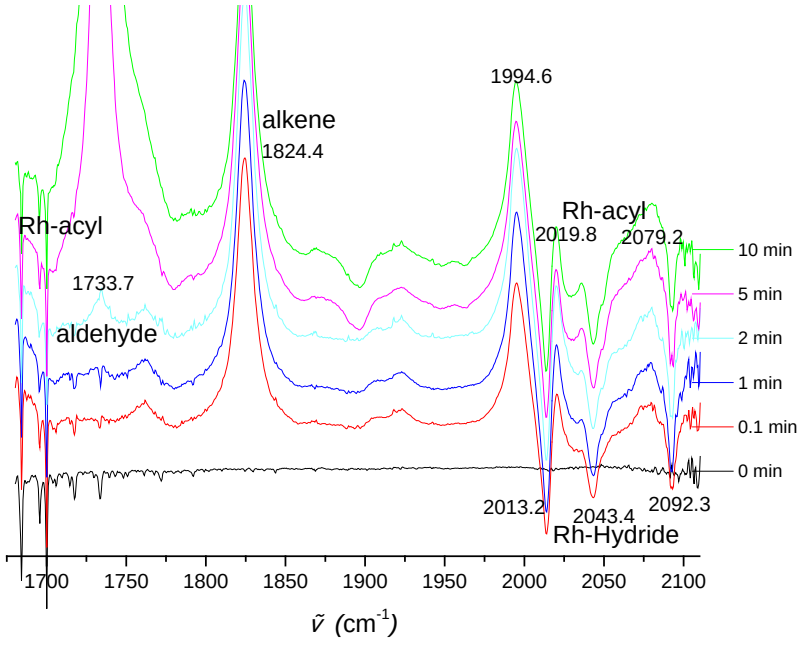

Figure 9 IR spectra recorded in the first ten minutes of neohexene hydroformylation, [neohexene] = 0.54 M, [Rh] =3.14x10^{-4} M, L/Rh=26, T=25°C, H_2=4.8 bar, CO=35.2 bar

The last peaks of these species, belonging to the acyl C=O bond, should be located in the organic CO region,[23,24] around 1690-1700 cm^{-1} and these are the ones that will enable us to determine the linear to branched Rh-acyl ratio. Selent et al.[14] recently determined this peak at 1690 cm^{-1} for this catalyst-substrate system. However, the aldehyde (1734 cm^{-1}) and neohexene (1642 cm^{-1}) peaks overlap in this region and it is not possible to observe the relatively small C=O signals, especially at higher conversions. Therefore, spectra of pure neohexene were subtracted from the reaction spectra recorded to eliminate the neohexene signal at 1824.4 cm^{-1}. The low pressure of hydrogen used in

these experiments (Table 5) enabled us to take a number of spectra before the Rh-acyl peak was concealed under the aldehyde peak at 1734 cm^{-1}. This enabled us to obtain the spectra of the acyl C=O bond of the Rh-acyl species such as given in Figure 10, with the desired species (**G** and **G'**) overlapping around 1690 cm^{-1}.

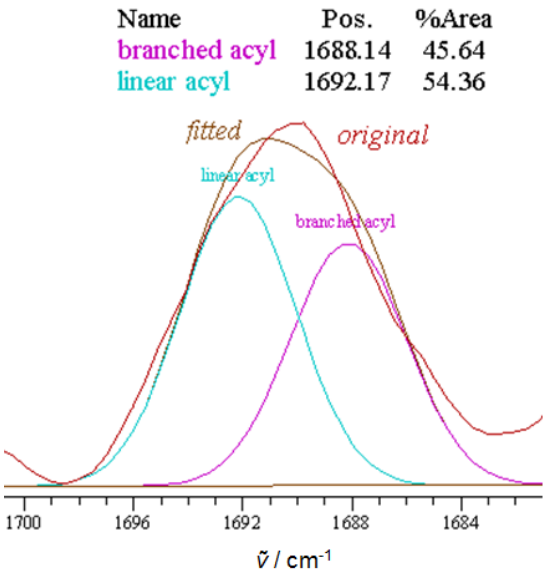

Figure 10 IR spectra recorded immediately after neohexene addition for the 40°C IR experiment, after neohexene subtraction, showing the deconvolution of Rh-acyl species ([neohexene] = 0.54 M, [Rh] =3.14x10^{-4} M, L/Rh=26, H_2=3.9 bar, CO=34.2 bar)

After deconvolution of this signal, linear and branched coordinatively saturated Rh-acyl species (**G** and **G'**) were characterized by the peaks at 1692 and 1688 cm^{-1} respectively with their acyl CO signals, with the values given in Table 5. The deconvolution was performed by CasaXPS.[25]

Table 5 Ratio of linear to branched Rh-acyl species and reaction conditions for the IR experiments

T (K)	H_2 (bar at 25°C)	CO (bar at 25°C)	[Linear Rh-acyl]/[Branched Rh-acyl]
298	4.85	35.15	1.04
313	3.87	34.21	1.12
328	6.59	29.75	1.50
343	3.75	31.00	1.68

Rearranging equation 16, the natural logarithm of the Rh-acyl ratios $ln\left(\frac{[G]}{[G']}\right)$ describes a line with the equation $\frac{(-\Delta H_{CG}+\Delta H'_{CG})}{R}\frac{1}{T}+\frac{(\Delta S_{CG}-\Delta S'_{CG})}{R}$. Linear regression of the data presented in Table 5 as given in Figure 11 allows to calculate $\Delta H_{CG}-\Delta H'_{CG}$ as 9.7 kJ/mol and a difference of changes in entropy $\Delta S_{CG}-\Delta S'_{CG}$ = 32.5 J/mol.K.

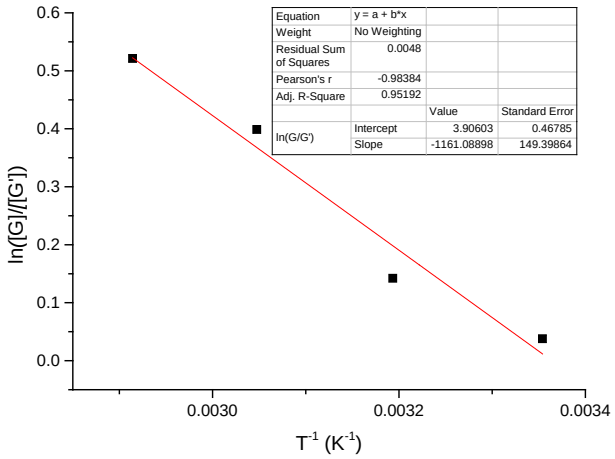

Figure 11 Linear fit to describe equation ln([G]/[G'])= ($-\Delta H_{CG}+\Delta H'_{CG}$)/RT+($-\Delta S_{CG}+\Delta S'_{CG}$)/R using data in Table 5

It would be justified to assume that the total free energy changes from species **C** to **F** should be negative, since the coordination of alkene is suggested to be a high energy change step by the IR-observable hydride species. This is also in line with energy profiles of hydroformylation of a range of substrates.[4,7,22,23,26] The free energy change of the equilibrium between **F** and **G** should also be negative. We also know that the difference in Gibbs free energy changes is negative ($\Delta G_{CG}-\Delta G'_{CG} < 0$), from which we can deduce $|\Delta G_{CG}| > |\Delta G'_{CG}|$. So a higher negative ΔG favors the forward reaction (**C** to **G**) of the linear path, even more so with increasing temperature because the entropy difference $\Delta S_{CG}-\Delta S'_{CG}$ is positive and increases the difference in Gibbs free energy changes with increasing temperature; as should be evident from the following expression:

$$\Delta G_{CG}-\Delta G'_{CG} = \Delta H_{CG}-\Delta H'_{CG} - T(\Delta S_{CG}-\Delta S'_{CG}).$$

It is possible to obtain $\left(\Delta E^{\#}_{FA} - \Delta H_{FG}\right) - \left(\Delta E^{\#'}_{FA} - \Delta H'_{FG}\right)$ and $(\Delta S_{FA} - \Delta S'_{FA}) - (\Delta S_{FG} - \Delta S'_{FG})$ using the data in Table 5 for linear regression of Equation 15 where the ratio of the pre-exponential factors A_{FA}/A'_{FA} can be written as given in Equation 17.

$$\frac{A_{FA}}{A'_{FA}} = \exp\left(\frac{\Delta S^{\#}_{FA} - \Delta S^{\#'}_{FA}}{R}\right) \qquad (17)$$

Figure 12 shows the linear regression carried out.

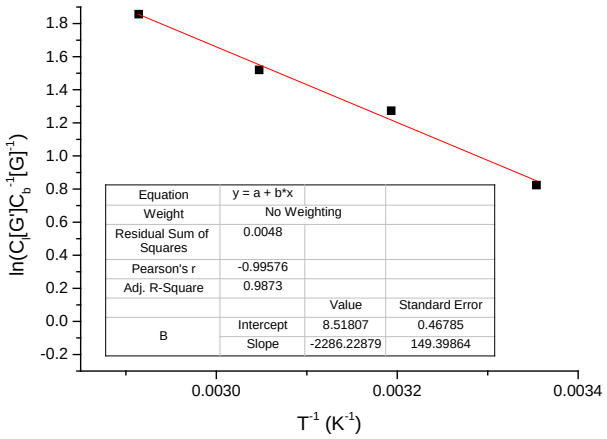

Figure 12 Linear fit using data in Table 5 to describe equation ln([linear aldehyde][G']/[branched aldehyde][G])= ($-\Delta H_{GA}+\Delta H'_{GA}$)/RT+($\Delta S_{GA}-\Delta S'_{GA}$)/R

$\left(\Delta E_{FA}^{\#}+\Delta H_{GF}\right)-\left(\Delta E_{FA}^{\#'}+\Delta H'_{GF}\right)=\Delta H_{GA}-\Delta H'_{GA}=19$ kJ/mol and $\Delta S_{FA}^{\#}-\Delta S_{FA}^{\#'}+\Delta S_{GF}-\Delta S'_{GF}=\Delta S_{GA}-\Delta S'_{GA}$ is determined as 71 J/mol.K. For the formation of the activated state, the entropy change should be positive. Garland et al.[27] reported an activation entropy of $\Delta S^{\#}$=121±14 J/mol.K for the hydrogenolysis step of neohexene hydroformylation catalyzed by the unmodified Rh catalyst. A positive activation entropy suggests that the transition state is highly unstable. Degrees of freedom are 'liberated' in going from the ground state to the transition state, which, in turn, increase the rate of the reaction. The entropy change involved in going from G to F or G' to F' should also be positive, meaning both ΔS_{GA} and $\Delta S'_{GA}$ are positive.

So hydrogenolysis of the 5-coordinated linear Rh-acyl, **G** at typical hydroformylation conditions is faster than that of the branched isomer **G'** although it has a higher activation energy ($\Delta H_{GA}-\Delta H'_{GA}$=19 kJ/mol) because it has a larger positive activation entropy ($\Delta S_{GA}-\Delta S'_{GA}$=71 J/mol.K).

4.4 Conclusions

Detailed analysis of the kinetics and mechanism of neohexene hydroformylation was carried out for the bulky phosphite, tris(2,4-di-*tert*-butylphenyl) phosphite modified Rh as catalyst. Both linear and branched aldehyde isomers were shown to have the hydrogenolysis of the Rh-acyl species as the rate limiting step. Rate equations were derived and equation parameters were estimated within very narrow confidence intervals using nonlinear regression. These estimates were used to predict the regioselectivity in very good agreement with the experimental data. Deuterioformylation and *in situ*

IR experiments were performed to reveal the reasons behind the increase in linear aldehyde selectivity with increasing temperature.

The deuterioformylation experiments showed that both linear and branched Rh-alkyl formation are reversible, and increasingly so with increasing temperature. This finding suggests that the entropy change involved in Rh-alkyl formation is negative, favoring the reverse reaction more and more with increasing temperature as $\Delta G = \Delta H - T\Delta S$. At 100°C; the linear Rh-alkyl formation was found to be even more reversible than the branched one, which means the negative entropy change for linear Rh-alkyl formation is larger than the one for branched Rh-alkyl formation: i.e. linear Rh-alkyl formation equilibrium (**C** to **D**) is more temperature sensitive than the branched Rh-alkyl equilibrium (**C** to **D'**). HP-IR experiments carried out to investigate the linear and branched Rh-acyl species (**G** and **G'**) showed an excess of linear Rh-acyl compared to the branched one. Moreover, the ratio of linear to branched Rh-acyl increased with increasing temperature. These findings suggest that the total forward reaction of non-common equilibrium steps of the linear and branched catalytic cycles (**C** to **G** and **C'** to **G'**) are favored for the linear aldehyde over the branched one. Accordingly, we calculated a higher negative ΔG for the linear cycle at all temperatures. The difference in Gibbs free energies, $\Delta G_{CG} - \Delta G'_{CG}$, gets even more pronounced at higher temperatures since $\Delta G_{CG} - \Delta G'_{CG} = \Delta H_{CG} - \Delta H'_{CG} - T(\Delta S_{CG} - \Delta S'_{CG})$ and the difference in entropy changes is positive ($\Delta S_{CG} - \Delta S'_{CG}$ = 32.5 J/mol.K).

Furthermore, the reverse step of the equilibrium from **G** to **F** and subsequent hydrogenolysis of the linear acyl (**F**) was found to have a larger enthalpy change associated compared to the branched equivalent (**G'** to **F'** and hydrogenolysis of **F'**). The contribution of this part of the cycle to the temperature dependence of regioselectivity is around twice as much compared to the part from Species **C** to **G** (and **C' to G'**). Finally, the larger positive entropy changes for both mentioned parts of the linear aldehyde cycle make the linear aldehyde the favored isomer at typical hydroformylation conditions.

4.5 Experimental

4.5.1 Materials

Chemicals were purchased from Aldrich, Merck, Acros or Biosolve. All air/water sensitive solutions were prepared under argon using Schlenk techniques. The substrate solution containing neohexene and decane as internal standard was filtered over neutral alumina and degassed. A stock solution of catalyst (Rh precursor: Rh(acac)$(CO)_2$ and Ligand) was prepared in dry and degassed solvent. Solvents were dried and degassed using a custom-made alumina-filled Ar-flushed column.

4.5.2 Kinetic batch experiments

Batch reactions for kinetics were performed in custom built stainless steel autoclaves (100 mL) equipped with a mechanical gas-impeller stirrer and a mass flow controller (MFC) to monitor the gas uptake and to keep the reaction pressure constant. A stirring rate of 1200 rpm was set for all kinetic experiments. Conversion was measured on a Shimadzu GC-2010 gas chromatograph (GC) using an Agilent DB1 column (30m x0.32mm i.d.) at the end of the reaction time to normalize the values obtained from gas uptake data.

The substrate solution was filled into a dropping funnel (30 ml) connected to the autoclave by a tube that keeps the funnel at the same pressure as the autoclave and a valve that enables controlled charge of the substrate solution into the autoclave. The catalyst solution was charged in the autoclave where it was preformed under reaction conditions for one hour, after which the reaction was started by adding the substrate solution.

Deuterioformylation reactions were performed with the same type of autoclave as mentioned before, equipped with a sampling unit that enables sampling during the reaction. ^{2}H NMR spectroscopy was performed on a Varian Unity Inova 500 spectrometer operating at 499.8 MHz for ^{1}H (76.72 MHz for ^{2}H), equipped with a 5 mm AutoX DB-PFG probe. Prior to measurement, the 90 degree pulse width was calibrated using a solution of C_6D_6 in $CHCl_3$. Spectra were recorded using a 1535 Hz spectral width, employing 90 degree pulses and a relaxation delay of 20 seconds. Data was processed using VNMRJ 2.2d Software and was filtered using 1 Hz line broadening. Integrals were normalized to the aldehyde signal at 10.1 ppm

4.5.3 *In situ* HP-IR experiments

In situ HP-IR experiments were carried out in a custom built stainless steel autoclave (50 ml) with an integrated flow cell equipped with ZnS windows and a mechanical gas-impeller stirrer (800 rpm for all FT-IR measurements). The spectra were recorded on a Shimadzu FT-IR 8300 spectrometer, in absorbance mode. The catalyst solution in hexane was preformed under syngas and the reaction was started after complete hydride formation by adding the substrate, kept in a dropping funnel. Background measurements were performed just before the addition of the substrate. FT-IR spectra of pure neohexene were later subtracted from the measurements in proper amounts. Catalyst and substrate concentrations are kept constant at [neohexene] = 0.54 M, [Rh] =3.14×10^{-4} M, L/Rh=26 for all IR experiments.

4.5.4 GC-MS

GC-MS analyses were done with a Shimadzu GCMS-QP2010 SE with a DB-1 MS column (10 m, 0.1 mm i.d.).

4.6 References

[1] P. W. N. M. van Leeuwen, C. Claver, *Rhodium Catalyzed Hydroformylation*, Springer, **2002**.
[2] S. C. van der Slot, J. Duran, J. Luten, P. C. J. Kamer, P. W. N. M. van Leeuwen, *Organometallics* **2002**, *21*, 3873–3883.
[3] A. van Rooy, E. N. Orij, P. C. J. Kamer, P. W. N. M. van Leeuwen, *Organometallics* **1995**, *14*, 34–43.
[4] G. Alagona, C. Ghio, R. Lazzaroni, R. Settambolo, *Organometallics* **2001**, *20*, 5394–5404.
[5] J. Feng, M. Garland, *Organometallics* **1999**, *18*, 417–427.
[6] A. L. Watkins, C. R. Landis, *J. Am. Chem. Soc.* **2010**, *132*, 10306–10317.
[7] R. Lazzaroni, R. Settambolo, G. Alagona, C. Ghio, *Coord. Chem. Rev.* **2010**, *254*, 696–706.
[8] R. Lazzaroni, G. Uccello-Barretta, M. Benetti, *Organometallics* **1989**, *8*, 2323–2327.
[9] R. Lazzaroni, R. Settambolo, G. Uccello-Barretta, A. Caiazzo, S. Scamuzzi, *J. Mol. Catal. Chem.* **1999**, *143*, 123–130.
[10] C. P. Casey, S. C. Martins, M. A. Fagan, *J. Am. Chem. Soc.* **2004**, *126*, 5585–5592.
[11] A. Van Rooy, J. N. H. de Bruijn, K. F. Roobeek, P. C. J. Kamer, P. W. N. M. van Leeuwen, *J. Organomet. Chem.* **1996**, *507*, 69–73.
[12] C. Kubis, R. Ludwig, M. Sawall, K. Neymeyr, A. Börner, K.-D. Wiese, D. Hess, R. Franke, D. Selent, *ChemCatChem* **2010**, *2*, 287–295.
[13] T. Jongsma, G. Challa, P. W. N. . van Leeuwen, *J. Organomet. Chem.* **1991**, *421*, 121–128.
[14] C. Kubis, D. Selent, M. Sawall, R. Ludwig, K. Neymeyr, W. Baumann, R. Franke, A. Börner, *Chem. - Eur. J.* **2012**, *18*, 8780–8794.
[15] J. H. Hildebrand, *Solubility of Non-electrolytes*, Reinhold Pub. Corp., **1936**.
[16] U. J. Jáuregui-Haza, E. J. Pardillo-Fontdevila, A. M. Wilhelm, H. Delmas, *Lat. Am. Appl. Res.* **2004**, *34*, 71–74.
[17] L. C. Yen, J. J. McKetta, *AIChE J.* **1962**, *8*, 501–507.
[18] M. V. Roux, M. Temprado, J. S. Chickos, Y. Nagano, *J. Phys. Chem. Ref. Data* **2008**, *37*, 1855.
[19] "NIST Chemistry WebBook," can be found under http://webbook.nist.gov/**.**
[20] R. Lazzaroni, P. Pertici, S. Bertozzi, G. Fabrizi, *J. Mol. Catal.* **1990**, *58*, 75–85.
[21] C. P. Casey, L. M. Petrovich, *J. Am. Chem. Soc.* **1995**, *117*, 6007–6014.
[22] C. Ghio, R. Lazzaroni, G. Alagona, *Eur. J. Inorg. Chem.* **2009**, *2009*, 98–103.
[23] G. Liu, R. Volken, M. Garland, *Organometallics* **1999**, *18*, 3429–3436.
[24] P. C. J. Kamer, A. van Rooy, G. C. Schoemaker, P. W. N. M. van Leeuwen, *Coord. Chem. Rev.* **2004**, *248*, 2409–2424.
[25] "Copyright © 2005 Casa Software Ltd," can be found under http://www.casaxps.com/**.**
[26] G. Alagona, R. Lazzaroni, C. Ghio, *J. Mol. Model.* **2010**, *17*, 2275–2284.
[27] M. Garland, P. Pino, *Organometallics* **1991**, *10*, 1693–1704.

Chapter 5

1-Pentene Hydroformylation:

Testing the Limits of Gas-Liquid Mass Transfer in a Jet Loop Rector and Optimizing Selectivity

---

The kinetics of 1-pentene hydroformylation were investigated for a Rh catalyst modified with the bulky monodentate tris(2,4-di-*tert*-butylphenyl) phosphite. Rate equations for isomerization of 1-pentene to 2-pentene and hydroformylation for both linear and branched aldehydes were derived and the kinetic parameters were estimated. Kinetic data was used to plan a continuous 1-pentene hydroformylation in a jet loop reactor with integrated membrane separation. The fast kinetics of this alkene makes it an excellent candidate to obtain very high total turnover numbers even within a couple of residence times. However, for this very active catalyst-substrate pair, gas-liquid mass transfer can be the limiting factor. We investigated the dissolved syngas concentration in the liquid during reaction using kinetic data and the results we have previously obtained on mass transfer characteristics of this reactor. Steady state selectivity of the reaction was shown to be a complex function of temperature and pressure.

5.1 1-Pentene Hydroformylation

Hydroformylation of alkenes to aldehydes is a very useful tool in chemistry, the first step in the route to important chemicals as alcohols via hydrogenation, carboxylic acids via oxidation and to amines via reductive amination of the aldehydes.[1]

Hydroformylation of terminal alkenes give linear and branched aldehydes, as given for 1-pentene in Scheme 1 below, not only because both sides of the double bond are active but also owing to double bond isomerization taking place as a side reaction. Linear aldehydes are economically more desired; and suppressing the isomerization activity by using different ligands,[2] using catalyst systems which selectively hydroformylate to the linear aldehyde,[3,4] or tuning the process conditions to minimize isomerization, are techniques applied to maximize the linear aldehyde selectivity.

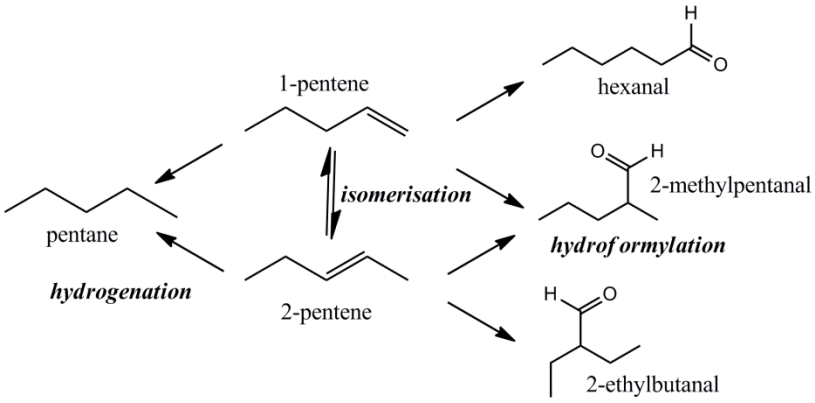

Scheme 1 1-pentene hydroformylation

The extent of isomerization is a combination of many parameters. To start with, the ligand used to modify the metal center has a tremendous effect. Unmodified Rh catalyst is known to be very active for isomerization[5] whereas quite some ligands have been developed to increase linear to branched ratios either by suppressing isomerization or by steering the selectivity to the linear aldehyde.[2,3,6–9] Other factors that affect isomerization are temperature and CO pressure; β-hydride elimination is favored at high temperatures and low CO pressures.[6,10] And of course the hydroformylation reaction, which is the 'competing' side reaction should also be taken into account: the relative activity of the catalyst towards isomerization and hydroformylation depending on process conditions might open up optimization possibilities in terms of selectivity.

Another important concern in hydroformylation is of course activity of the catalyst, which has a huge effect on the process economics, directly affecting the reactor size and conditions the system

operates at to achieve reasonable space time yields. Unfortunately, activity and selectivity does not come together most of the time; and when it does, it might be achieved via 'fancy' ligands which might be too expensive to be considered for feasible industrial processes of bulk chemicals.

Knowing the kinetics for a certain catalyst-substrate system is necessary not only to optimize the selectivity of a process via process conditions but also to avoid mass transfer limited operation conditions, which might have a negative effect on the catalyst stability in the long run, i.e. cluster formation.[1]

Bulky phosphite ligands studied by the group of van Leeuwen,[11] are famous for their activity, even for internal alkenes which are otherwise unreactive. However, they show only moderate selectivity towards the linear aldehyde.[10]

In this chapter, we will investigate the kinetics of 1-pentene hydroformylation catalyzed by the bulky monodentate tris(2,4-di-*tert*-butylphenyl) phosphite modified Rh catalyst (precursor: $Rh(acac)(CO)_2$), in order to elucidate the effects of process conditions on selectivity. Furthermore the operation window will be determined, where the reaction is kinetically limited rather than mass transfer limited. Finally continuous hydroformylation in a jet loop reactor will be demonstrated.

5.2 Gas Solubilities in Reaction Mixture

Solubilities of carbon monoxide and hydrogen in toluene and hexane, which are solvents used in this study, were calculated as explained in Chapter 4. Parameter values that were used for the reported method for hexane are given in Table 1.

Table 1 Parameters for Regular Solution Theory

Parameter (Unit)	Value
ϑ_{hexane} $(m^3 mol^{-1})$	$3.68x10^{-4}$
Δ_{hexane} $(J.m^3)$ [non-ploar solvent=0]	0
$\Delta H^{vap}_{hexane} (J.mol^{-1})$ [12]	28850

5.3 Kinetics

Literature reports that for the hydroformylation of 1-octene with a very similar ligand, tris(2-tert-butyl-4-methylphenyl) phosphite, a first order dependence in H_2 and a negative first order in CO concentration is observed.[10] This observation suggests that hydrogenolysis of the acyl species is the rate limiting step, which is supported by *in situ* IR studies showing that the major resting species during the reaction is the 5 coordinated acyl species (**G**) in Scheme 2.[13] At low conversions, i.e. higher substrate concentrations, the reaction rate is independent of 1-octene

concentration,[10,14] but turns slightly dependent (0.3th order[14]) at low concentrations. This suggests that the coordination of the alkene to form the π-complex (**C**) is still a high energy change step and that the hydride might be the co-existing resting species.

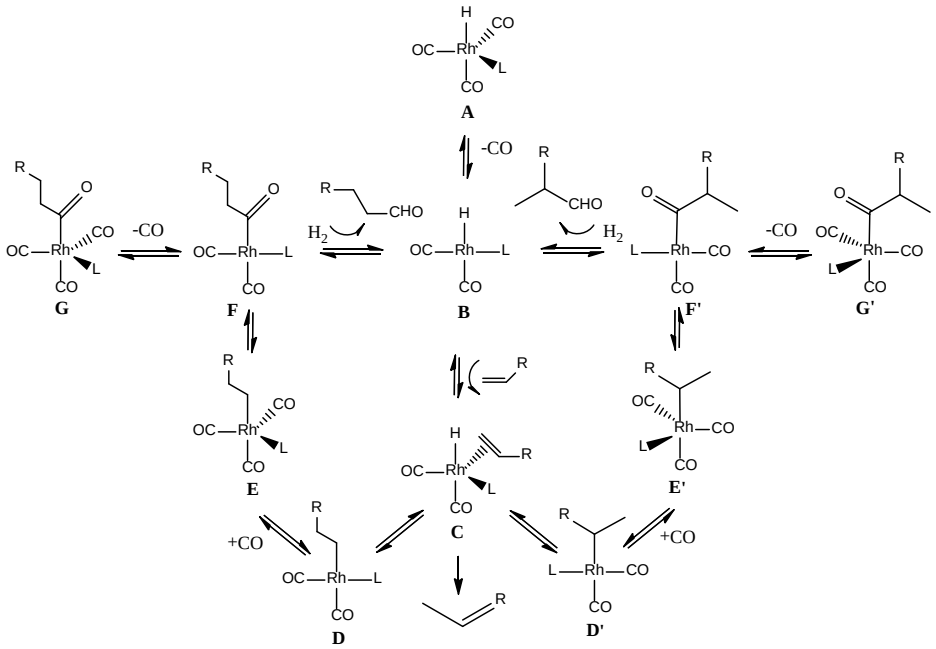

Scheme 2 Mechanism of Rh-catalyzed hydroformylation using bulky monophosphites[14]

Since 1-pentene is a terminal alkene like 1-octene, same type of kinetics are expected. A set of preliminary experiments as given in Figure 1 confirmed the first order in hydrogen and catalyst concentration. It is also possible to observe from the reaction profiles that in the beginning of the reaction the rate is independent of 1-pentene concentration.

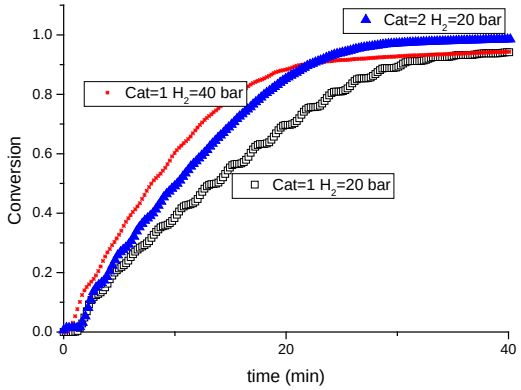

Figure 1 1-Pentene hydroformylation reactions (80°C, [1-pentene]=1 M, CO=20 bar, cat=1=>[Rh]=4.63x10^{-5} M and cat=2=>[Rh]=9.26x10^{-5} M, 1200 rpm)

An *in situ* IR experiment was performed to confirm that the hydrogenolysis is the rate limiting step. As can be seen in Figure 2, negative peaks appearing after the addition of 1-pentene belong to the Rh-H species (**A** in Scheme 2) characterized by absorptions at 2013, 2043 and 2092 cm^{-1}. These values are in close agreement with the ones reported by Selent et al.[15] ($\tilde{\nu}_{CO}$=2013, 2041 and 2091 cm^{-1}). They are negative since the background was measured after complete conversion of the catalyst into Rh-hydride and after substrate addition this species turns into Rh-acyl. Rh-acyl species (**G, G'**) is characterized by three peaks in the terminal CO region; 1994.6, 2019.8 and 2078 cm^{-1} appearing immediately after substrate addition, also in agreement with the values reported by Selent et al.[15] ($\tilde{\nu}_{CO}$ = 1995, 2017, 2079 cm^{-1}). In the beginning of the reaction, Rh-acyl species are the only resting state whereas the Rh-acyl species are restored back to Rh-H species as the reaction proceeds, and the species co-exist to the end of the reaction.

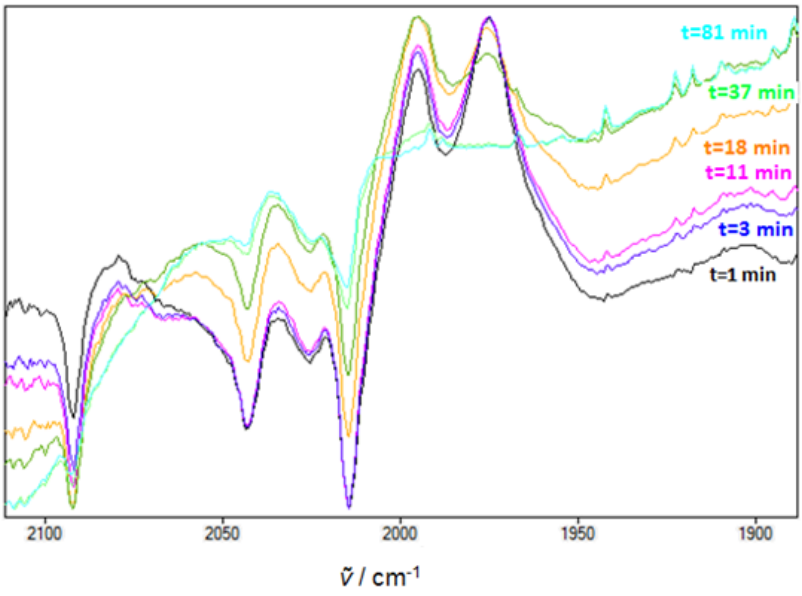

Figure 2 *In situ* HP-IR spectra of 1-pentene hydroformylation (70°C, [1-pentene]=1.8 M, [Rh]=3.88x10^{-4} M, L/Rh=30 , CO=20 bar, H_2=20 bar)

The rate equation proposed[14] for 1-octene hydroformylation is given in Equation 1 below.

$$r = \frac{k[Rh][H_2]}{1 + K[CO]} \qquad (1)$$

To extend the equation to take into account the alkene dependence showing up at low alkene concentrations, we decided to derive the rate equation again according to the reported mechanism given in Scheme 2 and with the following assumptions:

- The total Rh concentration is a sum of species **A** and **G**
- Pre-equilibrium between species **A** and **B**
- Steady state assumption for species **C** and **F**

The rate equation obtained according to these assumptions is given below in its simplified form in Equation 2. The derivation is very similar to the one carried out for neohexene hydroformylation in Chapter 4, and the details of this derivation are given in the Appendix.

$$r_{hydroformylation} = \frac{k[Alkene][Rh][H_2]}{K + [CO][Alkene]} \tag{2}$$

The rate equation for isomerization was modeled according to the observation in literature that increasing CO partial pressure inhibits isomerization.[10] The model we used is given below:

$$r_{isomerization} = \frac{k[Alkene][Rh]}{[CO]} \tag{3}$$

The reaction network was simplified by lumping the two branched products together and ignoring hydrogenation as given in Scheme 3.

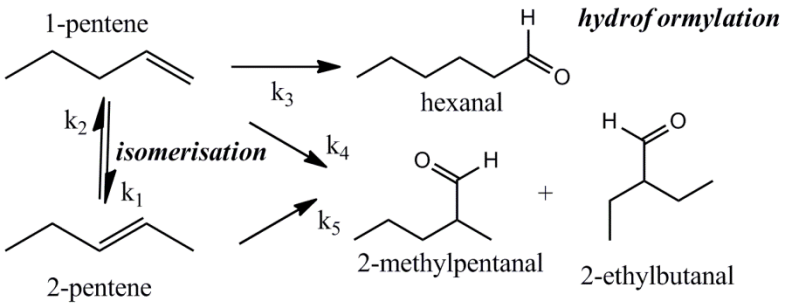

Scheme 3 Simplified reaction network for hydroformylation of 1-pentene

According to this simplified scheme, the following equations can be written:

$$\frac{d[1-pentene]}{dt} = r_2 - r_3 - r_4 - r_1 \tag{4}$$

$$\frac{d[2-pentene]}{dt} = r_1 - r_5 - r_2 \tag{5}$$

$$\frac{d[hexanal]}{dt} = r_3 \tag{6}$$

$$\frac{d[branched\ aldehydes]}{dt} = r_4 + r_5 \tag{7}$$

where

$$for\ i = 1{,}2\ \ r_i = \frac{k_i[Rh][i-pentene]}{[CO]} \tag{8}$$

$$for\ i = 3{,}4\ \ r_i = \frac{k_i[Rh][H_2][1-pentene]}{K + [CO][1-pentene]} \tag{9}$$

$$for\ i = 5\ \ r_i = \frac{k_i[Rh][H_2][2-pentene]}{K + [CO][2-pentene]} \tag{10}$$

$$k_i = A_i \exp\left(-{}^{E_{Ai}}/_{RT}\right) \tag{11}$$

A series of batch experiments were performed in autoclaves equipped with sampling units and mass flow controllers to keep the reaction pressure constant. This enables confirming the conversion values obtained by GC measurements with gas uptake values, as will be seen from Figure 3.

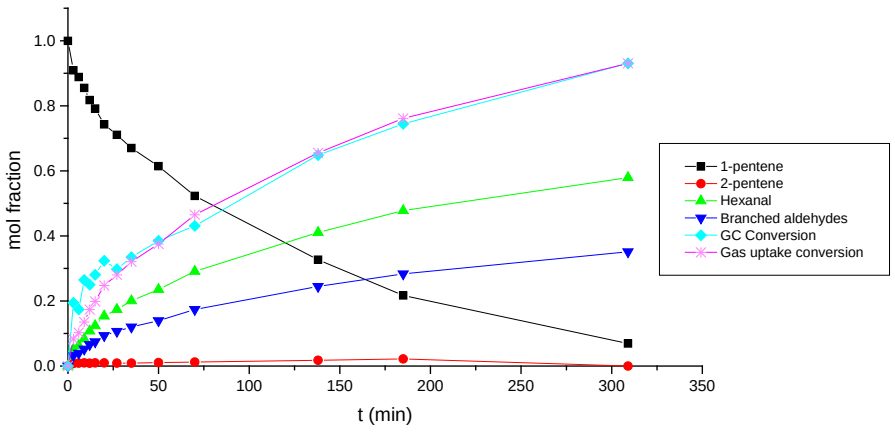

Figure 3 1-Pentene hydroformylation reaction followed by sampling and gas-uptake (70°C, [1-pentene]=1.37M, CO=31 bar, H_2=31 bar, Rh]=2.27x10^{-5} M, 1200 rpm)

Experiments performed for the kinetic investigation are given in Table 2 and more specific time-concentration data is included in the Appendix.

Table 2 Kinetic experiments performed for 1-pentene hydroformylation

Entry	T (°C)	P_{H2} (bar)	P_{CO} (bar)	[Rh] (M)	$[2\text{-pentene}]_0$ (M)	$[1\text{-pentene}]_0$ (M)	Solvent	l/b (end)
1	60	20	20	$2.27x10^{-5}$	0.00	1.37	toluene	1.59
2	60	20	20	$5.58\ x10^{-5}$	0.00	1.10	hexane	1.64
3	63	20	23	$2.27\ x10^{-5}$	0.00	1.37	toluene	1.51
4	63	19	38	$2.27\ x10^{-5}$	0.00	1.37	toluene	1.58
5	70	19	31	$2.27\ x10^{-5}$	0.00	1.37	toluene	1.66
6	70	19	31	$2.27\ x10^{-5}$	0.00	1.37	toluene	1.67
7	70	20	20	$3.72\ x10^{-5}$	0.00	1.37	hexane	1.63
8	70	20	20	$9.30\ x10^{-5}$	0.37	0.00	hexane	0.08
9	70	19	31	$2.27\ x10^{-5}$	0.00	1.37	toluene	1.69
10	70	19	31	$2.27\ x10^{-5}$	0.00	1.37	toluene	1.63
11	77	20	23	$2.27\ x10^{-5}$	0.00	1.37	toluene	1.58
12	77	19	39	$2.27\ x10^{-5}$	0.00	1.37	toluene	1.78
13	80	18	42	$2.27\ x10^{-5}$	0.00	1.37	toluene	1.57
14	80	10	10	$4.65\ x10^{-5}$	0.00	1.37	hexane	1.61
15	80	10	10	$7.44\ x10^{-5}$	0.37	0.00	hexane	0.13
16	80	20	20	$1.86\ x10^{-5}$	0.00	1.10	hexane	0.86
17	80	10	10	$3.49\ x10^{-5}$	1.37	0.00	hexane	0.19
18	80	20	20	$2.27\ x10^{-5}$	0.00	1.37	toluene	1.72
19	90	20	20	$5.58\ x10^{-5}$	0.37	0.00	hexane	0.23

From these 19 experiments, there are a total of 200 data points, each of which has concentration data for 4 compounds; 1-pentene, 2-pentene; hexanal and the branched aldehydes. A MATLAB routine was developed to carry out nonlinear regression analysis for the parameters given in Equations 8 to 11, minimizing the difference between experimental and estimated concentration values obtained by numerical integration of Equations 4-7. The following parameter values given in Table 3 are found to give the best solution to this optimization problem:

Table 3 Estimated values of the parameters in Equations 4-11 within 95% confidence intervals

A_1 (1/min)	$(2.88\pm0.03)\times10^{13}$
A_2 (1/min)	$(2.06\pm0.65)\times10^{13}$
A_3 (1/min)	$(2.15\pm0.0002)\times10^{14}$
A_4 (1/min)	$(2.64\pm0.03)\times10^{13}$
A_5 (1/min)	$(7.85\pm0.002)\times10^{13}$
E_{A1} (kJ/mol)	80.140±0.004
E_{A2} (kJ/mol)	81.868±0.0005
E_{A3} (kJ/mol)	73.729±0.004
E_{A4} (kJ/mol)	69.329±0.029
E_{A5} (kJ/mol)	76.856±0.654
K (mol^2/L^2)	0.3105±0.0007

Experimental and predicted concentration values from the kinetic experiments are compared in the parity plot, Figure 4.

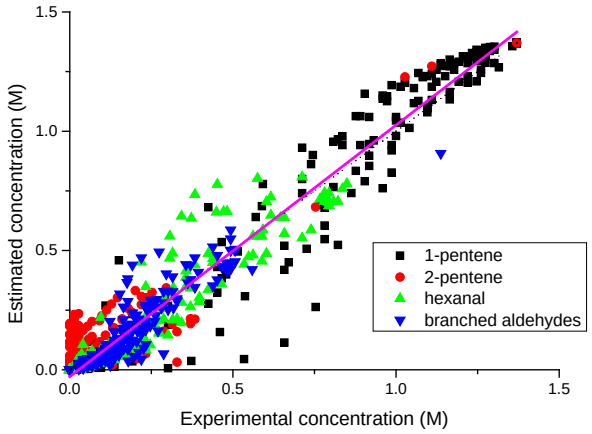

Figure 4 Parity plot comparing experimental concentration data to predicted data obtained using parameter estimates in Table 3 to evaluate Equations 4-11

Although there are some outliers, the general bulk of the data points are well around the y=x line and the models predict the experimental data quite well.

5.4 Continuous 1-Pentene Hydroformylation

Continuous 1-pentene hydroformylation reactions were planned using the kinetic information obtained; in this case it is important not to reach full conversion at steady state because this leads to a loss of kinetic data as well as information on leaching/deactivation behavior of the catalyst.

The concentration profiles are modeled assuming the total volume of the jet loop reactor system behaves as a CSTR:[16]

$$\frac{d[1-pentene]}{dt} = \frac{[1-pentene]_{feed} - [1-pentene]}{\tau} + r_2 - r_3 - r_4 - r_1 \quad (12)$$

$$\frac{d[2-pentene]}{dt} = \frac{[2-pentene]_{feed} - [2-pentene]}{\tau} + r_1 - r_5 - r_2 \quad (13)$$

$$\frac{d[hexanal]}{dt} = \frac{[hexanal]_{feed} - [hexanal]}{\tau} + r_3 \quad (14)$$

$$\frac{d[branched\ aldehydes]}{dt} = \frac{[branched\ aldehydes]_{feed} - [branched\ aldehydes]}{\tau} + r_4 + r_5 \quad (15)$$

These equations were integrated numerically using a MATLAB routine to determine the concentration of each species at a given time.

The first continuous experiment we performed was planned to prove the predictive power of kinetic data we obtained (Figure 5). The aldehyde profiles are predicted very well by the model, however, the extent of isomerization to 2-pentene is underestimated. This suggests that isomerization part of the model should be improved by performing more experiments starting with 2-pentene.

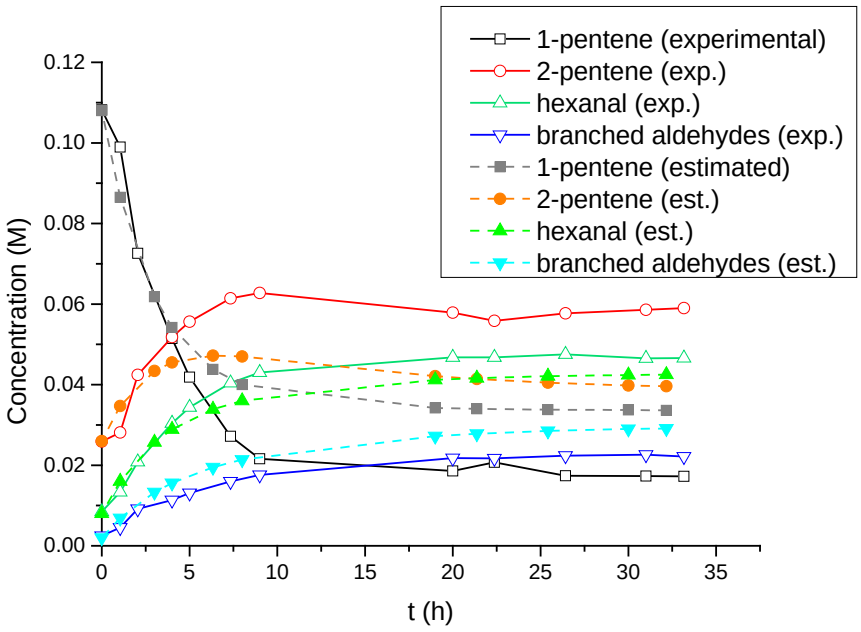

Figure 5 Continuous 1-pentene hydroformylation in the jet loop reactor ($[1\text{-pentene}]_{feed}$= 0.13 M, $[2\text{-pentene}]_{feed}$= 0.015 M, $[1\text{-pentene}]_0$= 0.108 M, $[2\text{-pentene}]_0$= 0.026 M, $[hexanal]_0$= 0.008 M, $[branched\ aldehydes]_0$= 0.002 M, [Rh] = 4.0×10^{-6} M, L/Rh= 30, 20 bar $CO:H_2$ (1:1) ,T = 80°C, τ = 14.3h, solvent=toluene)

We obtained a TTON of 47 600 in about 2 residence times. This number can be improved to almost one million only by using 1-pentene without a solvent, and increasing the temperature to 100°C at these conditions would give a TTON around two million! We were not able to realize these experiments due to some technical problems but hope to do so in the near future.

5.5 Selectivity

The regioselectivity of the reaction can be modeled as the ratio of the rates of linear and branched aldehyde formation, Equations 6 and 7 respectively, as given in Equation 16 below:

$$\frac{l}{b} = \frac{r_3}{r_4 + r_5} \tag{16}$$

Substituting r_3,r_4 and r_5 and simplifying the equation, one obtains the equation given in Equation 17 to express the regioselectivity of the reaction.

$$\frac{l}{b} = \frac{k_3[1-pentene](K + [CO][2-pentene])}{K(k_4[1-pentene] + k_5[2-pentene]) + [CO][1-pentene][2-pentene](k_4 + k_5)} \tag{17}$$

According to Equation 17, regioselectivity is a function of CO concentration, temperature and alkene concentration. This means that the regioselectivity of the reaction changes during batch

reactions according to changes in isomer alkene concentrations and this is what we observe as well. It is hard to predict any clear dependencies on the parameters listed, according to Equation 17, since it is very non-linear.

For continuous operation, the l/b ratio should be constant at steady state once the isomer alkene concentrations reach their steady state values. This is what we observed also for the continuous run given in Figure 5. As done for that experiment, we used kinetics to predict the steady state concentration of aldehydes for different operating conditions such as pressure and temperature. Figure 6 below shows the fraction of linear aldehyde in the product aldehyde mixture as a function of T and P.

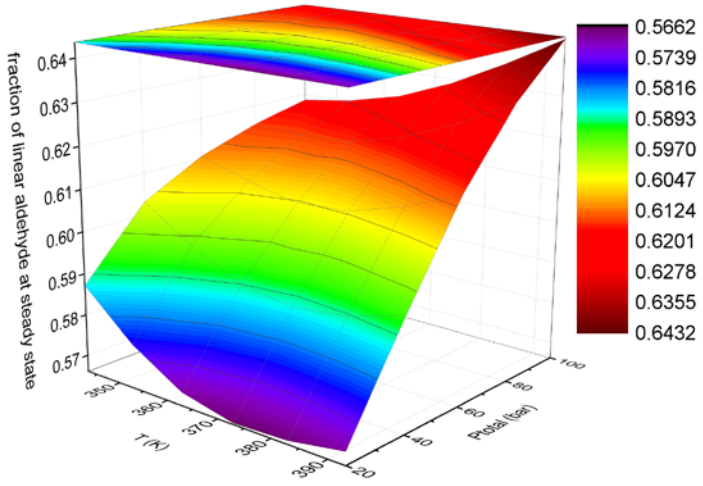

Figure 6 Calculated temperature and pressure dependence of the fraction of linear aldehyde in the product aldehyde mixture at steady state ($CO:H_2$=1, $[1\text{-pentene}]_{feed}$= 1 M, $[1\text{-pentene}]_0$= 1 M, [Rh] = 4.0×10^{-6} M, L/Rh= 30, τ = 14.3 h, solvent=toluene)

Figure 6 shows that the linear aldehyde is between 56-65% of the product aldehydes at process conditions 343-393 K, 20-100 bar and increases with increasing total pressure at a given temperature, since isomerization is suppressed by increased CO pressure. Increasing the temperature at 20 bar results in a decrease of the linear aldehyde fraction, whereas after 60 bar, this behavior is reversed and increasing the temperature increases the fraction of linear aldehyde. The difference probably arises from the fact that at higher pressures where isomerization is suppressed, the 4 kJ/mol difference between the activation energies E_{A3} and E_{A4} starts to show its effect more and more clearly, especially at elevated temperatures. The optimal operating point can be chosen according to the relative cost of operating at certain process conditions and the separation costs involved with the achieved selectivity.

5.6 Mass Transfer Limitations

According to the results presented in Chapter 2, we have discussed that a minimum volumetric mass transfer coefficient of $k_l a$ =0.1 s^{-1} should be available in the jet loop reactor for 1-pentene hydroformylation. Accordingly, we modeled the change in concentration of dissolved gas in the reactor for the jet loop reactor as follows:

$$\frac{d[CO]}{dt} = k_l a([CO]^{sat} - [CO]) - r_3 - r_4 - r_5 \quad (18)$$

$$\frac{d[H_2]}{dt} = k_l a([H_2]^{sat} - [H_2]) - r_3 - r_4 - r_5 \quad (19)$$

If we calculate the saturation gas concentrations as given in Section 5.2 and assume $k_l a$ =6 $min^{-1}$for both CO and H_2, we obtain the following H_2 concentrations in the liquid over time for the specified reaction conditions. We chose to show H_2 since it has a lower equilibrium concentration compared to CO and would be depleted faster given the two gases have similar $k_l a$ values.

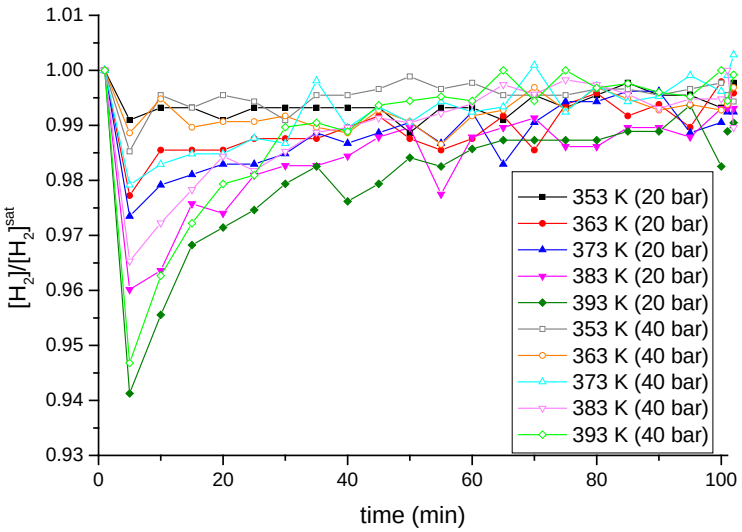

Figure 7 Estimated H_2 concentration normalized to its equilibrium concentration over time for reaction conditions specified in the legend, and CO:H_2=1, $[\text{1-pentene}]_{feed}$= 1 M, $[\text{1-pentene}]_0$= 1 M, [Rh] = 4.0x10^{-6} M, L/Rh= 30, τ = 14.3 h, solvent=toluene

As seen from Figure 7, between 353-393 K, for specified reaction conditions, the H_2 concentration does not fall below 94% of its saturation value, even at 20 bar. About 20 minutes after the start of the reaction, the H_2 concentration is above 97% of its saturation value for all temperatures and pressures presented in Figure 7. The values obtained for CO are slightly better. Changing the

concentration of 1-pentene or the residence time will of course also have an effect on these profiles. Furthermore, we assumed that mass transfer from syngas to reaction mixture takes places at a rate that we determined as the lower limit and is constant for all reaction mixture compositions. However, we showed in Chapter 2 that $k_l a$ increases with increased specific power input and the presence of polar aldehyde has a positive effect on $k_l a$; so it is also concentration dependent. In short, it is possible to obtain $k_l a$ values of 0.9 s^{-1} in the jet loop reactor. It should be clear that mass transfer limitations can be avoided by determining the specific mass transfer rate for the aimed steady state reaction mixture beforehand and choosing process conditions accordingly.

5.7 Conclusions

A detailed kinetic study of 1-pentene hydroformylation was carried out for a tris(2,4-di-*tert*-butylphenyl) phosphite modified Rh catalyst. Rate equations were derived for alkene isomerization and hydroformylation of both 1-pentene and 2-pentene. The parameters in the rate equations were estimated using non-linear regression. The kinetic information obtained was used to predict the concentration over time during continuous 1-pentene hydroformylation in a jet loop reactor and a continuous run was demonstrated. The extremely fast kinetics of this substrate makes it an excellent candidate for obtaining very high total turnover numbers in the jet loop reactor. We obtained a TTON of 47600 in just two residence times using a very dilute 1-pentene feed. The highest TOF was achieved in the beginning of the reaction: 3700 h^{-1}, which stabilized at 1200 h^{-1} at steady state. In principle it is possible to increase the TTON to one million at the same conditions only by changing to pure 1-pentene feed. The fast kinetics of this substrate also bears the possibility of mass transfer limitations, especially at elevated temperatures. We investigated the concentration of H_2 and CO in the reaction mixture at different temperatures and pressures, including the proposed reaction conditions to obtain one million TTON in two residence times. The calculations showed that even when using the minimum mass transfer coefficient value determined beforehand, the concentration of gases in the liquid remain very close to the equilibrium values. The steady-state selectivity of the reaction is a complex function of temperature and pressure. We showed that it can be optimized.

5.8 Experimental

5.8.1 Materials

1-Pentene was kindly supplied by Evonik Industries. All other chemicals were purchased from Aldrich, Merck, Acros or Biosolve. All air/water sensitive solutions were prepared under argon using Schlenk techniques. The substrate solution containing 1-pentene and decane as internal

standard was filtered over neutral alumina and degassed. A stock solution of catalyst (Rh precursor: $Rh(acac)(CO)_2$ and Ligand) was prepared in dry and degassed solvent. Solvents were dried and degassed using a custom-made alumina-filled Ar-flushed column. Gas chromatography (GC) measurements were done on a Shimadzu GC-2010 gas chromatograph using an Agilent DB1 column (30m x0.32mm i.d.).

5.8.2 Kinetic batch experiments

Batch reactions for kinetics were performed in custom built stainless steel autoclaves (100 ml) equipped with a mechanical gas-impeller stirrer and a mass flow controller (MFC) to monitor the gas uptake and to keep the reaction pressure constant. A stirring rate of 1200 rpm was set for all kinetic experiments. Samples were taken during the course of the reaction via a capillary through a valve connected to the reactor. The substrate solution was filled into a dropping funnel (30 ml) connected to the autoclave by a tube that keeps the funnel at the same pressure as the autoclave and a valve that enables controlled charge of the substrate solution into the autoclave. The catalyst solution was charged in the autoclave where it was preformed under reaction conditions for one hour. The reaction was started by adding the substrate solution.

Reactant and product compositions were measured by gas chromatography (GC) and gas uptake data was used to confirm the trend in aldehyde formation.

5.8.3 Continuous jet loop experiments

The reaction start-up was performed as follows: The reactor was purged with syngas pressure before the reactor was filled with substrate solution under argon flow to the designated level by the HPLC pump. The catalyst solution was added into the dropping funnel under argon which is connected to the reactor by a valve. It is possible to preform the catalyst in this heated compartment under pressure. The reactor was heated and pressurized to the reaction conditions and after the flux through the membrane reached steady state, preformed catalyst solution was added to start the reaction. A mass flow controller kept the reaction pressure constant and the gas uptake was monitored to confirm conversion values obtained by GC sampling.

5.8.4 In-*situ* HP-IR experiments

In situ HP-IR experiments were carried out in a custom built stainless steel autoclave (50 ml) with an integrated flow cell equipped with ZnS windows and a mechanical gas-impeller stirrer (800 rpm for all FT-IR measurements). The spectra were recorded on a Shimadzu FT-IR 8300 spectrometer, in absorbance mode. Catalyst solution in hexane was preformed under syngas and the reaction was

started after complete hydride formation by addition of the substrate, kept in a dropping funnel. Background measurements were performed just before the addition of the substrate.

5.9 References

[1] K.-D. Wiese, D. Obst, in *Catal. Carbonylation React.* (Ed.: M. Beller), Springer Berlin Heidelberg, **2006**, pp. 1–33.

[2] A. J. Sandee, L. A. van der Veen, J. N. H. Reek, P. C. J. Kamer, M. Lutz, A. L. Spek, P. W. N. M. van Leeuwen, *Angew. Chem. Int. Ed.* **1999**, *38*, 3231–3235.

[3] C. Vogl, E. Paetzold, C. Fischer, U. Kragl, *J. Mol. Catal. Chem.* **2005**, *232*, 41–44.

[4] M. Beller, B. Zimmermann, H. Geissler, *Chem. Eur. J.* **1999**, *5*, 1301–1305.

[5] R. Lazzaroni, P. Pertici, S. Bertozzi, G. Fabrizi, *J. Mol. Catal.* **1990**, *58*, 75–85.

[6] A. van Rooy, P. C. J. Kamer, P. W. N. M. van Leeuwen, K. Goubitz, J. Fraanje, N. Veldman, A. L. Spek, *Organometallics* **1996**, *15*, 835–847.

[7] S. C. van der Slot, J. Duran, J. Luten, P. C. J. Kamer, P. W. N. M. van Leeuwen, *Organometallics* **2002**, *21*, 3873–3883.

[8] C. Cai, S. Yu, B. Cao, X. Zhang, *Chem. Eur. J.* **2012**, *18*, 9992–9998.

[9] K. Takahashi, M. Yamashita, Y. Tanaka, K. Nozaki, *Angew. Chem. Int. Ed.* **2012**, *51*, 4383–4387.

[10] A. van Rooy, E. N. Orij, P. C. J. Kamer, F. van den Aardweg, P. W. N. M. van Leeuwen, *J. Chem. Soc. Chem. Commun.* **1991**, 1096–1097.

[11] P. W. N. M. van Leeuwen, C. F. Roobeek, *J. Organomet. Chem.* **1983**, *258*, 343–350.

[12] "NIST Chemistry WebBook," can be found under http://webbook.nist.gov/

[13] P. C. J. Kamer, A. van Rooy, G. C. Schoemaker, P. W. N. M. van Leeuwen, *Coord. Chem. Rev.* **2004**, *248*, 2409–2424.

[14] A. van Rooy, E. N. Orij, P. C. J. Kamer, P. W. N. M. van Leeuwen, *Organometallics* **1995**, *14*, 34–43.

[15] C. Kubis, R. Ludwig, M. Sawall, K. Neymeyr, A. Börner, K.-D. Wiese, D. Hess, R. Franke, D. Selent, *ChemCatChem* **2010**, *2*, 287–295.

[16] H. S. Fogler, *Elements Of Chemical Reaction Engineering*, Prentice Hall Professional Technical Reference, **2006**.

Chapter 6

Ceramic Membrane Nanofiltration: Permeability and Rejection Characteristics

---

In this part of the study, solvent permeability and ligand retention were characterized for a TiO_2 ceramic nanofiltration membrane used in a jet loop reactor setup. Three models reported in the literature to predict solvent permeability as a function of solvent characteristics were investigated. The results were used to model the permeate rate of any solvent (mixture) as a function of process variables. It was shown that two of these models can be used as well to predict the temperature dependence of permeability, when temperature dependence of physical properties were incorporated in the model.

Rejection of the ligand in toluene was modeled as a function of temperature, trans membrane pressure and ligand concentration in the reactor, extending the solution-diffusion model reported in the literature to take temperature dependencies into account. This model allows the prediction of the amount of ligand leaching through the membrane for pure toluene. Further investigation will be necessary to extend the model for real reaction mixtures.

6.1 Ceramic Membrane Nanofiltration

The first organic solvent nanofiltration membranes developed were polymeric membranes.[1] Although ceramic membranes have been used in aqueous processes like waste water treatment for a long time, they have been applied only lately in organic solvent nanofiltration[2] due to challenges in obtaining smaller pore sizes.[1] By the end of the 20th century, zirconia and titania doped, silica-based ceramic nanofiltration membranes were developed successfully and are commercially available under the name Inopor.[3] Their superior chemical and mechanical stability in organic solvents and wider operating range in terms of temperature compared to polymeric membranes makes ceramic nanofiltration membranes a promising separation tool in chemical applications.[4,5]

Figure 1 Ceramic membranes available from Inopor[3]

Although the separation of organometallic complexes by membrane separation started to appear in the patent literature in the early 1970s,[6–8] the separation and recycling of homogeneous catalysts by means of nanofiltration has been reported first around the early 2000s,[9–12] following the development of solvent resistant nanofiltration membranes.[1]

An elegant example of continuous hydroformylation using ceramic membrane nanofiltration has been recently reported by Vogt et al.[13] The researchers reported an accumulated turn over number of 120 000 using a POSS enlarged PPh_3 ligand Rh catalyst for 1-octene hydroformylation.

6.2 Solvent Permeability Models

As in every chemical operation, an important aspect of membrane nanofiltration is predictability. Modeling the solvent flux behavior is of great interest, since it determines design parameters such as membrane area and process parameters like trans membrane pressure and filtration temperature. It is also important to know if the flux behavior for mixtures leads to different mixture compositions in the retentate and permeate. This of course will be relevant for a reaction mixture, i.e. accumulation of certain species and changes in reactor concentration.

Thus, recent research on ceramic membranes is focused on the prediction of solvent flux and rejection characteristics.[2,5,14–16]

6.2.1 Coupled Series–Parallel Resistance Model

In 2009 Darvishmanesh et al.[5] proposed a model for predicting solvent fluxes through inorganic nano-filtration membranes: the Coupled Series–Parallel Resistance Model. The model introduces three different resistances to permeation of a solvent through the membrane: i) resistance at the active top layer $\mathbf{R_s}$, which acts in series to the following two that are "parallel" to each other: ii) pore resistance to viscous flow in the nanopores $\mathbf{R_p}$, and iii) matrix resistance for diffusive flow through the ceramic material $\mathbf{R_m}$.

The total resistance is then given as:

$$R_{total} = R_s + \frac{R_m \times R_p}{R_m + R_p} \tag{1}$$

where:

$$R_s = k_s \left(\frac{r_s}{r_p}\right)^2 exp(1-\beta) \tag{2}$$

$$\beta_{hydrophilic\ membrane} = \frac{\gamma_{LV}}{\gamma_{SV}} \tag{3}$$

$$R_m = k_m \left(\frac{\mu}{\alpha}\right) \tag{4}$$

$$\alpha_{hydrophilic\ membrane} = \frac{\epsilon_L}{\epsilon_M} \tag{5}$$

$$R_p = k_p \left(\frac{r_s}{r_p}\right)^2 \mu \tag{6}$$

In the equations above r_s: the solvent molecular size, r_p: the pore size of the membrane, γ_{LV} :surface tension of the solvent, γ_{SV}: surface tension of the membrane, μ:viscosity, ϵ_L: dielectric constant of the solvent and ϵ_M: dielectric constant of the membrane. Constants k_s, k_m and k_p are membrane specific and need to be estimated for the membrane in use by nonlinear regression. Once

determined, they can be used in the model to predict fluxes of other solvents. And the total solvent flux (J) is then written as the ratio of trans-membrane pressure ΔP and R_{total}:

$$J = \frac{\Delta P}{R_{total}} \tag{7}$$

The model can be extended to predict the permeation of a mixture by calculating a total resistance for the mixture using molar fractions:

$$R_{total,mix} = \sum x_i R_{total,i} \tag{8}$$

6.2.2 Phenomenological Model 1

Another study by Patrizia Marchetti et al.[2] proposed to use a correction factor to modify the Hagen-Poiseuille model, which takes the interaction between pore walls and the solvent into account. Hagen-Poiseuille model flux J_{HP} is a function of solvent viscosity μ and trans-membrane pressure ΔP and a membrane specific constant K_{HP} :

$$J_{HP} = \frac{K_{HP}}{\mu}\Delta P \tag{9}$$

And permeability L is given as follows:

$$L_{HP} = \frac{K_{HP}}{\mu} \tag{10}$$

This model describes the flux through ultra-filtration (UF) membranes quite well but fails to do so for nanofiltration (NF) membranes. The correction proposed is a combination of three effects: capillary rise in the nanopores, polarity and molecular dimensions of the solvent. Capillary rise in the nanopores is described by the Lucas-Washburn equation, which determines the capillary pressure as a function of liquid surface tension γ_{LV}, contact angle θ and membrane pore radius r_p. The polarity of the solvent is described by the dipole moment and the interaction between the solvent and membrane is accounted for by taking the difference between solvent dipole δ_s and membrane polarizability k_{pol}. The last contribution is the ratio between solvent radius r_s and membrane pore size radius r_p. The correction factor f_c is estimated as a sum of all three factors with membrane specific correction constants C_1, C_2 and C_3.

$$f_c = f_{Ccapillary} + f_{Cdipole} + f_{Csteric} = C_1 \frac{2\gamma_{LV} cos\theta}{r_p} + C_2 \left|\delta_s - k_{pol}\right| + C_3 \left(\frac{r_s}{r_p}\right)^2 \quad (11)$$

The contact angle θ is determined using the equation given below:

$$\cos\theta = \left(2\sqrt{\gamma_{sv}^d} + k_{pol}\frac{\gamma_{lv}^p}{\sqrt{\gamma_{lv}^d}}\right)\frac{\sqrt{\gamma_{lv}^d}}{\gamma_{lv}} - 1 \quad (12)$$

with

$$k_{pol} = 2\sqrt{\frac{\gamma_{sv}^p}{\gamma_{lv}^p}} \quad (13)$$

where $\gamma_{sv}^d, \gamma_{sv}^p, \gamma_{lv}^d$ and γ_{lv}^p are dispersion and polar components of solid and liquid surface tension, respectively. Then the permeability through the membrane can be estimated using the equation below:

$$L = L_{HP}(1 + f_c) \quad (14)$$

The model is extended to solvent mixtures using the equations given below:

$$L_{mix} = L_{HP}(1 + f_{c,mix}) \quad (15)$$

$$f_{c,mix} = \sum x_i f_{c,i} \quad (16)$$

6.2.3 Phenomenological Model 2

This very simple model has been proposed very recently by Buekenhoudt et al.[16] The solvent flux is given as follows:

$$\frac{J_i \times \mu_i}{J_{H_2O} \times \mu_{H_2O}} = (1 - C) + C\frac{\delta_{tot,i}}{\delta_{tot,H_2O}} \quad (17)$$

where δ_{tot} is the total Hansen solubility parameter, μ the viscosity and constant C is determined experimentally. The authors report C=1.45 for TiO_2 membranes with a pore size of 0.9 nm.

The origin of this model is the observation that flux times viscosity has a linear dependence on the Hansen solubility parameter:

$$J_i \times \mu_i = A + B\delta_{tot,i} \quad (18)$$

6.2.4 Estimation and sources of parameter values in the models

Table 1 Parameter values and sources to estimate the presented solvent permeability models

Parameter	Reference
r_s: the solvent molecular size (nm)	$r_s = \left(\frac{V_m}{N_A}\right)^{1/3}$
V_m: molecular volume (nm^3)	$V_m = \frac{MW}{density}$
r_p: the pore radius of the membrane (nm)	0.9 (Supplier [3])
γ_{LV} :surface tension of the solvent (mN/m)	Calculated using ASPEN Properties[17]
γ_{SV}: surface tension of the membrane (mN/m)	54.7 (reported for HITK275 TiO_2 membrane[2,5])
μ:viscosity (mPa.s , bar.h for P Model 1)	Calculated using ASPEN Properties[17]
ϵ_L: solvent dielectric constant	[18,19]
ϵ_M: membrane dielectric constant	86 (reported for HITK275 TiO_2 membrane[5])
δ_{tot} : total Hansen solubility parameter ($MPa^{1/2}$)	$\left((\Delta H_v - RT)/V_m\right)^{0.5}$
ΔH (kJ/mol)	$\frac{\Delta H}{\Delta H^0} = \left(\frac{1-T_r}{1-T_r^0}\right)^{0.38}$ [20]
γ_{sv}^d : dispersion component of solid surface tension (mN/m)	27.1[2]
γ_{sv}^p: polar component of solid surface tension (mN/m)	28.2[2]
γ_{lv}^d: dispersion component of liquid surface tension (mN/m)	[21],*
γ_{lv}^p : polar component of liquid surface tension (mN/m)	[21],*
δ_s:solvent dipole (Debye)	[22,23]

** Components of liquid surface tension are reported for some solvents.[21] Unknown liquid surface tension components can be estimated using contact angle data for the solvent in question measured on a surface where the contact angle is reported[24] for some other solvents with known liquid surface tension components. Rearranging equation 11 and plotting* $(\cos\theta + 1)/\left(2\sqrt{\gamma_{lv}^d/\gamma_{lv}}\right)$ *vs* $\sqrt{\frac{\gamma_{lv}^p}{\gamma_{lv}^d}}$ *gives* $\sqrt{\gamma_{sv}^p}$ *as the slope and* $\sqrt{\gamma_{sv}^d}$ *as the intercept. Then, for a solvent of known surface tension, it is possible to reduce the number of unknowns in Equation 11 to one and deduce both components of liquid surface tension, since* $\gamma_{lv} = \gamma_{lv}^p + \gamma_{lv}^d$*. This technique was used to calculate components of acetonitrile and methanol surface tension in this study. For apolar solvents (toluene, cyclooctene, cyclooctane and pentane), we used the following equations reported in literature;[25]*

$$\gamma_{lv}^p = \frac{I_{ll}^p}{2} \quad (19)$$

$$I_{ll}^p = \frac{n_s}{2} i_{ll} \quad (20)$$

$$n_s = \left(\frac{density}{MW} N\right)^{\frac{2}{3}} \tag{21}$$

$$i_{ll} = \frac{2\delta_l^2}{4\pi\varepsilon_0 r_{ll}^3} \tag{22}$$

$$r_{ll} = \left(\frac{1}{n_v}\right)^{1/3} \tag{23}$$

$$n_v = (n_s)^{3/2} \tag{24}$$

In the above given equations, ε_0=8.854x10^{-12} C^{2}J^{-1}m^{-1}, N=6.022x10^{23} is the Avogadro number, density has units kg/m^3, MW is in kg/mol, δ_l is the solvent dipole moment in C.m which equals $3.336x10^{-30}\delta_s$. γ_{lv}^p is then found in Jm^{-2} and can be converted to mN/m by multiplying with 1000.

6.2.5 Comparison of Model Performances

A comparison of the model performances was done using the data from 16 solvent permeation experiments, performed with 5 different solvent/mixtures at different temperatures. Temperature independent (or assumed to be so) properties of the solvents used are given in Table 2. These models have been evaluated at room temperature in the original reports, so these experiments will also allow an evaluation of their performance for temperature dependent flux prediction.

Table 2 Temperature independent properties of solvents used (dipole moment and dielectric constant are not temperature independent but assumed to be so)

Solvent	MW(g/mol)	δ_s (Debye)	ϵ_L	T_c (K)
Toluene	92.14	0.31	2.38	591.8
Cyclooctene	110.2	0.43	2*	636.5
Cyclooctane	112.2	0	2*	647.2
Pentane	72.14	0	1.84	469.8
Methanol	32.04	2.87	32.7	513
Acetonitrile	41.05	3.44	37.5	545

**Dielectric constant of cyclohexane*

The permeate rates obtained for these 16 experiments are reported along with temperature dependent parameters of models in Table 3.

Table 3 Permeate rates and temperature dependent parameter values for permeation experiments

Entry	Solvent	T (°C)	μ (mPA.s)	γ_{LV} (mN/m)		density (g/cm3)		γ^d_{lv} (mN/m)		ΔHvap (kJ/mol)	V_m (cm^3)	δ_{tot} ($MPa^{0.5}$)	L (L/m^2 h bar)
1	Toluene	28	0.58	26.81		0.87		26.81		37.77	105.82	18.3	0.57
2		40	0.5	25.57		0.86		25.57		37.17	107.60	17.9	0.67
3		50	0.44	24.55		0.84		24.55		36.65	109.13	17.6	0.78
4		60	0.39	23.52		0.83		23.52		36.13	110.71	17.4	0.95
5	80%C.octene 20%C.octane	35	1.32	27.34	27.63	0.84	0.84	27.22	27.63	40.91	131.71	17.1	0.12
6		50	1.1	25.91	26.18	0.82	0.83	25.80	26.18	40.19	134.11	16.7	0.17
7		60	0.97	24.96	25.21	0.81	0.82	24.85	25.21	39.70	135.76	16.5	0.2
8		70	0.87	24.00	24.24	0.80	0.81	23.90	24.24	39.20	137.46	16.3	0.21
9	Pentane	22	0.24	15.52		0.64		15.52		26.20	112.65	14.5	0.18
10		30	0.22	14.74		0.63		14.74		25.74	114.36	14.2	0.26
11		40	0.2	13.76		0.62		13.76		25.14	116.58	13.9	0.28
12		50	0.18	12.78		0.61		12.78		24.52	118.89	13.6	0.35
13	Methanol	32	0.49	22.39		0.79		12.94		37.60	40.67	29.4	3.58
14		40	0.45	21.55		0.78		12.45		37.04	41.17	28.9	4.45
15		50	0.4	20.50		0.77		11.85		36.33	41.81	28.4	6.31
16	Acetonitrile	22	0.34	28.66		0.79		18.28		33.23	52.23	24.3	10.12

Pentane experiments given in entries 9-12 of Table 3 were not used to estimate the parameters in the phenomenological Model 1 since γ_{lv}^{p} for pentene is zero and k_{pol} is therefore undefined. For the same reason, for the cyclooctene-cyclooctane mixture, k_{pol} for cyclooctane was assumed to be equal to that of cyclooctene. According to the data presented, parameter values given in Table 4 were estimated for CSPR and Phenomenological Model 1, using nonlinear regression.

Table 4 Parameter values estimated using nonlinear regression for CSPR and P. Model 1

Model	Parameter	Value
CSPR	k_m	0.15
	k_s	2.22×10^{-14}
	k_p	3.98×10^{4}
Model 1	C_1	0.025
	C_2	-0.1481
	C_3	4.6226

The K_{HP} value for Phenomenological Model 1 was determined by linear regression as 1×10^{-12} L/m^2. A linear fit was carried out for fitting parameters in Equation 18 of Phenomenological Model 2, as shown in Figure 2. Equation 25, which is the re-written form of Equation 18 with a change to obtain only positive permeate rates, gives parameters A and B. It is obvious from the methanol data

in Figure 2 that the model cannot predict the temperature dependence of permeability, and acetonitrile has a higher product of permeation rate times viscosity than methanol although its solubility parameter is lower.

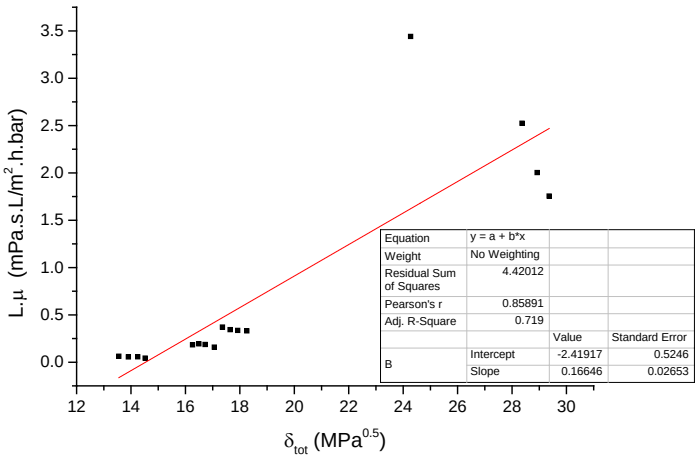

Figure 2 Linear fit for parameters in Phenomenological Model 2

$$L_i \times \mu_i = \left|-2.4192 + 0.1665\delta_{tot,i}\right| \quad (25)$$

Figure 3 shows a comparison of the experimental permeation data and values estimated using the models and parameter estimates reported. CSPR and P. Model 1 predict pretty close values. The standard deviations of the models calculated are 0.69, 0.90 and 1.44 for CSPR, P. Model 1 and P. Model 2 respectively. CSPR is the best performing model for prediction of permeation rate among the 3 models we considered here. Both CSPR and P. Model 1 allow a good incorporation of temperature in the model by including temperature dependencies of physicochemical properties. Including the temperature dependencies of dipole moment and dielectric constant as well would probably improve the model performances. Unfortunately, physicochemical data on these properties is very hard to find.

The models now can be used to predict the permeation of a reaction mixture through the membrane as a function of temperature and applied trans membrane pressure. However, it should be kept in mind that the parameters fitted for these models are membrane specific and probably will not be useful for another membrane of same specifications produced in a different batch by the same producer. Literature reports that three different batches of 0.9 nm TiO_2 membranes gave quite a span of toluene fluxes: 47, 1.5 and 10 L/m^{2}h. [16] On the other hand, ceramic membranes are pretty

stable under process conditions and the same membrane can be used for a long time. They can also be stored very easily, so buying a stock of membranes from the same batch is an attractive solution.

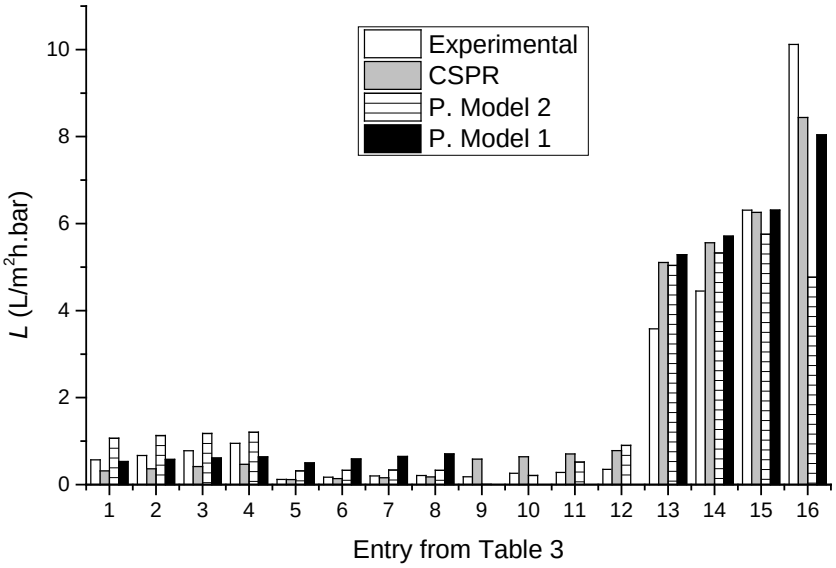

Figure 3 Experimental permeation data and values estimated using the permeation models

6.3 Rejection Behavior

High rejection of the catalyst by the membrane while supplying a reasonable permeate rate for the product is the key point in nanofiltration assisted continuous homogeneous catalysis. To determine the rejection behavior of the catalyst in advance and apply a make-up for the lost catalyst is essential for long term continuous operation.

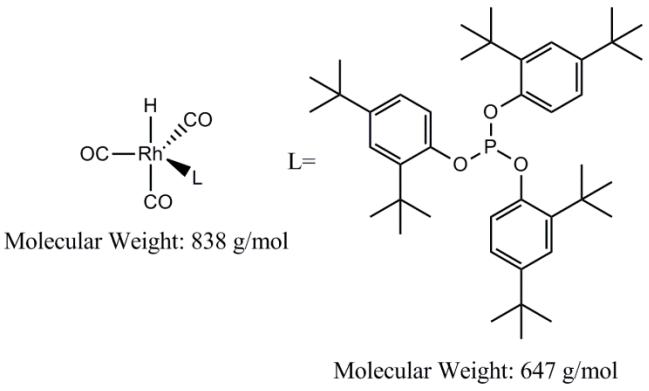

Scheme 1 Active catalyst (left) and the ligand (right) used in this study

The influence of solute size is proven to be the most important parameter that determines the rejection.[26,27] The active catalyst molecule we used in this study has a MW of 835 g/mol as given

in Scheme 1. A high excess of ligand to Rh is necessary to keep all the Rh centers coordinated with a ligand, in order to keep the catalyst active as well as to prevent metal leaching.

We studied the retention of the ligand as a function of process parameters such as temperature, applied trans membrane pressure and concentration of ligand. Toluene was used as the solvent, and the concentration in the permeate was determined using UV/Vis. Figure 4 shows the UV/Vis spectrum of bulky phosphite ligand, tris(2,4-ditert-butylphenyl) phosphite in toluene, measured on a reference of pure toluene, the ligand gives a peak around 286 nm. Peak areas were used to determine the concentration according to the calibration performed.

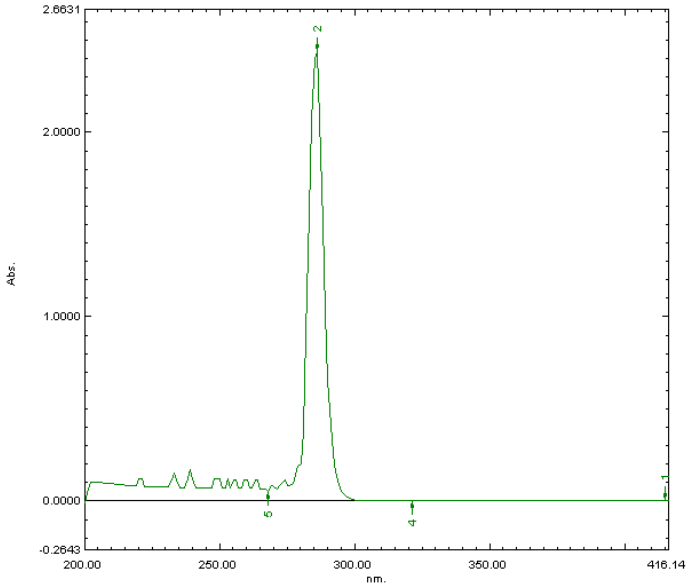

Figure 4 UV/Vis spectrum of tris(2,4-ditert-butylphenyl) phosphite ligand, concentration=6.4 mg/ml

Results of the retention experiments performed are given below in Table 5.

Table 5 Retention experiments performed with tris(2,4-ditert-butylphenyl) phosphite ligand in toluene

Entry	$\Delta P \times 10^{-5}$ ($kg.m^{-1}s^{-2}$)	T (°C)	$J \times 10^{3}$ ($kg.m^{-2}s^{-1}$)	C_{feed} ($kg.m^{-3}$)	$C_{toluene}$ ($kg.m^{-3}$)	$C_{permeate}$ ($kg.m^{-3}$)	C_f-C_p ($kg.m^{-3}$)
1	18.6	40	1.65	1.06	856.3	0.05	1.01
2	17.9	50	1.94	1.05	856.3	0.05	1.00
3	16.8	60	2.12	1.05	844.3	0.05	1.00
4	15.9	70	2.52	1.04	832.3	0.05	1.00
5	14.7	80	2.87	1.03	820.3	0.04	1.00
6	14.3	80	2.89	2.09	808.3	0.04	0.99
7	14.2	80	2.83	3.15	808.3	0.07	2.03
8	13.6	80	2.68	3.14	808.3	0.07	3.08
9	9.6	80	1.77	3.12	808.3	0.22	2.92
10	7.0	80	1.32	3.11	808.3	0.21	2.92

We used the solution-diffusion model reported in literature for aqueous systems[26,27] to analyze the data obtained, in order to model the ligand concentration in the permeate $C_{permeate}$. According to this model, $C_{permeate}$ is estimated as given in Equation 26.

$$C_{permeate} = \frac{C_{feed}}{1 + \frac{L_{solvent}\Delta P}{L_{solute}C_{solvent}} - \frac{\varphi C_{feed}L_{solvent}}{L_{solute}C_{solvent}}} \quad (26)$$

The concentration of ligand in the reactor originally is C_{feed} (kg/m^3), $L_{solvent}$ (s/m) and L_{solute} (s/m) are permeability of solvent and solute, respectively, and Ψ (m^2/s^2) is the osmotic pressure coefficient. $L_{solvent}$ is determined using pure solvent; so we will use the data presented in Table 3. The model as reported, does not take temperature dependence into account. We will extend the model to represent the temperature dependencies of solvent permeability and osmotic pressure coefficient. Plotting a graph of $L_{toluene}$ vs. temperature as given in Figure 5 allows us to determine the permeability as a linear function of temperature as expressed in Equation 27.

$$L_{toluene} = 2.88\text{x}10^{-11}\text{T(°C)} + 5.11\text{x}10^{-10} \quad (27)$$

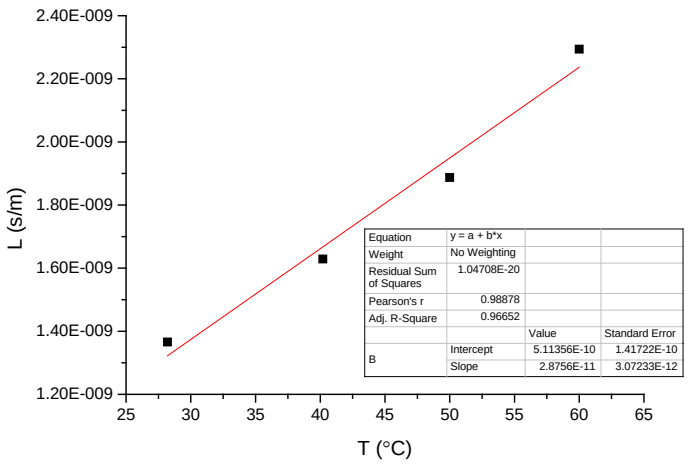

Figure 5 Temperature dependence of pure toluene permeability

L_{solute} is calculated from Equation 28

$$\frac{J.C_{permeate}}{C_{toluene}} = L_{solute}(C_{feed} - C_{permeate}) \quad (28)$$

Plotting flux times permeate concentration divided by temperature corrected toluene concentration vs. the difference between feed and permeate concentrations of the ligand then gives L_{solute} =1.50x10^{-7} as the slope as shown in Figure 6.

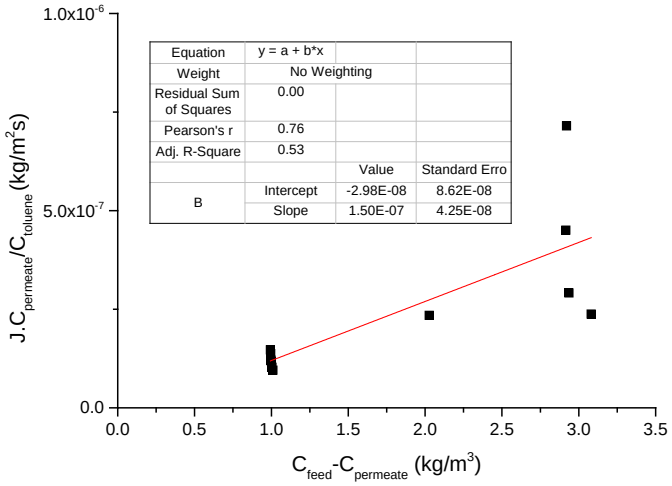

Figure 6 Determination of L_{solute} from the slope of the line given by Equation 28

The osmotic pressure coefficient Ψ is determined using Equation 29,

$$\Delta\pi = \varphi\left(C_{feed} - C_{permeate}\right) \tag{29}$$

Δπ in this equation is the difference between the trans membrane pressure applied to obtain the solute+solvent permeate and the trans membrane pressure that would be required to obtain the same permeate rate for the solvent only, as given in Equation 30

$$\Delta\pi = \Delta P - J/L_{solvent} \tag{30}$$

Because we would like to see the effect of temperature on the osmotic pressure coefficient, we first determined the pressure dependence of Δπ by plotting ΔP/(J/$L_{solvent}$) vs. temperature for the experiments performed at the same C_{feed}-$C_{permeate}$ values, i.e. entries 1 to 5 in Table 5. J/$L_{toluene}$ values were calculated using $L_{toluene}$ estimates obtained by Equation 27. Figure 7 shows that ΔP/(J/$L_{toluene}$) decreases linearly with increasing temperature, according to Equation 31 given below

$$\Delta P/(J/L_{toluene}) = -1.0769\text{x}10^{-2}T(°C) + 2.344 \tag{31}$$

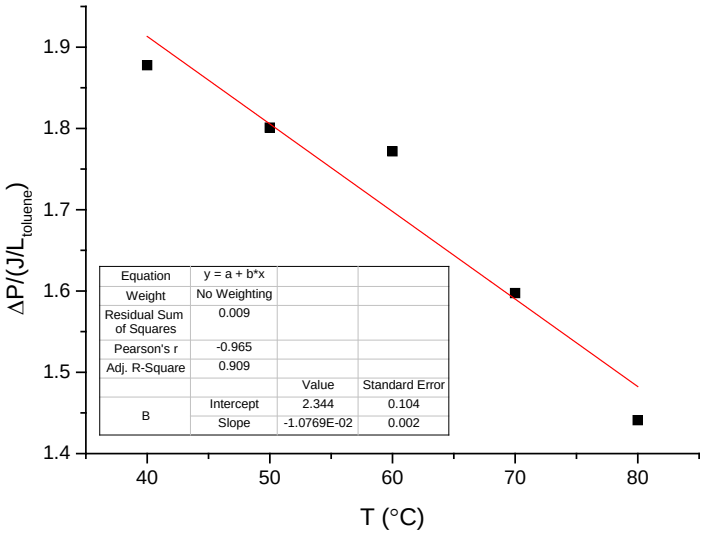

Figure 7 Temperature dependence of ΔP/(J/$L_{toluene}$)

The effect of concentration difference across the membrane, C_{feed}-$C_{permeate}$, on the osmotic pressure difference is determined by plotting ΔP/(J/$L_{toluene}$) vs. C_{feed}-$C_{permeate}$ for experiments performed at the same temperature, 80°C, which are entries 5 to 10 in Table 5.

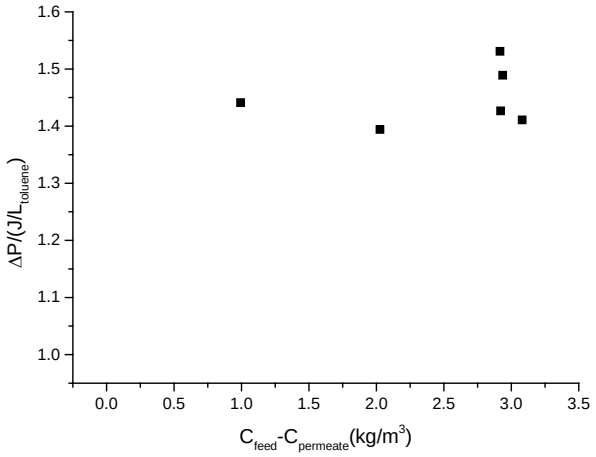

Figure 8 ΔP/(J/$L_{toluene}$) at 80°C as a function of C_{feed}-$C_{permeate}$

According to Figure 8, ΔP/(J/$L_{toluene}$) at 80°C is not a function of C_{feed}-$C_{permeate}$, but is constant around 1.45; which might be due to the fact that at 1kg/m^3 already, the concentration reaches its maximum effect. Further investigation with lower feed concentration is required to clear this question. Equation 31 then gives the final expression for ΔP/(J/$L_{toluene}$) as a function of temperature.

Finally we simplify Equation 29 to express osmotic pressure coefficient Ψ as a function of temperature, applied trans membrane pressure and solute feed concentration as given in Equation 32. Since we would like to be able to use the model for predicting $C_{permeate}$, we assumed C_{feed}-$C_{permeate}$ = C_{feed} for dilute permeate concentrations like we have.

$$\varphi = \frac{\Delta\pi}{C_{feed}} = \frac{\Delta P\left(1 - \frac{1}{(-1.0769x10^{-2}T(°C) + 2.344)}\right)}{C_{feed}} \quad (32)$$

The last parameter missing in Equation 26 is $C_{toluene}$ which we also expressed as a function of temperature as given in Equation 33,

$$C_{toluene} = -1.20\mathrm{T}(°\mathrm{C}) + 904.30 \quad (33)$$

If we insert all these parameters into Equation 26, we can now estimate the permeate concentration of the ligand as a function of temperature, trans membrane pressure and feed concentration of the ligand. Figure 9 shows the comparison of predicted and experimental permeate ligand concentrations for the experiments presented in Table 5.

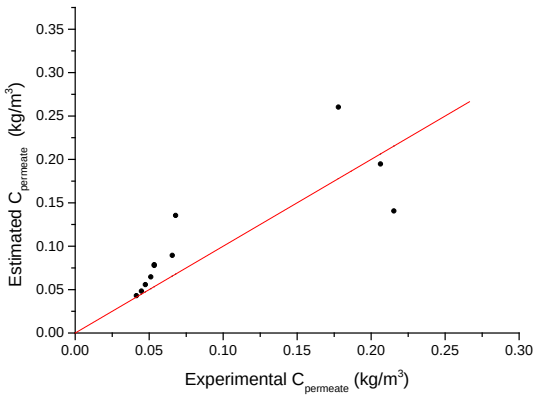

Figure 9 Permeate ligand concentrations for toluene, estimated using solution diffusion model compared to the experimental values

Although the lower permeate concentration values are predicted well by the model, at higher concentrations there is a large scatter, as is expected from the linear fits performed for the parameter values like L_{solute}. The fact that we cannot see the whole ligand peak in UV-Vis probably also contributes to the poor fits. Toluene has a UV Cutoff of 284 nm and we only see part of the peak that comes at higher wavelengths. Measuring the ligand in tetrahydrofuran which has a UV Cutoff of 212 nm shows this quite obviously as seen in Figure 10.

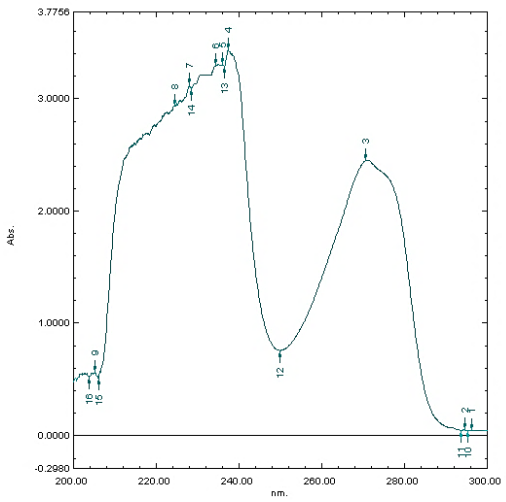

Figure 10 UV/Vis spectrum of tris(2,4-ditert-butylphenyl) phosphite ligand in THF, concentration=0.5 mg/ml

To see the effect of temperature and pressure on retention, we used the model we developed to calculate the retention, R% according to Equation 34.

$$R\% = 100\left(1 - \frac{C_{permeate}}{C_{feed}}\right) \tag{34}$$

Figure 11 shows predicted retention values of the bulky phosphite ligand in toluene, depending on the pressure differential across the membrane and reaction temperature. Increasing the pressure differential increases the retention; and so does increasing the temperature, especially evident at lower ΔP. These dependencies however, cannot be considered final. The scatter of data is quite high for parameter estimates in the model and a more thorough investigation including higher pressure differentials is necessary to conclude on the effect of temperature and pressure on retention. Furthermore, the experiments were performed in the order they are presented in Table 5, and the higher temperatures were applied later in the study. So if there are history effects such as 'clogging'; the data was affected the more, the higher the temperature.

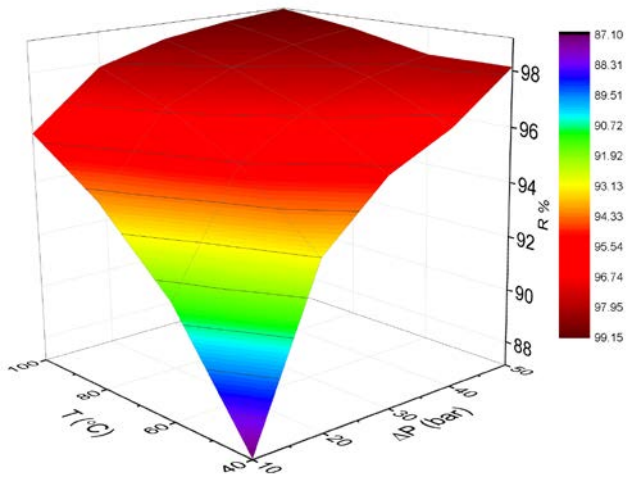

Figure 11 Estimated temperature and trans membrane pressure dependence of bulky phosphite ligand (C_{feed}=1 kg/m^3) retention in toluene

Table 6 below shows the permeate concentrations of Rh and P (ligand) determined for three continuous reactions performed. The concentrations are determined by elemental analysis. Samples were collected up until different residence times (also given in Table 6) to determine the effect of residence time on especially the Rh leaching. Retentions calculated for rhodium and phosphorus are given in Table 6 along with the predicted phosphorus retention.

Table 6 Retention of Rh and P during continuous reactions in the jet loop reactor

Entry	Substrate	ΔP (bar)	T (°C)	τ	$[P]_0$ (kg/m^3)	$[Rh]_0$ (kg/m^3)	$[P]_p$ (kg/m^3)	$[P]_{p\_predicted}$ (kg/m^3)	$[Rh]_p$ (kg/m^3)	P_R%	Rh_R%
1	Cyclooctene	10.6	80	0.42	3.84	0.051	$4.13x10^{-3}$	$2.13\ x10^{-1}$	$2.42\ x10^{-4}$	99.89	99.53
2	Cyclooctene	14.9	80	0.90	3.84	0.051	$1.59\ x10^{-2}$	$1.54\ x10^{-1}$	$6.36\ x10^{-4}$	99.59	98.75
3	1-pentene	6.2	80	2.11	0.05	0.001	$3.24\ x10^{-4}$	$4.71\ x10^{-3}$	$4.26\ x10^{-4}$	99.37	95.99

Entries 1&2: [cyclooctene] = 1.34 M, [Rh] = $2.0x10^{-4}$ M, [L] = $5.9x10^{-3}$ M, P = 20 bar CO:H_2 (1:1), T = 80°C, solvent=toluene

Entry 3: $[1\text{-pentene}]_{feed}$= 0.13 M, $[2\text{-pentene}]_{feed}$= 0.015 M, $[1\text{-pentene}]_0$= 0.108 M, $[2\text{-pentene}]_0$= 0.026 M, $[hexanal]_0$= 0.008 M, $[branched\ aldehydes]_0$= 0.002 M, [Rh] = $4.0x10^{-6}$ M, L/Rh= 30, P = 20 bar CO:H_2 (1:1) ,T = 80°C, solvent=toluene

The permeate concentration of phosphorus detected by elemental analysis is much lower than the predicted amount for all three experiments and the retention is higher than 99%. The predicted permeate concentration values are calculated for pure toluene according to the model derived, and apparently cannot represent the reaction mixtures. The model should be extended for liquid mixtures as a function of solvent physicochemical properties, to be able to predict the permeate concentration of ligand correctly. The different measurement technique applied for these experiments can be another source of error.

Although different reaction conditions are used and a one to one comparison is not possible among the entries of Table 6, Rh retention decreases almost linearly with increasing residence time; i.e. leaching of Rh increases over time. This can be due to the fact that with increased loss of the ligand, there are some catalyst species which exchange the phosphorus ligand with a CO. Or another deactivation mechanism can be active, where the deactivating agent accumulates over time. An experiment where the leached ligand is compensated for via the feed would help to determine the extent of the effect of ligand loss on the increased Rh leaching in time. And finally, the increased amount of aldehyde in the reactor with increased residence time can also be responsible for the increase in Rh loss. Indeed, literature reports that polar solvents decrease the retention of solutes by ceramic TiO_2 membranes.[15] We need to investigate the Rh leaching at steady state over time to eliminate this possibility.

6.4 Conclusions

The ceramic nanofiltration membrane used in the jet loop reactor setup was characterized for solvent permeation and ligand retention as a function of process variables like trans-membrane pressure and temperature. Three models from literature were investigated for the prediction of solvent permeability. Two of these models were used successfully to predict the temperature dependence of permeability as well, by including the temperature dependence of physical properties in the model. These models can be used to predict the permeate rate of a reaction mixture through the membrane as a function of temperature, trans membrane pressure and liquid mixture composition.

Retention of the bulky phosphite ligand by the membrane was also modeled as a function of temperature, trans membrane pressure and ligand concentration in the reactor, extending the solution-diffusion model reported in the literature to take temperature dependencies into account. This model allows a prediction of the amount of ligand leaching in pure toluene. The model predicts that increased temperature and trans membrane pressure should increase the retention of the phosphorus ligand in toluene, which we approach tentatively. Further investigation is required to extend the model for liquid mixtures and finalize our conclusions on the pressure and temperature dependence of retention.

Three continuous reaction permeate samples were investigated for Rh and P leaching. P was found to be rejected more than 99% for all three measurements. Rh retention, on the other hand, shows a clear decrease from 99.5% to 96%, according to the amount of sample collected. This suggests that the Rh loss rate is not constant and increases over time. The reason can be the shift in ligand

coordinated species to form only CO coordinated Rh centers due to ligand leaching, or another deactivation mechanism where the deactivating agent accumulates over time. It can also be due to the increase in aldehyde concentration over time before steady state is reached, since polar solvents are reported to reduce retention of solutes by TiO_2 membranes. Further investigation is required to clear out the reasons behind this behavior.

6.5 Experimental

6.5.1 Solvent Permeation Experiments

All solvent flux measurements were performed in the jet loop reactor setup with integrated membrane separation. Details of the experimental setup are given in Chapter 2. One single Inopor TiO_2 membrane with 0.9 nm pore size and molecular weight cutoff of 450 D was used for all the reported data in this Chapter. The flow in the membrane channel was set to 1.5 L/min during the measurements. Reactor pressure and trans membrane pressure were kept constant to obtain the reported pressure differential values during the measurements. The system was rinsed 3 times with the solvent to be measured beforehand and at least 100 mL of solvent was permeated through the membrane before the measurement was started to prevent 'history effects' in the measurements. Furthermore, solvent permeations were measured in the order they are given in Table 2, measuring the more polar methanol and acetonitrile in the end. The permeate rate was followed by logging the weight of the permeate every 0.5 minutes.

6.5.2 Ligand Retention Experiments

Retention experiments were performed similar to the solvent permeation experiments. Toluene was used as solvent and the retention samples were collected after steady state solvent permeation was achieved at the specified temperature and pressure differential. For samples 1-7 in Table 5, 50 mL of permeate was collected for each sample and concentrated to 3 mL by evaporating the solvent. For samples 8-10, 10 mL permeate was collected for each measurement. The ligand concentration was measured using Shimadzu UV-1650 PC UV-VIS Spectrophotometer. Elemental analyses were performed by H. Kolbe, Mikroanalytisches Laboratorium, Mülheim a.d. Ruhr (Germany).

6.6 References

[1] "Koch Membrane Systems - Membrane Products- Microfiltration, Ultrafiltration, Nanofiltration, and Reverse Osmosis Membranes," can be found under http://www.kochmembrane.com/Membrane-Products.aspx**.**

[2] P. Marchetti, A. Butté, A. G. Livingston, *J. Membr. Sci.* **2012**, *415-416*, 444–458.

[3] "inopor," can be found under http://www.inopor.com/**.**

[4] C. Guizard, A. Ayral, A. Julbe, *Desalination* **2002**, *147*, 275–280.

[5] S. Darvishmanesh, A. Buekenhoudt, J. Degrève, B. Van der Bruggen, *Sep. Purif. Technol.* **2009**, *70*, 46–52.

[6] A. Goldup, M. T. Westaway, G. Walker, *Separation of Organometallic Catalysts by Silicon Latex Membranes Under Pressure*, **1971**, DE 1953641.

[7] A. Goldup, M. T. Westaway, G. Walker, *Separation of Organometallic Compounds from Organic Liquids*, **1972**, US 3645891.
[8] E. Bayer, V. Schurig, **1974**, DE 2326489.
[9] S. S. Luthra, X. Yang, A. G. Livingston, L. M. Freitas dos Santos, L. S. White, *Chem. Commun.* **2001**, 1468–1469.
[10] D. Nair, S. S. Luthra, J. T. Scarpello, L. S. White, L. M. Freitas dos Santos, A. G. Livingston, *Desalination* **2002**, *147*, 301–306.
[11] K. De Smet, S. Aerts, E. Ceulemans, I. F. J. Vankelecom, P. A. Jacobs, *Chem. Commun.* **2001**, 597–598.
[12] D. Nair, J. T. Scarpello, L. S. White, L. M. Freitas dos Santos, I. F. J. Vankelecom, A. G. Livingston, *Tetrahedron Lett.* **2001**, *42*, 8219–8222.
[13] M. Janssen, J. Wilting, C. Müller, D. Vogt, *Angew. Chem., Int. Ed.* **2010**, *49*, 7738–7741.
[14] S. Darvishmanesh, A. Buekenhoudt, J. Degrève, B. Van der Bruggen, *J. Membr. Sci.* **2009**, *334*, 43–49.
[15] A. Dobrak, B. Verrecht, H. Van den Dungen, A. Buekenhoudt, I. F. J. Vankelecom, B. Van der Bruggen, *J. Membr. Sci.* **2010**, *346*, 344–352.
[16] A. Buekenhoudt, F. Bisignano, G. De Luca, P. Vandezande, M. Wouters, K. Verhulst, *J. Membr. Sci.* **2013**, *439*, 36–47.
[17] "Aspen Properties®" can be found under http://www.aspentech.com/products/aspen-properties.aspx.
[18] "Dielectric Constant," can be found under http://macro.lsu.edu/HowTo/solvents/Dielectric%20Constant%20.htm,
[19] "Dielectric Constants of various materials," can be found under http://www.clippercontrols.com/pages/Dielectric-Constant-Values.html#C**.**
[20] "NIST Chemistry WebBook," can be found under http://webbook.nist.gov/**.**
[21] "Surface Tension Components and Molecular Weight of Selected Liquids," can be found under http://www.accudynetest.com/surface_tension_table.html?sortby=sort_cas**.**
[22] "Dipole Moment," can be found under http://macro.lsu.edu/howto/solvents/Dipole%20Moment.htm**.**
[23] N. L. Allinger, *J. Am. Chem. Soc.* **1958**, *80*, 1953–5.
[24] D. Janssen, R. De Palma, S. Verlaak, P. Heremans, W. Dehaen, *Thin Solid Films* **2006**, *515*, 1433–1438.
[25] A. Carré, *J. Adhes. Sci. Technol.* **2007**, *21*, 961–981.
[26] S. Darvishmanesh, J. Vanneste, E. Tocci, J. C. Jansen, F. Tasselli, J. Degrève, E. Drioli, B. Van der Bruggen, *J. Phys. Chem. B* **2011**, *115*, 14507–14517.
[27] B. Van der Bruggen, J. Schaep, D. Wilms, C. Vandecasteele, *J. Membr. Sci.* **1999**, *156*, 29–41.
[28] A. M. Hidalgo, G. León, M. Gómez, M. D. Murcia, E. Gómez, J. L. Gómez, *Chem. Eng. Technol.* **2011**, *34*, 1753–1759.
[29] A. M. Hidalgo, G. León, M. Gómez, M. D. Murcia, D. S. Barbosa, P. Blanco, *Desalination Water Treat.* **2013**, *51*, 2244–2252.

Appendix

A.1 Derivation of the rate equations

In the simplified mechanism given in Scheme 1, total amount of Rh is given below:

$$Rh = A + G + G' \tag{A1}$$

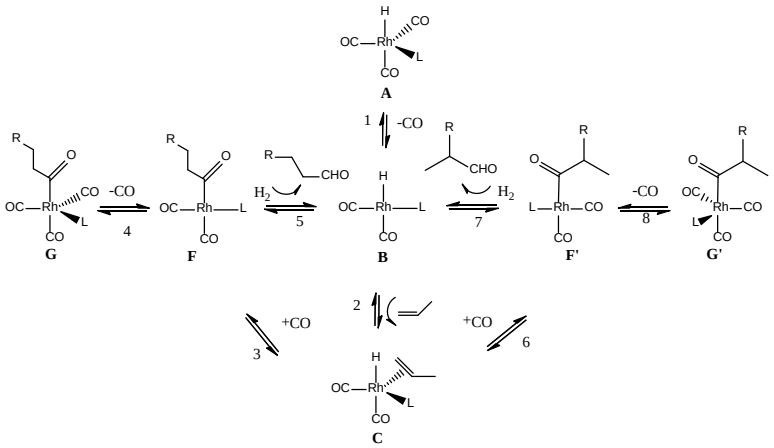

Scheme A1. Mechanism of Rh-catalyzed hydroformylation using bulky monophosphites

And the rest of the derivation is as follows:

Pre-equilibrium assumptions:

$$[B] = K_1[A]/[CO] \tag{A2}$$

$$[G] = K_4[F][CO] \tag{A3}$$

$$[G'] = K_7[F'][CO] \tag{A4}$$

Steady-state assumptions:

$$\frac{d[C]}{dt} = 0 \tag{A5}$$

$$\frac{d[F]}{dt} = 0 \tag{A6}$$

$$\frac{d[F']}{dt} = 0 \tag{A7}$$

Using the steady-state assumptions:

$$[F] = \frac{K_1K_2K_3[Rh][Alkene] + \left(\frac{k_{-6}K_3}{k_{-2}K_7} - K_1K_2K_3[Alkene]\right)[G']}{1 + \frac{k_6}{k_{-2}}[CO] + K_1K_2K_3K_4[CO][Alkene]} \tag{A8}$$

$$[F'] = \frac{K_1K_2K_3[Rh][Alkene] + \left(\frac{k_{-3}K_6}{k_{-2}K_4} - K_1K_2K_6[Alkene]\right)[G]}{1 + \frac{k_3}{k_{-2}}[CO] + K_1K_2K_6K_7[CO][Alkene]} \tag{A9}$$

To replace the dependencies on Rh-acyl compositions , we need to determine [F]/[F']

$$[\mathrm{F}] = \frac{\mathrm{a} + \mathrm{bK_7[F']CO}}{\mathrm{c}} \tag{A10}$$

$$[\mathrm{F'}] = \frac{\mathrm{d} + \mathrm{eK_4[F]CO}}{\mathrm{f}} \tag{A11}$$

$$[\mathrm{F}] = \frac{\mathrm{a} + \mathrm{bK_7[CO]}\,\frac{\mathrm{d} + \mathrm{eK_4[F]CO}}{\mathrm{f}}}{\mathrm{c}} \tag{A12}$$

$$[\mathrm{F}] = \frac{\mathrm{af} + \mathrm{bdK_7[CO]}}{\mathrm{cf} - \mathrm{beK_4K_7[CO]^2}} \tag{A13}$$

$$[\mathrm{F'}] = \frac{\mathrm{dc} + \mathrm{aeK_4[CO]}}{\mathrm{cf} - \mathrm{beK_4K_7[CO]^2}} \tag{A14}$$

$$\frac{[\mathrm{F}]}{[\mathrm{F'}]} = \frac{\mathrm{af} + \mathrm{bdK_7[CO]}}{\mathrm{dc} + \mathrm{aeK_4[CO]}} \tag{A15}$$

where

$a = K_1K_2K_3[Rh][Alkene]$, $\quad b = \frac{k_{-6}K_3}{k_{-2}K_7} - K_1K_2K_3[Alkene]$, $\quad c = 1 + \frac{k_6}{k_{-2}}[CO] + K_1K_2K_3K_4[CO][Alkene]$

$d = K_1K_2K_6[Rh][Alkene]$, $\quad e = \frac{k_{-3}K_6}{k_{-2}K_4} - K_1K_2K_6[Alkene]$, $\quad f = 1 + \frac{k_3}{k_{-2}}[CO] + K_1K_2K_6K_7[CO][Alkene]$

And re-writing

$a = K_3[Rh]\alpha$, $where\ \alpha = K_1K_2[Alkene]$; $b = \beta - K_3\alpha$, where $\beta = \frac{k_{-6}K_3}{k_{-2}K_7}$; $\quad c = 1 + \frac{k_6}{k_{-2}}[CO] + K_3K_4\alpha[CO]$

$d = K_6[Rh]\alpha$, $\quad e = \gamma - K_6\alpha$, where $\gamma = \frac{k_{-3}K_6}{k_{-2}K_4}$; $\quad f = 1 + \frac{k_3}{k_{-2}}[CO] + K_6K_7\alpha[CO]$

$$\frac{[F]}{[F']} = \frac{K_3[Rh]\alpha\left(1 + \frac{k_3}{k_{-2}}[CO] + K_6K_7\alpha[CO]\right) + (\beta - K_3\alpha)(K_6[Rh]\alpha)K_7[CO]}{(K_6[Rh]\alpha)\left(1 + \frac{k_6}{k_{-2}}[CO] + K_3K_4\alpha[CO]\right) + (K_3[Rh]\alpha)(\gamma - K_6\alpha)K_4[CO]} \tag{A16}$$

$$\frac{[F]}{[F']} = \frac{K_3[Rh]\alpha\left(1 + \frac{k_3}{k_{-2}}[CO] + K_6K_7\alpha[CO]\right) + K_3[Rh]\alpha\left(\frac{k_6}{k_{-2}} - \alpha K_6K_7\right)[CO]}{K_6[Rh]\alpha\left(1 + \frac{k_6}{k_{-2}}[CO] + K_3K_4\alpha[CO]\right) + K_6[Rh]\alpha\left(\frac{k_3}{k_{-2}} - \alpha K_3K_4\right)[CO]} \tag{A17}$$

$$\frac{[F]}{[F']} = \frac{K_3[Rh]\alpha\left[1 + \frac{k_3}{k_{-2}}[CO] + \alpha K_6K_7[CO] + \frac{k_6}{k_{-2}}[CO] - \alpha K_6K_7[CO]\right]}{K_6[Rh]\alpha\left[1 + \frac{k_6}{k_{-2}}[CO] + \alpha K_3K_4[CO] + \frac{k_3}{k_{-2}}[CO] - \alpha K_3K_4[CO]\right]} \tag{A18}$$

$$\frac{[F]}{[F']} = \frac{K_3[Rh]\alpha\left[1 + \frac{k_3}{k_{-2}}[CO] + + \frac{k_6}{k_{-2}}[CO]\right]}{K_6[Rh]\alpha\left[1 + \frac{k_6}{k_{-2}}[CO] + + \frac{k_3}{k_{-2}}[CO]\right]} \tag{A19}$$

$$\frac{[F]}{[F']} = \frac{K_3}{K_6} \tag{A20}$$

Which allows us to write the following

$$[G] = \frac{K_3K_4}{K_6}[F'][CO] \tag{A21}$$

$$[G'] = \frac{K_6K_7}{K_3}[F][CO] \tag{A22}$$

With this, we can insert the Rh-acyl concentrations [G] and [G'] as given in Equations 11 and 12 into the equations describing [F] and [F'] , Equations 8 and 9 to write down the final rate equations:

$$r_l = k_5[F][H_2] = \frac{k_5 K_1 K_2 K_3 [Rh][Alkene][H_2]}{1 + K_1 K_2 [CO][Alkene](K_3 K_4 + K_6 K_7)} \quad \text{(A23)}$$

$$r_b = k_8[F'][H_2] = \frac{k_8 K_1 K_2 K_6 [Rh][Alkene][H_2]}{1 + K_1 K_2 [CO][Alkene](K_3 K_4 + K_6 K_7)} \quad \text{(A24)}$$

A.2 Batch 1-pentene experiments for kinetics

Table A1. Concentration-time data of species during 1-pentene hydroformylation for conditions specified in Chapter 5 Table 2, (The entries in this table are equivalent to the ones in Chapter 5 Table 2)

Entry	Time (min)	[1-pentene] (M)	[2-pentene] (M)	[hexanal] (M)	[branched aldehydes] (M)
1	0.00	1.37	0.00	0.00	0.00
1	3.00	1.29	0.01	0.04	0.03
1	6.00	1.29	0.01	0.04	0.03
1	9.00	1.26	0.01	0.07	0.04
1	12.00	1.22	0.01	0.10	0.05
1	30.00	1.12	0.01	0.15	0.08
1	46.00	1.07	0.01	0.18	0.11
1	77.50	1.00	0.01	0.22	0.14
1	131.00	0.81	0.01	0.34	0.21
1	270.75	0.47	0.01	0.55	0.33
1	366.25	0.19	0.01	0.71	0.44
1	425.25	0.16	0.03	0.74	0.45
1	1290.00	0.05	0.00	0.81	0.51
2	0.00	1.10	0.00	0.00	0.00
2	20.00	0.75	0.04	0.19	0.12
2	70.00	0.52	0.09	0.32	0.16
2	171.00	0.11	0.04	0.59	0.36
2	340.00	0.03	0.03	0.65	0.39
3	0.00	1.37	0.00	0.00	0.00
3	3.00	1.27	0.01	0.05	0.03
3	6.00	1.25	0.01	0.07	0.04
3	9.00	1.23	0.01	0.08	0.05
3	12.00	1.19	0.01	0.11	0.07
3	15.00	1.16	0.01	0.12	0.08
3	20.00	1.11	0.01	0.15	0.10
3	27.75	0.99	0.01	0.23	0.14
3	35.00	0.96	0.01	0.25	0.15
3	50.00	0.88	0.01	0.30	0.18
3	70.00	0.81	0.01	0.34	0.21
3	116.00	0.71	0.01	0.40	0.25
3	997.98	0.08	0.01	0.77	0.51
4	0.00	1.37	0.00	0.00	0.00

Entry	Time (min)	[1-pentene] (M)	[2-pentene] (M)	[hexanal] (M)	[branched aldehydes] (M)
4	3.25	1.30	0.01	0.04	0.03
4	6.00	1.27	0.01	0.05	0.04
4	9.00	1.23	0.01	0.08	0.05
4	12.00	1.21	0.01	0.10	0.07
4	15.00	1.16	0.01	0.12	0.08
4	20.00	1.14	0.01	0.14	0.08
4	27.50	1.07	0.01	0.18	0.11
4	35.00	1.03	0.01	0.21	0.12
4	50.00	0.97	0.01	0.23	0.15
4	96.00	0.93	0.01	0.26	0.16
4	131.00	0.88	0.01	0.29	0.19
4	1118.00	0.08	0.01	0.78	0.49
5	0.00	1.37	0.00	0.00	0.00
5	3.00	1.25	0.01	0.07	0.04
5	6.00	1.22	0.01	0.08	0.05
5	9.00	1.18	0.01	0.11	0.07
5	12.00	1.12	0.01	0.15	0.10
5	15.00	1.08	0.01	0.16	0.10
5	20.00	1.01	0.01	0.21	0.12
5	27.00	0.97	0.01	0.23	0.15
5	35.00	0.92	0.01	0.27	0.16
5	50.00	0.84	0.01	0.33	0.19
5	70.00	0.71	0.01	0.40	0.23
5	138.00	0.45	0.03	0.56	0.33
5	185.00	0.30	0.03	0.66	0.38
5	309.00	0.10	0.00	0.79	0.48
6	0.00	1.37	0.00	0.00	0.00
6	3.00	1.30	0.01	0.04	0.03
6	6.00	1.27	0.01	0.05	0.03
6	9.00	1.22	0.01	0.08	0.05
6	12.00	1.18	0.01	0.11	0.07
6	15.00	1.15	0.01	0.12	0.08
6	20.00	1.11	0.01	0.15	0.10
6	28.00	1.05	0.01	0.19	0.11
6	35.00	1.00	0.01	0.22	0.14
6	50.00	0.89	0.01	0.29	0.16
6	89.00	0.78	0.03	0.36	0.21
6	313.00	0.05	0.05	0.79	0.47
6	360.00	0.04	0.01	0.82	0.49
7	0.00	1.37	0.00	0.00	0.00
7	10.00	1.03	0.04	0.19	0.11
7	20.00	1.00	0.05	0.21	0.11
7	30.00	0.92	0.04	0.26	0.14

Entry	Time (min)	[1-pentene] (M)	[2-pentene] (M)	[hexanal] (M)	[branched aldehydes] (M)
7	40.00	0.96	0.05	0.23	0.12
7	60.00	0.82	0.07	0.32	0.18
7	90.00	0.75	0.10	0.34	0.18
7	120.00	0.66	0.14	0.38	0.19
7	150.00	0.53	0.16	0.45	0.22
7	210.00	0.30	0.23	0.58	0.27
7	340.00	0.01	0.21	0.71	0.44
8	0.00	0.00	0.37	0.00	0.00
8	11.00	0.01	0.30	0.02	0.04
8	21.00	0.01	0.25	0.03	0.07
8	33.00	0.00	0.23	0.03	0.10
8	50.00	0.00	0.22	0.03	0.12
8	71.00	0.00	0.19	0.02	0.15
8	93.00	0.00	0.16	0.03	0.18
8	120.00	0.00	0.14	0.02	0.21
8	150.00	0.00	0.11	0.02	0.23
8	202.00	0.00	0.08	0.02	0.26
8	264.00	0.00	0.06	0.02	0.28
9	0.00	1.37	0.00	0.00	0.00
9	3.00	1.27	0.00	0.05	0.04
9	6.00	1.21	0.00	0.10	0.07
9	9.00	1.14	0.00	0.14	0.08
9	12.00	1.12	0.01	0.15	0.10
9	15.00	1.10	0.01	0.16	0.11
9	50.00	0.99	0.01	0.23	0.14
9	62.00	0.92	0.01	0.27	0.16
9	79.00	0.86	0.01	0.30	0.18
9	102.00	0.78	0.03	0.36	0.21
9	121.00	0.73	0.03	0.38	0.23
9	141.00	0.66	0.03	0.42	0.25
9	1180.00	0.05	0.00	0.84	0.49
10	0.00	1.37	0.00	0.00	0.00
10	5.00	1.27	0.00	0.05	0.04
10	8.00	1.25	0.00	0.07	0.04
10	12.00	1.26	0.00	0.07	0.04
10	15.00	1.22	0.00	0.08	0.05
10	53.00	0.99	0.00	0.23	0.15
10	66.00	0.99	0.00	0.25	0.14
10	87.00	0.77	0.01	0.37	0.23
10	360.00	0.10	0.01	0.78	0.48
11	0.00	1.37	0.00	0.00	0.00
11	5.00	1.32	0.00	0.03	0.03
11	8.00	1.25	0.00	0.07	0.04

Entry	Time (min)	[1-pentene] (M)	[2-pentene] (M)	[hexanal] (M)	[branched aldehydes] (M)
11	12.00	1.16	0.00	0.12	0.07
11	15.00	1.10	0.01	0.16	0.10
11	53.00	0.78	0.03	0.36	0.19
11	63.00	0.67	0.03	0.44	0.23
11	87.00	0.42	0.07	0.58	0.30
11	358.00	0.10	0.00	0.78	0.49
12	0.00	1.37	0.00	0.00	0.00
12	6.00	1.30	0.01	0.04	0.03
12	9.00	1.26	0.01	0.05	0.04
12	12.00	1.22	0.01	0.10	0.05
12	15.00	1.16	0.01	0.12	0.07
12	20.00	1.10	0.01	0.16	0.10
12	27.00	1.04	0.01	0.21	0.12
12	47.00	0.90	0.01	0.29	0.16
12	77.00	0.66	0.03	0.44	0.25
12	107.00	0.45	0.03	0.56	0.32
12	138.00	0.30	0.04	0.66	0.37
13	0.00	1.37	0.00	0.00	0.00
13	3.00	1.27	0.00	0.07	0.04
13	6.00	1.15	0.04	0.11	0.07
13	9.00	1.08	0.04	0.16	0.10
13	12.00	1.05	0.00	0.19	0.12
13	15.00	0.96	0.04	0.23	0.14
13	20.00	0.89	0.05	0.27	0.16
13	27.00	0.82	0.05	0.32	0.19
13	35.00	0.74	0.04	0.37	0.22
13	50.00	0.59	0.05	0.47	0.26
13	65.00	0.47	0.07	0.53	0.30
13	205.00	0.04	0.01	0.79	0.51
14	0.00	1.36	0.01	0.00	0.00
14	5.00	0.90	0.14	0.22	0.11
14	10.00	0.84	0.16	0.26	0.12
14	20.00	0.42	0.33	0.42	0.19
14	30.00	0.15	0.37	0.59	0.26
14	42.50	0.11	0.38	0.59	0.29
14	61.00	0.07	0.37	0.62	0.32
14	91.00	0.10	0.32	0.60	0.36
14	121.00	0.08	0.29	0.62	0.38
15	0.00	0.00	0.37	0.00	0.00
15	10.00	0.00	0.20	0.04	0.12
15	20.00	0.00	0.15	0.04	0.18
15	30.00	0.00	0.13	0.04	0.20
15	40.00	0.00	0.11	0.04	0.21

Entry	Time (min)	[1-pentene] (M)	[2-pentene] (M)	[hexanal] (M)	[branched aldehydes] (M)
15	51.00	0.00	0.10	0.04	0.23
15	61.00	0.00	0.09	0.04	0.23
15	110.00	0.00	0.06	0.04	0.27
15	1116.00	0.00	0.01	0.04	0.32
16	0.00	1.10	0.00	0.00	0.00
16	10.00	0.71	0.04	0.23	0.11
16	20.00	0.59	0.08	0.25	0.19
16	30.00	0.57	0.09	0.25	0.19
16	61.00	0.54	0.09	0.31	0.16
16	84.00	0.46	0.19	0.31	0.15
16	127.00	0.37	0.18	0.37	0.18
16	305.00	0.02	0.33	0.45	0.30
16	444.00	0.01	0.13	0.47	0.48
16	580.00	0.00	0.05	0.48	0.56
17	0.00	0.00	1.37	0.00	0.00
17	20.00	0.01	1.11	0.03	0.22
17	30.00	0.01	1.03	0.04	0.29
17	190.00	0.01	0.75	0.10	0.49
17	1110.00	0.00	0.01	0.22	1.14
18	0.00	1.37	0.00	0.00	0.00
18	3.00	1.27	0.03	0.05	0.03
18	6.00	1.19	0.04	0.10	0.05
18	9.00	1.11	0.04	0.15	0.08
18	13.00	1.01	0.04	0.22	0.11
18	17.00	0.92	0.04	0.27	0.14
18	52.00	0.48	0.01	0.60	0.29
18	149.00	0.19	0.00	0.79	0.37
18	226.00	0.14	0.00	0.78	0.45
18	1190.00	0.01	0.00	0.85	0.49
19	0.00	0.00	0.37	0.00	0.00
19	10.00	0.01	0.22	0.06	0.08
19	20.00	0.01	0.18	0.06	0.11
19	30.00	0.00	0.16	0.05	0.15
19	40.00	0.00	0.13	0.06	0.18
19	50.00	0.00	0.11	0.06	0.20
19	60.00	0.00	0.09	0.06	0.21
19	80.00	0.00	0.07	0.06	0.24
19	105.00	0.00	0.05	0.06	0.26
19	130.00	0.00	0.03	0.06	0.27

Continuous Homogeneous Hydroformylation with Integrated Membrane Separation: Kinetics, Mechanism and Jet Loop Reactor Technology

Hydroformylation is the reaction that converts alkenes to aldehydes in the presence of a Co or Rh based catalyst and syngas. Product aldehydes are important intermediates in the production of surfactants, softeners, and fragrances. Hydroformylation is one of the most important examples of homogenously catalyzed reactions in industry. However, the separation and reuse of the homogeneous catalyst is a grand challenge in continuous hydroformylation. This is relevant not only for recycling of the expensive metal but also for the product purity. Recycling of the homogeneous catalyst is achieved conventionally by phase separation, distillation, or heterogenization of the homogeneous catalyst. These techniques however have their limitations: limited alkene solubility in the aqueous phase that contains the catalyst for biphasic hydroformylation, catalyst deactivation and accumulation of heavies for distillation, and a loss in activity and /or selectivity for the heterogenization. It is therefore of great interest to build an optimal reaction-separation system that enables recycling of the homogeneous catalyst. Recently, it was shown by our research group that molecular weight enlarged catalysts kept in the reactor by taking the products out as permeate from a nanofiltration membrane represents a viable solution to this challenge. In this study we chose to use a naturally bulky, commercially available ligand to modify the Rh catalyst.

Based on the expertise in the group and taking into account the other challenge of a fast two phase reaction, mass transfer limitation; we constructed a jet loop reactor with integrated membrane separation. Jet loop reactor technology enables a very good dispersion of gaseous reactants in the liquid without introducing extra energy demands. ***Chapter 2*** introduces the reactor setup and explains the design considerations taken into account. A good selection of equipment gave us a flexible reaction system in terms of operating conditions like residence time and the power input per unit volume on the fluid flow through the jet (P/V), which is an important parameter for achieved gas to liquid mass transfer rates.

The first step in planning a continuous reaction is to determine the reaction kinetics, which also makes it possible to understand the reaction mechanism. We investigated the hydroformylation kinetics of cyclooctene in order to plan a continuous hydroformylation reaction in the new setup. ***Chapter 3*** gives the kinetic results obtained from batch experiments. A continuous hydroformylation run was successfully performed in the developed reaction setup, giving a total

turnover number of 44300 in a total reaction time of 47 hours, which corresponds to 5 residence times. Steady state conversion was reached after about one residence time and remained constant till the experiment was stopped. This result is important since it is achieved with a commercially available ligand without any further MW enlargement or immobilization on a support and can be improved by applying higher reaction temperatures or simply by running the reaction longer.

Hydroformylation kinetics of neohexene was also investigated, representing a different class of alkenes, i.e vinylic. The kinetic investigation led us to an interesting study on regioselectivity. We investigated the reasons behind the temperature dependence of the l/b aldehyde selectivity using deuterium labeling and ^{2}H NMR as well as in-situ high pressure IR in ***Chapter 4***. The deuterioformylation experiments showed that both linear and branched Rh-alkyl formation are reversible, and increasingly so with increasing temperature. At 100°C, the linear Rh-alkyl formation was found to be even more reversible than the branched one, which means the increase in linear aldehyde selectivity with increasing temperature cannot be explained by relatively increased branched Rh-alkyl reversibility at elevated temperatures. Indeed, we showed that the hydrogenolysis of the five-coordinated Rh-acyl species has a larger activation energy for the linear acyl, which contributes more than the rest of the cycle to the temperature dependence of regioselectivity.

Also a rather fast reaction, the hydroformylation of 1-pentene, was investigated. The extremely fast kinetics of this substrate makes it an excellent candidate for obtaining very high total turnover numbers in the jet loop reactor. The results of the kinetic study are presented in ***Chapter 5***. We obtained a TTON of 47600 in just two residence times using a very dilute 1-pentene feed. In principle it is possible to increase the TTON to one million at the same conditions only by changing to pure 1-pentene feed. The fast kinetics of this substrate also bears the possibility of mass transfer limitations, especially at elevated temperatures. We investigated the concentration of H_2 and CO in the reaction mixture at different temperatures and pressures, including the proposed reaction conditions to obtain one million TTON in two residence times. The calculations showed that even when using the minimum mass transfer coefficient value determined beforehand, the concentration of gases in the liquid remain very close to the equilibrium values. The steady-state selectivity of the reaction is a complex function of temperature and pressure. We showed that it can be optimized.

Prediction of membrane permeability as a function of process variables and reaction mixture composition are obviously necessary to be able to operate a continuous reactor where the product flow is the permeate of a nanofiltration membrane. Three models reported in the literature to

predict solvent permeability as a function of solvent characteristics were investigated. The results were used to model the permeate rate of any solvent (mixture) as a function of process variables. It was shown that two of these models can be used as well to predict the temperature dependence of permeability, when temperature dependence of physical properties were incorporated in the model. Also, characterizing the catalyst/ligand leaching behavior allows compensating for the lost ligand at an appropriate rate. Make-up of the lost ligand makes it possible to keep the ligand excess constant and prevent metal leaching since the metal centers will be more prone to leaching once they lose the ligand attached due to a shift in equilibrium. Rejection of the ligand in toluene was also modeled as a function of temperature, trans membrane pressure and ligand concentration in the reactor, extending the solution-diffusion model reported in the literature to take temperature dependencies into account. This model allows the prediction of the amount of ligand leaching through the membrane for pure toluene. Further investigation will be necessary to extend the model for real reaction mixtures. Membrane characterization is discussed in ***Chapter 6***.

Curriculum Vitae

Snezhana Hristova was born on 18-09-1985 in Kardzhali, Bulgaria. She took a Turkish name: ‘Sabriye Güven’ according to her family’s origin, after she moved to Turkey with her family in 1989. After finishing her high school degree at Gazi Anadolu Lisesi in 2003 in Bursa/Turkey, she studied Chemical Engineering at Boğaziçi Universitesi in Istanbul/Turkey. She acquired her bachelor degree in 2007, with a specialization in process engineering. In 2009, she obtained her master degree within the group of Chemical Catalyst Technology and Reaction Engineering under the supervision of Prof. Ahmet Erhan Aksoylu. From October 2009 she started a PhD project in the group of Prof. Dieter Vogt at Eindhoven University of Technology at Eindhoven, The Netherlands; where she was registered with her birth name ‘Snezhana Hristova’ which she could not manage to correct to date. The results of her PhD work are presented in this dissertation.

List of Publications

- Sabriye Güven, Bart Hamers, Robert Franke, Markus Priske, Marc Becker, Dieter Vogt*

  Kinetics of Cyclooctene Hydroformylation for Continuous Homogeneous Catalysis

  (submitted for publication)

- Sabriye Güven, Marko Nieuwenhuizen, Bart Hamers, Robert Franke, Markus Priske, Marc Becker, Dieter Vogt*

  Kinetic Explanation for the Temperature Dependence of Regioselectivity in Neohexene Hydroformylation

  (submitted for publication)

- Leen E.E. Broeckx, Sabriye Güven, Frank J.L. Heutz, Martin Lutz, Dieter Vogt, and Christian Müller*

  Cyclometalation of aryl substituted phosphinines via C-H bond activation: a mechanistic investigation

  Chemistry - A European Journal, **2013**, 19, 13087

Acknowledgements

When I was little I would say ‘I will be a *writer* when I grow up’, when they asked the famous question. I am pretty sure I didn’t mean this type of writing; back then I was more imaginative and would not require 4 years of experimenting to come up with a story! Well, a book is a book I guess...

I would like to thank Dieter for giving me the opportunity to write this book: Dieter, it was a pleasure to work with you; actually maybe too much so! I really appreciated the positive atmosphere you created in the group, and the fact that you were so humble and friendly as a boss. Despite your suspicions(!) of the abilities of my kind (engineers), you allowed me tremendous freedom in my research and I am grateful for it. I learned to appreciate the insight in chemistry in solving engineering problems and I think I managed to give a hint of the ‘beauty of engineering’ to my chemist colleagues.

And I should thank Christian for his guidance, corrections and last but not least all the barbecues that would not have been possible without him. It was fun working on the cyclometalation paper together and I was happy to visit the lab in Berlin.

I am also grateful to my committee members, who took the time to read and comment on my thesis.

I would also like to thank my colleagues from Evonik: Bart, Frank, Marc, Markus, Robert Franke and Horst; for the help with the setup and all the discussions and good company in the numerous F3/subproject meetings.

Ton, my setup would not have been possible without you! Thank you for all the help you offered so warmly over the years. Wout, heel erg bedankt voor uw hulp met de reactor en uw geduld met mijn Nederlands. And of course the GTD team for building my setup and helping me with the troubles: Harrie, Herbert, Jeroen and the others.

And my group members, past and present: Leen, we started our PhD projects the same day and shared the same office for 4 years, isn’t it weird we still like each other? ☺ Thank you for: all the ‘Leens’ you taught me, your softening effect on my Dutch, all the Styrofoam you imported from Belgium, my office chair at home, the rapid change of mood in the office which made it so exciting☺, all these little things which made life at work more fun and for being there to listen to the inevitable frustrations of a PhD project. Fanni; creator of the chocolate drawer, that was one evil thing you did in the office ☺ Thank you for being ‘Fanni’, and for being my friend. Why have you moved to Berlin, again? Iris, one woman SKO army; for being a super smooth office mate: absolutely tidy (you know how picky I am about that!), calm, never complaining, never in a bad mood…Come on Iris, is it something you discovered in the lab? Atilla; grupta gerçekten her aklıma geleni söyleyebildiğim tek insandın, ve sadece aynı anadili konuştuğumuzdan değil. ☺ Memleket kurtardığımız kahve molaları dahil doktoraya kattığın tüm pozitif enerji için teşekkürler! Olivier; thank you for all the training on drinking, all the times we were out having fun, all the barbecues in your(!) garden, the now conventional Easter trips and being there when I needed (also for NMR). It is always a pleasure to have you around. Andreas for the wellness trips to Aachen. Alberto especially for sharing the know-how on the spaghetti sausage. Coen for making the effort to speak clear and slow Dutch and the ‘private’ Nijmegen trip. Dennis for being startled so easily. Evert for making one feel good about herself about the amount of desert one eats. Jarno for all the whistling to the music in the lab. Michèle; for your help during the initial period of my PhD, it was nice

learning from you and not only science. Hybrids Jos, Arjan, Gijsbert and Erik for being there when one needed advice or tools. Patrick and Laura for the good company during the promotion parties. Master students: William, Yoran and Frank for all the bottles they opened for me in the lab. Our first immigrant from SMK, Georgy for being such a jolly good sport. Thank you all, very much, for the fun and the friendly atmosphere in the group, for all the borrels, Fort evenings, group weekends and conference trips. I really enjoyed being part of this group.

And of course the usual suspects of the coffee breaks and Friday borrels: Tiny, Gilbère, Remco, Ivo, Evgeny, Adelheid, Jan and other occasional SKE members; thank you for all the 'gezelligheid' in the coffee room.

Sympathetic people who made life in Eindhoven more fun with their warmth: Benjamin, Camille, Florence, Fabian, Natta, Matthieu, Isabelle, Ard; thank you for all the parties, refreshing politeness, the good food&mood and everything we drank together. And of course other Mediterraneans: Iliana&Sokratis (for the fantastic food, the 'swing' machine ☺ and the vinyl player), Dario, Maria, Daniele, Bruno&Valentina, Domenico, Lili, Sami, Maurizio along with the Turkish community: Eralp; yazık ki buradaki zamanımız pek uzun olmadı, ama senin burda olman bana ilk senemde çok büyük destek verdi. Eindhoven'daki ilk günlerimde bana evini açtığın için, ve ne zaman ihtiyacım olsa yanımda olan gerçek bir dost olduğun için çok teşekkürler. Yediğin peyniri de helal ettim ☺ Altuğcum, seni Boğaziçi'nden ziyade burda tanıdım, iyi ki böyle bir ikinci şansımız oldu: Beraber içtiğimiz tüm kahveler için, pişirdiğin tüm güzel yemekler için, Utrect'teki kano turu için ve tabii ki bu kadar sevecen ve fedakar bir arkadaş olduğun için çok teşekkür ederim. Elacım; güler yüzün, samimiyetin ve sıcaklığınla Eindhoven'in vazgeçilmezisin ☺. İçten dostluğun için çok teşekkürler ve bir sonraki maceran için bol şans. Ayşegül; Eindhoven'daki nesli tükenmekte olan yakın kız arkadaşlarımdan biri olduğun, sıkıntılı zamanlarda dinleyip destek olduğun, kahve için biraraya gelişlerimizde bolca güldürdüğün için, ve tabii ki tüm zumba akşamları için çok teşekkürler. Burcu; seni her gördüğümde yüzünden eksik olmayan gülümsemeyi bana da bulaştırdığın için, hem bana hem setup'a verdiğin reiki için, tüm zumbalamalar ve pişirdiğin leziz kek/pasta/börek/çörek için, ve tabii dostluğun için sonsuz teşekkürler. Ve tabii ki öğle yemeklerini, Fort'u, Antep'i neşelendiren diğer arkadaşlar: Abidin, Ali Can, Başar, Bahar, Ceylan, Döndü, Gökhan, Gözde, İlkin, İsa, Kamil, Müge, Sinan, Selçuk, Serkan; Eindhoven'daki varlığınız her zaman büyük bir güç kaynağıydı, aynı dili konuşmanın ve aynı kültürü paylaşmanın keyfini yaşatan harika insanlar olduğunuz için çok teşekkürler.

And partners I am very happy to have met: Roos, thanks for all the good food you served us with Atilla, and for offering that genuine smile of yours so readily. Micha, thank you for taking so good care of Fanni (who means a lot to me!), for all the advice on the printing and forms, and for staying positive on the gloomy day on the beach (actually whenever I met you ☺). Sanne, thanks for the nice canoe tour in Utrecht and the icecream☺.

Burakçım, burada doktoraya başlamamda payın büyük. Konukseverliğin, güleryüzün, samimiyetin, gösterişsiz bilgeliğin için ve zor zamanlarda beni şımartıp keyfimi yerine getirdiğin için çok teşekkürler. Ingrid, I wish we could meet more often, I always enjoy the time we spend together. Thank you for your hospitality, for your incredible openness, for being so easy to talk to and for introducing me to your family: Paul & Gea thank you very much for opening your house to me when I came for my PhD interview and your support back then and now. And Kirsten, thank you for being so unconditionally warm, positive and supportive.

My extended circle of friends (thanks to Hans): Ola&Johanna, Malin&Leo, Kajsa&Tobbe, Hanna&Olle, Oskar&Katta, Tony&Sanna, Henrik&Kristina, Sandra and Kristian: Thank you for making me feel welcome, I appreciate your friendship, although it could sure help to spend some

more time together ☺. Well, maybe that will be possible in the future, who knows? Elisabeth&Niklas, the most stylish couple with Dr. titles ever: thank you for your hospitality in your A'dam mansion, for being so warm hearted, all the fun we had together and hope will keep having, for having corrected my upcoming Swedish declaration, but especially for having introduced me to Chunky Monkey (yummy!!)

İstanbul'un güzelliğine güzellik katan arkadaşlarım: Filizim, sevgili paranimf'im, İstanbul'daki favori adresim, güzel arkadaşım; her geldiğimde evini ve kalbini sonuna kadar açtığın için, ne kadar uzun süre görüşmesek hep kaldığımız yerden başlayabildiğimiz için, sarıldığında insanda kendinden bir parça bıraktığın için…Herşey için çok teşekkürler! Görkemcim, istediğimiz kadar sık görüşemesek de kalbimdeki yerin ayrı, içten dostluğun için teşekkür ederim. Oğuz&Pınar: kocaman kalpli sevimli insanlar, gülümsemelerinizle içimi ısıttığınız için ve yuvanızdaki hatırlanası yılbaşı kutlaması için, İlker&Begüm: Konukseverliğiniz, candan dostluğunuz ve harika sofralarınız için, Miraycım: en zor zamanlarda insanın yanında olan gerçek bir dost olduğun için ve tüm kuaför maceralarımız için, Sadi ve Yaver: gözlerinizden ışıyan pozitif enerjiyi cömertçe paylaştığınız için, Can: ayaklı Wikipedia servisi ve bitip tükenmeyen bir hevesle anlatılan tüm anektodlar için, Umut: her daim kibar ve güleryüzlü dostluğun için. Ve tabii Ayfer: bir çocuktan yetişkine dönüşüm zamanlarımda yanımda olduğun için.

Hans: för att du gör Eindhoven till ett hem för mig, för din ständigt så positiva attityd till livet, för ditt tålamod då jag klagar på kylan, för alla äventyr vi har delat hittills, för stödet du alltid ger mig utan att tveka, för att du är en så omtänksam, kärleksfull, sympatisk och rolig partner.Tack så mycket älskling för att du vill vara en del av mitt liv. Och; Torsten och Britt: tack så mycket för att ni välkomnat mig in i er familj, för den goda maten, och för att ni gett mig Hans. Familjerna Söderström och Strand för den härliga tiden vi hade tillsammans.

Ailem; kuzenlerim, teyzelerim, halam, dayılarım, amcam, enişte ve yengelerim, dedem, hepinize desteğiniz ve sevginiz için ayrı ayrı teşekkürler.

Ablacım, koşulsuz sevgin, anlayışın ve desteğin için; dünyanın en tatlı yeğeni için; en çok da sadece 2.5 yaş büyük olduğun halde her zaman gerçek bir 'abla' olduğun için sonsuz teşekkürler. Seni seviyorum.

En son ve en çok da anne ve babama, beni yetiştirmek için gösterdikleri tüm çaba ve fedakarlıklar için bütün kalbimle teşekkür ederim. İyi ki varsınız, sizi seviyorum.

Sabriye